Photo-Physical Properties, and Quenching of the Excited State of Chlorophyll A

Daweena Masen

A Thesis Submitted in Partial Fulfillment of the Requirements
for the Degree of Master of Science in Chemical Studies
Prince of Songkla University
2010

Thesis Title	Photo-Physical Properties, and Quenching of the Excited State of Chlorophyll A
Author	Miss Daweena Masen
Major Program	Chemical Studies

Major Advisor:

…….....
(Dr.Nararak Leesakul)

Co-advisor:

…….....
(Asst. Prof. Dr.Kanidtha Hansongnern)

Examining Committee:

……...Chairperson
(Asst. Prof. Dr.Siwaporn Meejoo Smith)

…….....
(Dr.Nararak Leesakul)

…….....
(Asst. Prof. Dr.Kanidtha Hansongnern)

…….....
(Dr.Pongsaton Amornpitoksuk)

The Graduate School, Prince of Songkla University, has approved this thesis as partial fulfillment of the requirement for the Master of Science Degree in Chemical Studies.

…….....
(Assoc. Prof. Dr.Krerkchai Thongnoo)
Dean of Graduate School

ชื่อวิทยานิพนธ์ สมบัติเชิงแสงและปฏิกิริยาการระงับของคลอโรฟิลล์ เอ ที่สภาวะกระตุ้น

ผู้เขียน นางสาวดาวีน่า หมะเส็น

สาขาวิชา เคมีศึกษา

ปีการศึกษา 2552

บทคัดย่อ

สมบัติเชิงแสงของคลอโรฟิลล์ เอ สามารถศึกษาโดยใช้เทคนิคการเปล่งแสงฟลูออเรสเซนซ์ และเทคนิคการหาช่วงชีวิตของสารที่เปล่งแสงได้โดยวิธีการมอดูเลชันแสดงผลด้วยออสซิลโลสโคป คลอโรฟิลล์ เอ เป็นรงควัตถุที่สามารถดูดกลืนแสงได้ เนื่องจากมีโครงสร้างเป็นพันธะคู่อยู่มาก ส่งผลให้เกิดการดูดกลืนแสงได้ดีในช่วงแสงที่มองเห็นได้ คลอโรฟิลล์ เอ จึงนิยมนำมาเป็นโมเลกุลเซนซิไทเซอร์ในเซลล์พลังงานแสงอาทิตย์แบบสีย้อม การถ่ายโอนอิเล็กตรอนของคลอโรฟิลล์ เอ โดยใช้ tris(acetylacetonato)Iron(III); $Fe(acac)_3$ เป็นตัวระงับ สามารถศึกษาการถ่ายโอนอิเล็กตรอนผ่านปฏิกิริยาการระงับ (quenching reaction) ค่าการเปลี่ยนแปลงพลังงานอิสระของปฏิกิริยาการถ่ายโอนอิเล็กตรอนเหนี่ยวนำด้วยแสง คำนวณโดยใช้สมการของเรม-เวลเลอร์ (Rehm-Weller equation) โดยปฏิกิริยาการระงับศึกษาในช่วงความเข้มข้นของ $Fe(acac)_3$ 1.0×10^{-5} โมลาร์ ถึง 2.0×10^{-4} โมลาร์ พบว่าความเข้มของการเปล่งแสงจะลดลงเมื่อความเข้มข้นของ $Fe(acac)_3$ เพิ่มขึ้น โดยกราฟการพล็อตของสเติร์น-โวลเมอร์ (Stern-Vlmer plot) จากปฏิกิริยาการระงับได้กราฟที่มีลักษณะเป็นเส้นโค้งเนื่องมาจากผลของการบดบังภายใน (inner filter effect) มากกว่าผลที่เกิดการรวมตัวกันเป็นสารเชิงซ้อนที่สภาวะพื้น (ground state complex formation) ค่าคงที่อัตราการระงับ (k_q) สามารถหาได้จากการพล็อตกราฟของสเติร์น-โวลเมอร์ ที่กำจัดผลของอินเนอร์ฟิลเตอร์แล้ว (correction) พบว่าประสิทธิภาพของการถ่ายโอนอิเล็กตรอนระหว่างคลอโรฟิลล์ เอ และ $Fe(acac)_3$ สามารถเกิดขึ้นได้ดี ค่าคงที่อัตราการระงับ (k_q) และค่าคงที่ของการรวมตัวที่สภาวะพื้น (K_{app}) ขึ้นอยู่กับความหนืดของตัวทำละลาย การถ่ายโอนอิเล็กตรอนสามารถเกิดขึ้นได้เร็วขึ้นในตัวทำละลายที่มีความหนืดสูง

Thesis Title	Photo-Physical Properties, and Quenching of the Excited State of Chlorophyll A
Author	Miss Daweena Masen
Major Program	Chemical Studies
Academic Year	2009

ABSTRACT

The photo-physical properties of chlorophyll a were studied by spectrofluorimetric method and lifetime modulation technique with digital storage oscilloscope. Chlorophyll a is known as the prevailing light absorbing pigment. The network of multi double bonds in its structure shows very strong absorption in visible region. At present it has been widely used as sensitizer in DSSC. Electron Transfer performance of chlorophyll a by $Fe(acac)_3$ can be investigated from oxidative quenching reactions. Herein the simplified Rehm-Weller relationship was used to calculate the free energy change of a photoinduced electron transfer reaction. The studied $Fe(acac)_3$ concentration range was 1.0×10^{-5} M to 2.0×10^{-4} M. Emission intensity decreases when increasing the concentration of $Fe(acac)_3$ quencher. The curvature profiles of Stern-Volmer plots are significantly from inner filter effect more than the ground state complex formation. Rate of quenching reactions (k_q) can be determined from the Stern-Volmer plots with corrected inner filter effect. It reveals that an efficient photoinduced-electron transfer (PET) between the chlorophyll a and $Fe(acac)_3$ precisely occurred. The k_q and K_{app} values are dependent to the viscosity of solvents. The electron transfer occurs faster in more viscous solvents.

CONTENTS

CONTENTS (CONTINUED)

CONTENT (CONTINUED)

LIST OF TABLES

LIST OF TABLES (CONTINUED)

LIST OF FIGURES

LIST OF FIGURES (CONTINUED)

LIST OF FIGURES (CONTINUED)

LIST OF FIGURES (CONTINUED)

CHAPTER 1

INTRODUCTION

1.1 Chlorophyll a

Chlorophyll is a green pigment in chloroplast of plant's cell. It is mostly found in green leaves of plants. Chlorophyll can be divided into 4 types which are chlorophyll type a, chlorophyll type b, chlorophyll type c and chlorophyll type d. These types of chlorophyll can be found in the different kind of plants. Chlorophyll a can be most abundant in blue-green algae, cyanobacteria and general plants. Each type of chlorophyll is different only on the side chain as shown in figure 1 (http://www.chm.bris.ac.uk/motm/chlorophyll/chlorophyll_h.jpg).Chlorophyll a exists of 4 tetrapyrrole rings. Four nitrogen atoms interact with central atom of magnesium ion. Magnesium atom plays a coordinating role. Chlorophyll a has the methyl group ($-CH_3$) on the pyrrole ring while chlorophyll b has aldehyde (-CHO) instead (Kobayashi *et al*., 2007).

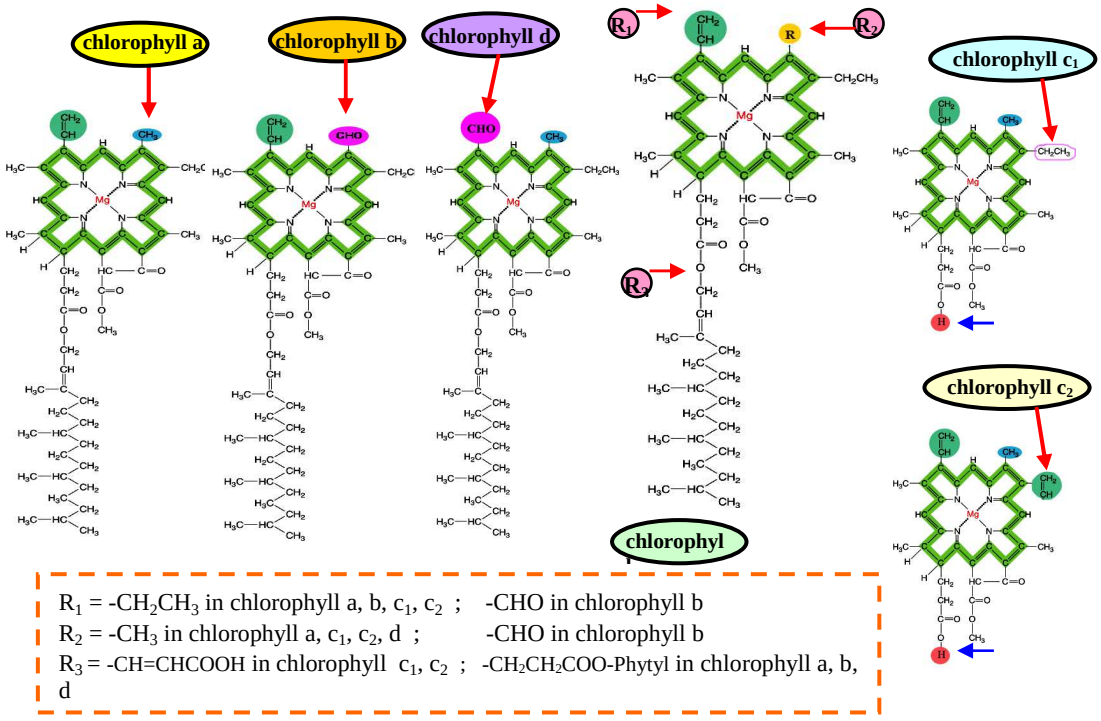

Figure 1 Structure of chlorophyll type (a, b, c and d)
Source: http://www.chm.bris.ac.uk/motm/chlorophyll/chlorophyll_h.jpg

Chlorophyll a, very well dissolve in the solvent at pole available, while Chlorophyll a is an effective photoreceptor in photosystem I. The pyrrole moiety absorbs light and transfer electron and energy to phytol side chain. The orbitals can delocalize electrons stabilizing the structure. The delocalized polyenes have enormous strong absorption in visible region, allowing the absorption of energy from sunlight. Chlorophyll a absorbs light in visible region at longer wavelength comparing with other types. It gives an intensive fluorescence in longer wavelength close to near IR region. Because of its structure and photo-physical properties, chlorophyll a is widely used to be a donor molecule in photochemistry frameworks. One of an interesting application of chlorophyll a and its derivatives is being a sensitized molecule in dye sensitized solar cell. It can harvest enormous light in the visible region and giving luminescence intensively. The electron transfer can occur from chlorophyll a to metal oxide like TiO_2 (Liu *et al*., 2008; Wang *et al*., 2006; Durrant *et al*., 2004; Amao *et al*., 2004). Furthermore, chlorophyll a can be used in artificial photosynthetic model (Ngweniform *et al.,* 2007; Jennings *et al.,* 1989). Chlorophyll a and its derivatives are not just only frequently used in electron transfer but also being a donor molecule in energy transfer process in plants (Xiaoqing *et al.,* 2007). A lot of researches try to replace the metal center of Mg to be other transition metal ions in order to explore photo-physical properties of its derivatives (Medforth *et al.,* 1997; Li and Inoue, 1991; Nonomura *et al.,* 1994; Yamashita and Inoue, 1991).

In this research, the chlorophyll a is a donor molecule to transfer electrons to an appropriate acceptor. In our preliminary work, we expected to use a free metal ion like Fe^{3+}. We tried to see how good of electron can be transferred via quenching reaction. However, we encountered a lot of problems of a limit of chlorophyll a solubility, ionic strength control and a forming of $Fe(acac)_3$-Chlorophyll a (Fe-Chl a) complex at ground state. These problems cannot be avoided. The idea of carrying out electron transfer had to be changed. In order to avoid such problems, the acceptor molecule must be changed. The tris(acetylacetonato)Iron (III), $Fe(acac)_3$ (Figure 2) is selected as a new acceptor complex owing to its neutral charge. The ligand acetylacetonate ($acac^-$) shows -1 charge though the $Fe(acac)_3$ complex is neutral. Therefore, the ionic strength can be neglected. Besides, the bond of the complex is strong. The replacing of Fe^{3+} in the porphyrin of chlorophyll a yielding Fe-Chl a

complex is least possible to occur. Finally, the solubility of both species can be solved. Chlorophyll a cannot dissolve in water but completely well soluble in organic solvent while $Fe(acac)_3$ can dissolve for all type of solvents. Even if the free Fe^{3+} was used as an acceptor, Fe^{3+} could dissolve absolutely in water but it could not do so in organic solvent. According to a criteria of selecting a quencher, the reduction potential of Fe(III/II) in $Fe(acac)_3$ is available to accept an electron from chlorophyll a. The $Fe(acac)_3$ is our best acceptor or so called quencher in the system.

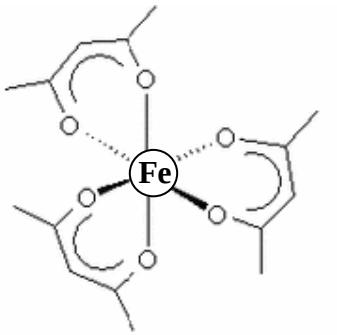

Figure 2 Structure of tris(acetylacetonato)Iron(III), $Fe(acac)_3$

The complex of $Fe(acac)_3$ has been extensively use as the essential catalyst in many reactions. An important one is photodegradation of diquat and paraquat herbicides by titanium dioxide (TiO_2) (Flor^encio *et al.*, 2004). The Fe(III) exists of $[Ar]3d^5$ electron figuration. The $Fe(acac)_3$ is high spin complex (Diaz-Acosta *et al.*, 2007). After it accepts an electron, the electron configuration has been changed to be $[Ar]3d^5$ which is still stable.

In the present work, the electron transfer of chlorophyll a fluorescence to $Fe(acac)_3$ in various types of solvents were investigated by steady-state measurement. Quenching reactions were measured. The photo-physical properties of both fluorophore and quencher were explored. The rates of reactions were determined in term of quenching rate constant (k_q). High k_q value is primary supposing to be good electron transfer.

1.2 Theory of electron transfer

Electron transfer reaction is the basic reaction in chemistry to transfer an electron from a reactant A to another reactant B. Electron transfer consists of electron movement between two orbitals. An electron may flow from an occupied orbital of the donor to a fully unoccupied or half-unoccupied orbital of the acceptor. Electron transfer also requires a close approach for effective orbital overlap as like as the case of energy transfer by electron exchange. Electron transfer quenching were originated from the ideas of Taube, Libby, Marcus and Hush. These concepts were expanded to the electron transfer quenching of photoexcited metal complexes by Sutin and Balzani who demonstrates the various scope and applicability of these reactions to solar energy conversion and the photoinduced decomposition of water. However, the most well known and succesful theory of electron transfer is Marcus theory addressed by R. A. Marcus in the mid of 1950s (Marcus., 1997). Marcus theory aims to find the rate constant of electron transfer by using the classical transition state theory. The theory concerns to the relation between the driving force of the reaction and its rate constant. In this work, the electron transfer reaction occurs in the system of chlorophyll a to tris(acetylacetonato)Iron(III), $Fe(acac)_3$. The electron transfer reaction was investigated via quenching reaction. The effort was concerned with the bimolecular quenching of the excited states of transition metal complexes by energy and electron transfer. The excited state donor molecule (D) which exists long enough can be quenched in bimolecular deactivation pathways. The singlet state (fluorescence) can be quenched by energy or electron transfer to another molecule (quencher, Q) in solution according to the following expressions

$D + h\nu$	$\longrightarrow$	$^*D$	absorption
$^*D + Q$	$\longrightarrow$	$D + {}^*Q$	quenching by energy transfer
$^*D + Q$	$\longrightarrow$	$D^+ + Q^-$	quenching by electron transfer (oxidative quenching)
$^*D + Q$	$\longrightarrow$	$D^- + Q^+$	quenching by electron transfer (reductive quenching)

Marcus theory is used for outer-sphere electron transfer reactions between a donor D and acceptor A. In the simple electron transfer reactions no chemical bonds are broken or formed. Either D or A may be in an excited state (D* or A*). This process is called photoinduced electron transfer (PET) which will be described in the next chapter. The principles of electron transfer theory apply equally well to photoinduced and to ground state electron-transfer reactions. The electron transfer steps can be shown in the equation 1.

$$D + A \underset{k_{-d}}{\overset{k_d}{\rightleftharpoons}} [D\cdots A] \underset{k_{-et}}{\overset{k_{et}}{\rightleftharpoons}} [D^{+}\cdots A^{-}] \xrightarrow{k_{diss}} D^{+} + A^{-} \qquad (1)$$

The reactants D and A diffuse together forming outer-sphere precursor complex (encounter complex) [D···A] with the rate of diffusion (diffusion controlled limit), k_d while the k_{-d} is the reversed rate of diffusion. The precursor complex undergoes the reorganization toward a transition state in which electron transfer takes place to form a successor complex $[D^{+}\cdots A^{-}]$ with the rate of electron transfer (k_{et}). Following the Franck-Condon principle, the nuclear configuration of the precursor complexes at the transition state is unchanged. Eventually, the successor complex dissociation, k_{diss}, to form the product of electron transfer D^{+} and A^{-}.

A steady-state treatment of precursor and successor complex yields the following expressions:

$$\frac{1}{k_{obs}} = \frac{1}{k_d} + \frac{1}{K_A k_{et}}\left[1 + \frac{k_{-et}}{k_{diss}}\right] \qquad (2)$$

where k_{obs} refers to quenching rate constant (k_q) which obtained from Stern-Volmer plot. $K_A = k_d/k_{-d}$. If $k_{diss} >> k_{-et}$, (Equation 2) reduces to

$$\frac{1}{k_{obs}} = \frac{1}{k_d} + \frac{1}{K_A\, k_{et}} \qquad (3)$$

photoinduced electron transfer is a process of electron transfer of a certain photoexcited molecules (molecules which are excited by photon) which can either act as the electron donor or acceptor regarding to another species in studied system. The photoexcited molecules can also be called “photosensitizers or sensitizers” which oftenly show better oxidizing or reducing species than its ground state. the driving force of the system must be the fundamental thermodynamic condition for spontaneous electron transfer between neutral reactants, $\Delta G^0 < 0$. Value of ΔG^0 for a photoinduced electron transfer can be estimated by Rehm-Weller equation (Clark and Hoffman,1995) which is shown in below

$$\Delta G^0 = E^0(D/D^+) - E^0(A/A^-) - E_{00}(D^*) + w_p - w_r \quad (4)$$

where $E^0(D^+/D)$ and $E^0(A/A^-)$ are the standard reduction potentials of the ground state donor and acceptor couples, respectively. The term w_p and w_r are the coulombic work terms of the products and reactants, respectively. It is corrected for the work involved in bringing ionic species together. The coulombic work terms are usually small, and zero for neutral species.

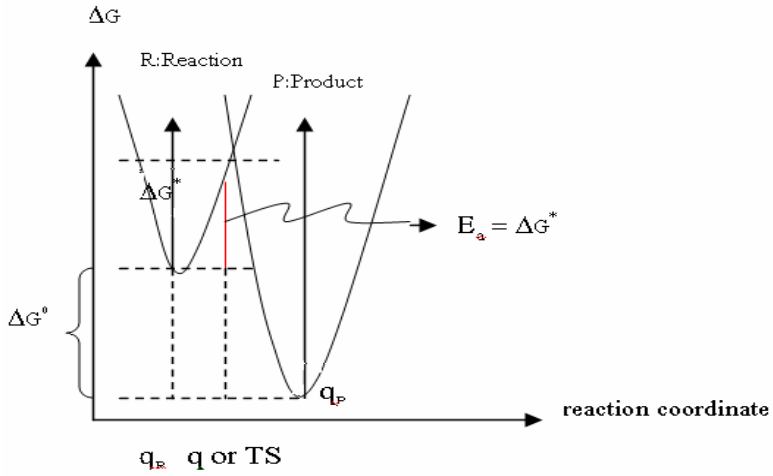

Figure 3 Gibbs free energy from electron transfer of cross reaction.

In quenching reaction, the observed rate constant (k_{obs}) can be calculated from quenching rate constant (k_q). This rate is taken from the linearity part of Stern-Volmer equation (Figure 4).

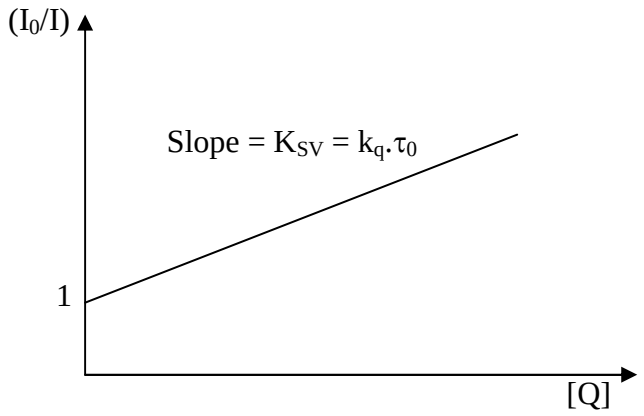

Figure 4 Stern–Volmer plot

The quenching rate constant can be measured from steady state measurement by spectrofluorimetric method. Fluorescence intensity from sensitizer molecule decreases when higher concentrations of quencher are added. We do control the concentration of sensitizer constant. The Stern-Volmer plot is the graph plotted between (I_0/I) versus concentration of quencher molecule $Fe(acac)_3$. I_0 and I are the fluorescence intensities in absence and presence of quencher, respectively.

$$\frac{I_0}{I} = 1 + k_q\tau_0[Q] = 1 + K_{SV}[Q] \quad (5)$$

1.3 Luminescence quenching of excited states

Quenching means to any processes which decreases the luminescence intensity of a sample. The interactions which result in quenching can be

- Excited state reactions
- Molecular rearrangements
- Energy transfer
- Ground state complex formation

- Collisional quenching(or dynamic quenching) between fluorophore and quencher
- Static quenching
- Combined Dynamic and Static quenching (or Pseudostatic-quenching)
- Trivial type : optical properties of the sample

In this stage, the collisional quenching, static quenching, Pseudostatic-quenching and the optical properties will be emphasized. The primary process in quenching can be shown below. The subject is the second order of quenching rate constant, k_q, for the bimolecular reaction between an electronically excited species, *D, and a quencher, Q. The reaction is irreversible occurring in a single step.

$$*D + Q \xrightarrow{k_q} \text{products} \qquad (6)$$

In the microscopic details of quenching, the diffusion of *D and Q together to form *D-Q is considered. The *D-Q is an outer-sphere encounter complex which is held within the solvent cage for a short period of time before deactivates to yield products with a rate constant k_r (Equation 22, below). This process must compete with the breaking up of the solvent cage and the release of *D and Q into the bulk solvent.

$$*D + Q \underset{k_{-d}}{\overset{k_d}{\rightleftharpoons}} \{*D\text{-}Q\} \xrightarrow{k_r} \text{products} \qquad (7)$$

1.3.1 Dynamic or collisional quenching mechanism

Collisional quenching of fluorescence is described by the Stern-Volmer equation as described above:

The Stern-Volmer quenching constant is given by $K_{SV} = k_q\tau_0$. If the quenching is known to be dynamic, the Stern-Volmer constant will be represented by K_{SV}. Quenching data are usually presented as plots of I_0/I versus [Q]. This is because I_0/I is expected to be linearly dependent upon the concentration of quencher. A plot of I_0/I versus [Q] yields an intercept of one on the y-axis and a slope equal to K_{SV} (Figure 5). A linear Stern-Volmer plot is generally indicative of all equally accessible to quencher. It is important to recognize that observation of a linear Stern-Volmer plot does not prove that collisional quenching of fluorescence has occurred. We will see that static quenching also results in linear Stern-Volmer plots. Static and dynamic quenching can be distinguished by their differing dependence on temperature and viscosity, or preferably by lifetime measurements. Higher temperatures result in faster diffusion and hence larger amounts of collisional quenching (Figure 5). Higher temperature will typically result in the dissociation of weakly bound complexes, and hence smaller amounts of static quenching.

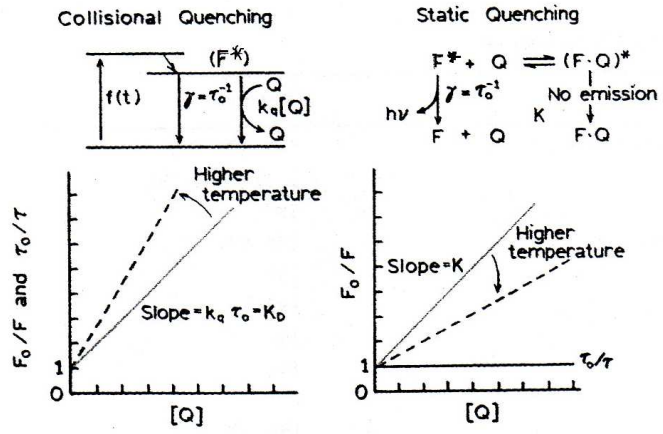

Figure 5 Comparison of dynamic and static quenching. I_0/I is the same abbreviation as F_0/F.

1.3.2 Static quenching mechanism

This type of quenching occurs from the formation (or ion - pairs) of a non-

fluorescence complex between fluorophore and quencher in ground state. The extent of adduct formation is governed by the concentrations of D and Q, and the equilibrium constant of the process in equation 8.

$$D + Q \overset{K_{app}}{\rightleftharpoons} [D\text{-}Q] \tag{8}$$

When this complex absorbs light, it immediately returns to the ground state without emission of a photon. The dependence of the fluorescence intensity upon quencher concentration for static quenching is derived by considering the association constant for complex formation which is given in equation 9.

$$K_{app} = \frac{[D\text{-}Q]}{[D][Q]} \tag{9}$$

Where [D-Q] is concentration of the complex, [D] is the concentration of the original fluorophore, and [Q] is the concentration of original quencher. K_{app} obtained from the Debye-Smoluchowski and Eigen equations (Hoffman, *et al*., 1989). If the ground state complex does not give the fluorescence, then the fraction of the fluorescence that remains, I_0/I, is given by the fraction of total fluorophores that are not complexes. The concentration of fluorophore, $[D_0]$ can be simply calculated from

$$[D_0] = [D] + [D\text{-}Q] \tag{10}$$

then

$$K_{app} = \frac{[D] + [D\text{-}Q]}{[D][Q]} = \frac{[D_0]}{[D][Q]} - \frac{1}{[Q]} \tag{11}$$

The Stern-Volmer equation for static quenching can be written as following:

$$\frac{I_0}{I} = 1 + K_S[Q] \quad (12)$$

The dependence of I_0/I on [Q] is linear which is identical to that observed for dynamic quenching, except that the quenching constant is now the association constant. Unless additional information is provided, fluorescence quenching data obtained by intensity measurements alone can be explained by either dynamic or static processes. As will be shown below, the magnitude of K_S can sometimes be used to demonstrate that dynamic quenching cannot account for the decrease in intensity. The measurement of fluorescence lifetimes is the most definitive method to distinguish static and dynamic quenching. Static quenching removes a fraction of the fluorophores from observation. The complexed fluorophores are nonfluorescent, and the only observed fluorescence is from the uncomplexed fluorophores. The uncomplexed fraction is unperturbed, and hence the lifetime is τ_0. Therefore, the static quenching $\tau_0 / \tau = 1$ in contrast with dynamic quenching, $\tau_0 / \tau = I_0 / I$. One additional method to distinguish static and dynamic quenching and dynamic quenching is by careful examination of the absorption spectra of the fluorophore. Collisional quenching only affects the excited states of the fluorophores, and thus no changes in the absorption spectra are expected. In contrast, ground state complex formation will frequently result in perturbation of the absorption spectrum of the fluorophore. In fact, a more complete from of equation 9 would include the possibility of different extinction coefficients for the free and complexed forms of the fluorophore (Figure 5).

1.3.3 Combined dynamic and static quenching mechanism

In many instances the fluorophore can be quenched both by collisions and by complex formation with the same quencher. The characteristic feature of the Stern-Volmer plots in such circumstances is an upward curvature, concave towards the y-axis (Figure 6). Then the fractional fluorescence remaining (I_0/I) is given by the product of the fraction not complexed (*f*) and the fraction not quenched by collisional encounters. Hence

$$\frac{I}{I_0} = f \frac{\gamma}{\gamma + k_q[Q]} \quad (13)$$

In the previous section we found that $f^{-1} = 1 + K_S[Q]$. Inversion of equation 14 and rearrangement of the last term on the right yields.

$$\frac{I_0}{I} = (1 + K_D[Q])(1 + K_S[Q]) \quad (14)$$

This modified from of the Stern-Volmer equation is second order in [Q], which accounts for the upward curvature observed when both static and dynamic quenching occur for the same fluorophore.

The dynamic portion of the observed quenching can be determined by lifetime measurements. That is $\tau_0/\tau = 1 + K_{SV}[Q]$, the dashed line in figure 6. If lifetime measurements are not available, then equation 15 can be modified to allow a graphical separation of K_S and K_{SV}. Multiplication of the terms in parentheses yields.

$$\frac{I_0}{I} = 1 + (K_{SV} + K_S)[Q] + K_{SV}K_S[Q]^2 \quad (15)$$

$$\frac{I_0}{I} = 1 + K_{app}[Q] \quad (16)$$

where

$$K_{app} = \left(\frac{I_0}{I} - 1\right)\frac{1}{[Q]} = (K_{SV} + K_S)[Q] + K_{SV}K_S[Q] \quad (17)$$

The apparent quenching constant is calculated at each quencher concentration. A plot of K_{app} versus [Q] yields a straight line with an intercept of $K_{SV} + K_S$ and a slope of K_SK_{SV} (Figure 6). The individual values can be obtained from the two solutions of the quadratic equation. The dynamic component can generally be selected to be the

solution comparable in magnitude to the expected diffusion-controlled values, or from other available information about the sample.

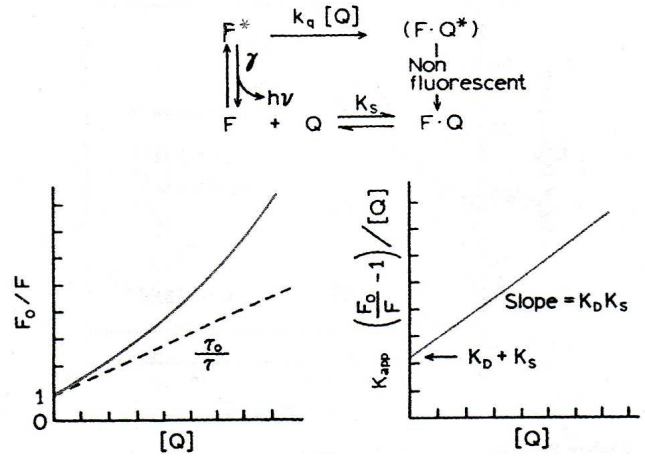

Figure 6 Dynamic and static quenching of the same population of fluorophores I_0/I is the same abbreviation as F_0/F.

1.4 Diffusion rate constant (k_d)

The rate of a diffusion-controlled reaction is calculated by considering the rate at which the reactants diffuse together. As shown in the equation below, the rate constant for a reaction in which the two reactant molecules react if they come within a distance R^* of one another is

$$k_d = 4\pi R^* DN \qquad (18)$$

here D is the sum of the diffusion coefficients of the two reactant species in the solution ($D = D_A + D_B$). Equation 18 can be taken further by incorporating the Strokes-Einstein equation ($D = kT / 6\pi\eta a$; a is radius of a studied reactant, η is the solution viscosity). The diffusion coefficients of reactant A and B can be written in equation 19.

$$D_A = \frac{kT}{6\pi\eta R_A} \qquad D_B = \frac{kT}{6\pi\eta R_B} \qquad (19)$$

R_A and R_B are hydrodynamic radius of A and B molecules in a medium of viscosity η. If sizes of two reactants are difference, the diffusion rate constant is

$$k_d = \frac{4RT}{6\eta}\left(R_A + R_B\right)\left(\frac{1}{R_A} + \frac{1}{R_B}\right) \quad (20)$$

When η was dynamic viscosity of solvent to use at experiment temperature in unit of kg–forces/m^2. But R_A and R_B are hydrodynamic radius of A and B molecules in a medium of viscosity η and R was rate constant equal to 8.314 $J.mol^{-1}K^{-1}$ and T was temperature for test in the Kelvin unit (K).

If we write $R_A = R_B = ½ R^*$ and the charges of reactants are neutral, it will leads to equation 20.

$$k_d = \frac{8RT}{3\eta} \quad (21)$$

1.5 Review of literatures

Amao *et al*., (2004) studied a dye sensitized solar cell using the visible light sensitization of chlorophyll a derivative, chlorine-e_6 (Chl-e_6) immobilized on TiO_2 film was developed. This work investigated spectroscopic measurements of Chl-e_6 in methanol. The maximum of the luminescence located at 675 nm. In contrast, the fluorescence intensity of Chl-e_6 immobilized on TiO_2 film was decreased. It indicated that the emission of Chl-e_6 was effectively quenched by TiO_2. The quenching of emission of Chl-e_6 was due to electron injection from excited singlet state of Chl-e_6 into the conduction band of TiO_2.

Borissevitch., (2009) studied the steady-state fluorescence quenching of 2, 6-bis(diethanolamino)-4, 8-dipiperidino-pyrimido[5, 4-d]pyrimidine(di pyridamole) by a stable nitroxyl radical 2, 2, 6, 6-etramethyl-piperidine-N-oxyl (TEMPO). It was used to clear up the influence of the quencher light absorption on the values of the

Stern-Volmer quenching constants (K_{SV}). The K_{SV} correction can be done by concerning the quencher absorbance (A_q) already at very low A_q and gives rather high K_{SV}. Thus, for $A_q < 0.02$ and K_{SV} was 50 M^{-1}. The uncorrected K_{SV} value appears about 50% higher than the real (corrected) one. Moreover, the uncorrected K_{SV} values do depend on the excitation and emission wavelengths, while the corrected ones are independent of them.

David *et al*., (2007) reported the electron transfer to a nearby acceptor molecule (A). A clear green chlorophyll (Chl) solution can be made by grinding spinach (either from fresh or frozen samples) in a mortar and pestle, adding the broken leaves to a beaker of acetone, and then filtering the solution through cheesecloth or coarse filter paper to remove the solid plant materials. Chlorophyll a and chlorophyll b molecules present in plants. When UV light irradiated, these molecules emit fluorescence at 650 nm giving a bright red solution. As with quinine sulfate, the mean fluorescence lifetime for both compounds is very short - about 5 ns. When present in plant cells, instead of fluorescing, an electronically excited chlorophyll molecule (Chl*) transfer an electron to a nearby acceptor molecule (A) as follows:

$$\begin{aligned} Chl^{*} + A &\longrightarrow Chl^{+} + A \\ A^{-} &\longrightarrow A + e^{-} \end{aligned} \qquad (22)$$

Gazdaru *et al*., (2001) studied the parameters of the fluorescence quenching of chlorophyll a by 1,4-benzoquinone in ethanol using the nonlinear analysis. The fluorescence intensity was measured at 670 nm. The modified Stern-Volmer plots of the quenching data have revealed two ways of the quenching mechanism and have offered the possibility to obtain the quenching parameters.

Kathiravan *et al*., (2009) studied the quenching reaction process of chlorophyll a adsorbed on the surface of colloidal TiO_2. In the presence of colloidal TiO_2 the optical density at the wavelength of 480 nm was increased without changing in wavelength. The apparent association constant (K_{app}) was determined by absorption and fluorescence intensity measurements. An increasing of colloidal TiO_2

concentration influences to the fluorescence emission spectrum of chlorophyll. An addition of colloidal TiO_2 to the solution of chlorophyll a resulted in the gradual decrease in emission intensity of chlorophyll which indicates the quenching occurs. The apparent association constant (K_{app}) can be calculated by following:

$$K_{app}; \quad \frac{1}{I^0 - I} = \frac{1}{I^0 - I'} + \frac{1}{K_{app}(I^0 - I')[TiO_2]} \qquad (23)$$

where

K_{app} = the apparent association constant
I_0 = the initial fluorescence intensity of chlorophyll
I' = the fluorescence intensity of TiO_2 adsorbed chlorophyll a
I = the observed fluorescence intensity at its maximum

The dynamics of photo-induced electron transfer from chlorophyll to the conduction band of colloidal TiO_2 nanoparticle was observed. The mechanism of electron transfer was confirmed by the calculation of free energy change (ΔG_{et}) by applying Rehm-Weller equation as well as energy level diagram.

$$\Delta G_{et} = E^{ox}_{1/2} - E^{red}_{1/2} - E_s + C \qquad (24)$$

where

$E_{(ox)}^{1/2}$ = the oxidation potential of chlorophyll (0.57 V)
$E_{(red)}^{1/2}$ = the reduction potential of TiO_2 (i.e.) conduction band potential of TiO_2 −0.1V.
Es = the excited state energy of chlorophyll
C = the coulombic term. Since one of the species is neutral and the solvent used is polar in nature.

The G_{et} value was calculated as −1.17 eV and this higher negative ΔG_{et} value indicates electron transfer processes which is thermodynamically favorable.

Kuroiwa *et al*., (2009) studied the spectroscopic and electrochemical properties of chlorophyll (Chl a) aggregation in mixed solvents of acetonitrile and an ionic liquid, 1-ethyl-3-methylimidazoliumtetrafluoroborate($EMIBF_4$), were examined. Chl a was homogeneously suspended in AN, and $EMIBF_4$. It was added. After stirring , the solution suspending. Chl a was incubated for 3 hr in the dark. The Chl a concentration was 250 μM. To investigate the emission spectra, the excitation wavelength was used at 430 nm. The redox potentials of Chl a in the mixed solvents were measured by square wave voltammetry (SWV). The red-shifted absorption in the Soret and Q_y band regions were found. For square wave voltammetry, a high signal-to-noise ratio of SWV was useful especially for investigating redox couples with high molecular weights at such relatively low concentration.

Larsson *et al*., (2007) studied fluorescence excitation-emission matrix (EEM) spectroscopy. This technique is a useful tool for interpretation of fluorescence information from natural water samples. The major problem with this technique is the inner-filter effect (IFE). Larsson *et al.,* propose a mathematical correction procedure based on the intensity of Raman scatter from water. This procedure was found to reduce the error after correction by up to 50% in comparison with two absorbance correction procedures.

Moreira *et al*., (2009) studied the role of different metal centers (magnesium, zinc and copper) on the enhancement of the hydrophilic character of metallochlorophylls, was evaluated by fluorescence. The present results denote that magnesium and zinc chlorophyll have a higher potential to be employed as photosensitizers in PDT as function of their highest absorption and emission intensities.

Nanomura *et al*., (1997) studied photo-physical and electrochemistry properties. Many techinques measured oxidation and reduction potential of chlorophyll a in H_2-Chl a, Mg-Chl a, Cu-Chl a and Zn-Chl a. The oxidation and

reduction potentials of porphyrins, were measured by cyclic voltammetry. The absorptions of metal porphyrins are the behaviour of Q band because they reflect the HOMO and LUMO energy levels of the macrocyclic 7π system. The difference of E_{ox}^{I} - E_{red}^{I} between the first oxidation potential (E_{ox}^{I}) and the first reduction potential (E_{red}^{I}) depends on the absorption maximum of the Q_y band in divalent metallochlorophylls.

Sergio *et al*., (2008) studied the process of quenching reaction is decrease fluorescence. Find that is quenching reaction such as reaction of the excited state, the electron transfer of collisional quenching mechanism depend on pressure and temperature. Therefore explain the mechanism of electron transfer and energy transfer. In this research to study carotenoids derivative have been conjugate in system 5-11 bonds and 5-(4–amino-phenyl)-10, 15, 20–tris (4-methylphenyl) porphyrin (TPPA). The quenching reaction of fluorescence of porphyrin but carotenoids derivative have been conjugate in system 10 or 11 bonds. Find out its can be quenching fluorescence of porphyrin 10%. Efficient of quenching fluorescence moreover depend on the structure of conjugate and solvent effect.

Song *et al*., (2006) introduced a new method to measure the chlorophyll a content, using 660 nm laser diode as a new kind of light source to stimulate fluorescence as well as combining a fiber and spectrum technique. The characteristic of fluorescence spectrum was determined. Relative fluorescence intensity at F685/F735 was used to measure the content in water and green leaves.

Smestad., (1998) studied a major role of luminescence of excited molecule on many applications. One of them is the present application of chlorophyll and its derivatives on dye sensitized solar cell (DSSC) of TiO_2 semiconductor.

Zvezdanovic *et al*., (2009) investigated chlorophyll bleaching by UV irradiation. It has been studied by absorption and emission spectroscopy of techniques the mixture of photosynthetic pigments, in acetone and n-hexane solutions, and in aqueous thylakoid suspensions. Chlorophyll undergoes destruction (bleaching)

accompanied by fluorescent transient formation obeying first-order kinetics. The bleaching kinetics is followed at chlorophyll absorption maximum (A_{max}), in the range between 660 and 680 nm. It was found that UV-irradiation induces a gradual decrease of the Q-band intensity. An increase of absorbance was observed between 485 and 563 nm. The maximum intensity of chlorophylls fluorescence decreased during increasing irradiation time periods, t_{irr}.

1.6 Objectives

5.1 To study the solubility and photo–physical properties of chlorophyll a.

5.2 To identify the rate of quenching reaction (k_q).

5.3 To investigate the solvent effect of photo-physical properties of chlorophyll a.

CHAPTER 2

EXPERIMENT

The successful application of photo-induced electron transfer theory requires considerable attention to experimental details and good understanding of the instrumentations. For this work, quenching reactions were determined by both steady-state phosphorescence and time-resolved technique. The details of modulation technique using digital storage oscilloscopes, a method of time resolved technique to determine emission lifetime, will be described mainly. Additionally, the optical properties of the sample, the determination of the ionic charges by conductivity measurement, changing the viscosity in the studied system and the determination of the standard reduction potentials of the studied complexes by cyclic voltammetry, will be given in details.

2.1 Materials

Chemical reagents were purchased from following companies as collected in table 1. All substances were analytical reagent grades. Quenching reactions of chlorophyll a fluorescence by tris(acetylacetonato)Iron(III) were carried out in various solvents. Chlorophyll a was used as received. Solvents were dried by 4 and 5 angstroms of molecular sieves over two nights before using. For lifetime determination, colloidal silica was used as reference in order to be collected scattering light sine wave. Ferrocencemethanol was used as the internal reference in electrochemical study.

Table 1 Data of chemical reagents.

Chemical reagents	Company
Chlorophyll a (spinach)	Fluka
Tris(acetylacetonato)Iron(III)	Sigma Aldrich
Acetonitrile	LAB – SCAN
chemical reagents	company
Benzene	BDH
Dimethyl sulfoxide (DMSO)	BDH
Ethanol	MERCK
Methanol	LAB – SCAN
N, N – Dimethylformamide (DMF)	Fluka Riedel-deHäen
Tetrahydrofuran (THF)	Fisher Scientific / Fisher ChemAlert Guide
Toluene	MERCK
Ferrocenemethanol	Sigma – Aldrich
Tetrabutylammonium-hexafluorophosphate electrolyte	Fluka
Colloidal silica	MERCK

2.2 Instruments and apparatuses

2.2.1 Absorption spectroscopy

UV-Vis absorption spectra were recorded on a UV-Vis Spectrophotometer model Specord S100 with standard cuvette, path length 1 cm. Deuterium and tungsten were used as light sources covering wavelengths in UV and visible region respectively.

Figure 7 UV-Vis spectrophotometer model Specord S100

2.2.2 Steady state luminescence spectroscopy

Emission spectra were recorded with a Luminescence spectrometer LS55 manufactured by Perkin Elmer (Figure 8). The spectrometer uses a xenon arc lamp as light source covering wavelengths from 250 nm to 800 nm. A grating monochromator with variable bandwidths is used for the excitation and emission. PMT voltage was automatically selected by the instrument and is a function of the slit width of the excitation monochromator. Luminescence cuvette is a standard transparent cuvette with a screw cap. Path length of the cuvvette is 1 cm. Excitation and emission slit widths are 5 nm widely.

Figure 8 Luminescence spectrometer LS55

2.2.3 Time-resolved technique

There are two types of time resolved techniques which are commonly used for measuring fluorescence lifetimes, *pulse fluorometry* and *phase-modulation fluorometry*. The pulse fluorometry relates to measurements performed in the time domain, while the phase-modulation fluorometry relates to the frequency domain. The basic principle of pulses fluorometry is that exciting pulses of light from a lasers or spark sources are focused to the sample. The time dependence of the fluorescence decay is recorded. Phase-modulation fluorometry traditionally incorporates a modulated excitation source which causes the fluorescence emission waveform to be phase shifted and having different in amplitudes with respect to the excitation waveform. The latter technique will be given in detail because it was used in the lifetime measurements of the system studies.

The modulated light source and the measurement of the phase shift of the emitted fluorescence are used to measure the fluorescence nanosecond lifetime. A sinusoidal excitation wave is used to excite a sample. The emission which is modulated with same frequency as excitation is observed. Because of the time lag between excitation and the emission, the emission is delayed in time relative to the modulated excitation (Figure 9). The degree of modulation and/or phase shift (Φ) of the emitted light is compared with the excitation light waveform. The phase shift increases from 0^o-90^o with increasing modulation frequency. The finite time response of the sample also results in demodulation of the emission by a factor *m*, which decreases from 1.0 to 0.0 with increasing the modulation frequency.

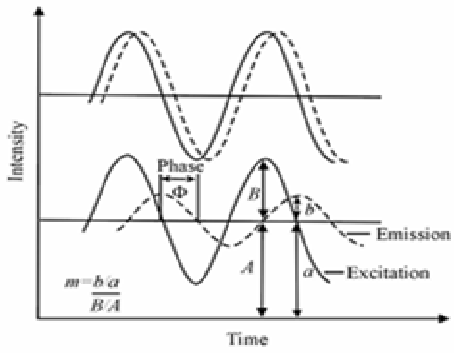

Figure 9 Phase and modulation of fluorescence in response to intensity-modulated excitation using single frequency.

There is a delay of time (Δt) between excitation and emission signal which relates to the phase shift (Φ). In addition, the amplitude signal is decreased ($b < B$) which is called demodulation (Lakowicz., 2006). For a fluorophore which decays monoexponentially with lifetime τ, the lifetime values can be analysed from the phase shift (τ_p) and from the demodulation (τ_m) which are given by

$$\tau_p = \frac{\tan \Phi}{\omega} \approx \frac{\Phi}{\omega} \quad (\Phi < 0.2) \tag{25}$$

$$\tau_m = \frac{1}{\omega}\sqrt{\frac{1}{m^2} - 1} \tag{26}$$

where θ is the measured phase shift, m is the measured modulation, ω is the angular frequency of light modulation = $2\pi f$, f is the modulation frequency. For the monoexponential decay the fluorescence lifetime $\tau = \tau_p = \tau_m$. The accuracy for this case is higher than that of TCSPC. However for the multiexponential decay, the data evaluation is very complex and less accurate compared to TCSPC. The lifetime τ_p and τ_m are obtained from fitting of equation 25 and equation 26 (Landgraf., 2001). Nevertheless, the interrelationship among the modulation frequencies, the phase angles and the modulation amplitudes have to be also considered. At higher modulation frequencies, the phase angles of the emission increase and the modulation decreases.

2.2.3.1 Modulation technique with digital storage oscilloscope

This technique was devised in 1995 and applied in many works (Landgraf., 1996; 2000; 2004). The principle of this technique is described in section 2.2.3. The experimental device is shown in figure 10. The advantages of this technique over other commercial instrument are that the lower cost. The excitation light source can easily to be replaced. Therefore, a large number of wavelengths are

possible for excitation of the sample. A working set-up has been used. The main devices are summarized in table 2.

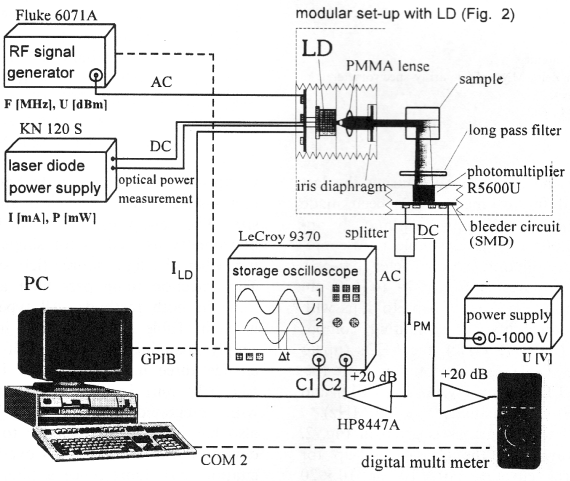

Figure 10 The scheme of the electronics used in our experimental set-up.

Table 2 The modulation apparatus used in our laboratory. The experiments was performed at 25 ^{o}C.

Instruments	**Modulation specification**
Oscilloscope	LeCroy 9450 WaferSurfer 16 Hz
Generator	LM. 04, max. 1.056 Hz
Amplifier	HP 8447A (20 dB, 400 MHz)
Detector	R5600U-04 (185-850 nm)
Modular set-up	bias tee, lens, filter holder, filters, sample holder (Figure 11)
LED	370 nm
PC control	LD_CALC program (version 2.04 from 08-
Filters	gray filter U 340 nm (Excitation filter) (Figure 11) and long pass filter RG 610 (Emission filter) (Figure 11)
Frequencies	5, 10, 15, 20, 25 and 30 MHz - Minimum frequency was calculated from

	$1/\tau_F$ / 36. Maximum frequency was calculated from $1/\tau_F$ / 7.2. ; τ_F is the fluorescence lifetimes
Phase angle	between 10^o to 50^o
Amplitude	- 45 to +13 dBm

*LeCroy (Geneva, CH), Fluke (new Gigatronics, San Ramon, USA), HP (Palo Alto, USA) Hamanitsu (Herrcling, D) modified DDS-generator based on AD9851 from Analog Device (Norwood, USA).

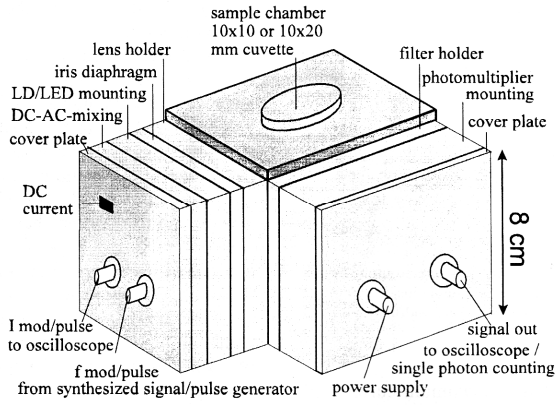

Figure 11 The modular set-up (Landgraf., 2001).

The single signal (frequency) synthesizer generates a sinusoidal radiation for the LED or LD. The modulated light beam excites the fluorophore sample. The modulation frequencies (*f*) have to be associated to the fluorescence lifetime in order to obtain measurable values for Φ and *m*. The lowest modulation frequency can be estimated from $1/(36\tau)$. The samples fluorescence is detected by a PM in a perpendicular position to the excitation light. The data generated from excitation and emission signals are stored in the oscilloscope and transferred to a PC global fit of all data points by LD_CALC program. The program is also used to handle the data from the DSO and to control the frequency generator by GBIP protocol as shown in Figure 16. In the same manner, a scattering sample (colloidal silica or Ludox, Aldrich, Austria) is applied which acts as reference.

2.2.3.2 Data analysis of the modulation technique with digital storage oscilloscope

As mentioned above the excitation light source, reference and fluorescence signals are recorded on the DSO, An example of the original data is shown in figure 12 (Landgraf., 2001). The data files compose with 4 sinusoidal waves which are:

- curve 1 : electronic signal of light source for exciting the reference
- curve 2 : amplified signal from the reference (colloidal silica)
- curve 3 : electronic signal of light source for exciting the sample
- curve 4 : amplified fluorescence signal from the sample

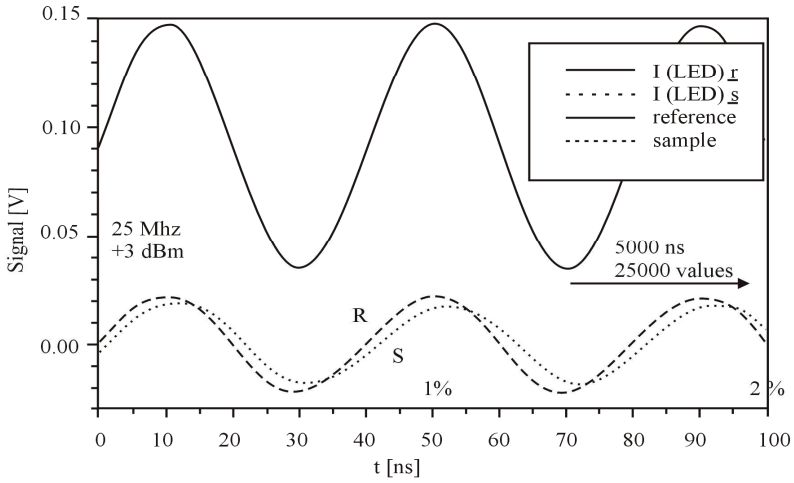

Figure 12 An example of the original data recorded on a digital storage oscilloscope (DSO).

Curve R and S refer to the reference signal and sample signal, respectively which are different in phase and modulation amplitude. I(LED) r and I(LED)s are the recorded data from the measurements through the LED during the measurement of reference and sample, respectively. They are both identical and are used for triggering the oscilloscope.

"Sample analysis is done by finding the zero crossing points in those four curves. The time values t_1- t_4 are optimized by a linear regression of the data points within a phase angle $\Phi = \pm 0.1$, where the approximation $\sin\Phi \approx \Phi$ is valid. This procedure is able to calculate values with a resolution better than the one from the oscilloscope but even in frequency scans of 10 different modulation frequencies results are rather poor. Therefore, a new method has been developed. A mathematical fit using simplex algorithm optimizes the following function to the complete data set including all experimental values." (Landgraf., 2001).

For fluorescence lifetime measurements, It is necessary to measure at different modulation frequencies in order to determine whether the decay is single exponential or not. The measured lifetimes are expected to be independent of varied frequencies, with reproducibility. To calculate the fluorescence lifetime from the frequency response of the devices applied it is necessary to consider the phase angle. The most precise results are in between 10^o – 40^o. Below 10^o the error occurs from the limited number of points on the DSO while above 40^o the signal is decreasing significantly by demodulation. Results are available independently from the controlling (modulation frequency set manually or by the LD_CALC program).

2.2.3.3 Fluorescence lifetime experiments via modulation technique with digital storage oscilloscope

Apart from the phase angle consideration as mentioned above, an important aspect to perform lifetime measurements is to select the appropriate LED wavelength and filters. Data from absorption and emission spectra of the studied quenching reaction must be considered. The LED should be selected at a wavelength which provides a high optical density. The filter is selected from the type which transmits most fluorescence of an emission band and reflects other wavelengths especially. Long pass filters (LPFs) is used to pass or transmit a range of a wavelengths and to block or reflect other wavelengths on one side of the passed band. In the case of long pass filters, the transmitted wavelength is long wavelength radiation, while short wavelength radiation is reflected. The filter is specified by their center (50% transmission) wavelength.

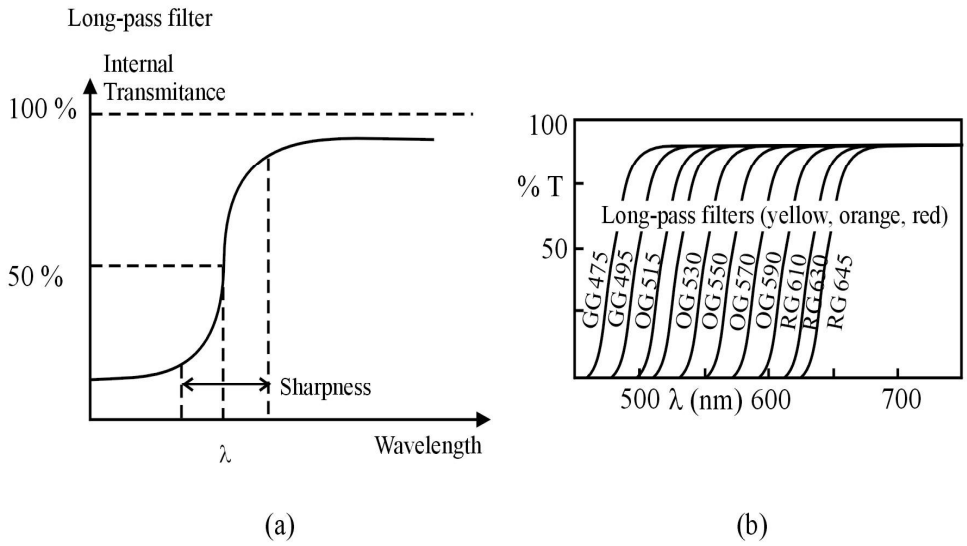

Figure 13 (a) Long pass filter characteristic and (b) Transmission spectra of long pass filters (product information from SCHOTT company)

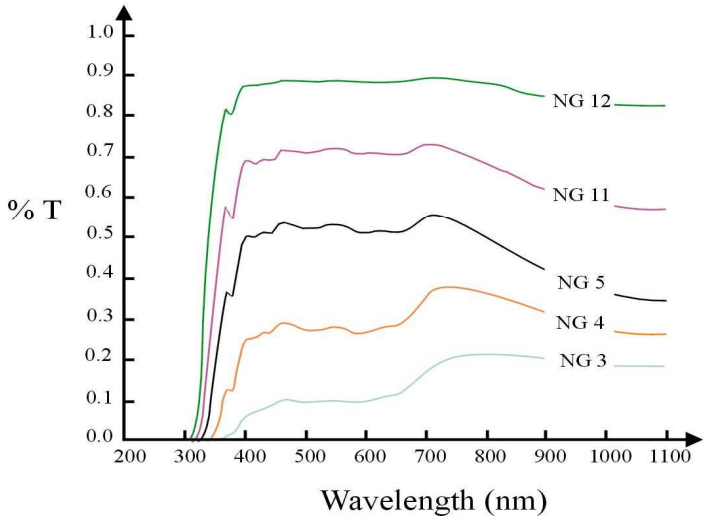

Figure 14 Transmission spectra of NG (gray) filters (product information from SCHOTT company)

Figure 15 Modulation technique with digital storage oscilloscope

2.2.4 Cyclic voltammetry technique

As already mentioned in the theoretical chapter, the driving force of the photoinduced electron transfer system is the most important thermodynamic property. The driving force can be determined by Rehm-Weller equation as already shown in equation 1. It is necessary to know the standard reduction potentials of the ground state donor, $E^0(D^+/D)$, and acceptor, $E^0(A/A^-)$ of each solvent studied using CV experiments. The electrochemical cell was used with temperature controlled by a thermostat at 25°C.

The cyclic voltammetry is an electrochemical method which allows to measure redox potentials. It can be used to investigate the rates and mechanisms of charge transfer reactions, kinetic studies, and so on. Typically, a voltammetric experiment utilizes three types of electrodes which are the working electrode, the reference electrode, and the counter or auxiliary electrode.

- ***Working electrode.*** It is normally made from inert conducting materials like glassy carbon, platinum or gold. The studied redox reactions take place at the surface of the electrode. Therefore it requires frequent cleaning by polishing with the proper size of diamond pastes. In order to remove absorbed species and

obtain the reproducible results. In this work, glassy carbon and gold electrodes are used. Diameters of the disk electrodes are 2 mm.

- ***Reference electrode*** provides a fixed reference potential versus the potential of the working electrode. The reference electrode uses a stable and reversible half-cell process. The half-cell is separated by a glass frit or membrane in order to avoid mixing of both components, but still allow charge transport.

- ***Counter electrode*** or auxillary electrode consists of a large surface area of the inert material such as platinum. Since the current flows through the counter electrode, it must have a sufficiently large surface area comparing relative to the working electrode in order to prevent limitation of current flowing in the total circuit. The current measured in a voltammetric experiment flows between the working and counter electrode.

- ***Supporting electrolyte*** plays important roles to decrease the resistivity of the solvent, suppress migration of charged electroactive analytes and reduce distortion of the voltammetry. The supporting electrolyte must be ionic and inert for electrochemical work. In this work tetrabutylammoniumhexafluorophosphate was used as supporting electrolyte which can be soluble in many kinds of organic solvents.

To understand the cyclic voltammetry principle, it is worth to brief shortly about linear sweep voltammetry. “Voltammetry” is an electrochemical method which records the relation between current and the applied potential. The potential is changed with time. Linear sweep voltammetry corresponds to the linear change (sweep) from the starting potential, $E_{1,}$ to the ending potential, E_2, with respect to time. The scan rate is the derivative of changing of potential with time, d*E*/dt. The scan proceeding to more positive potentials ($E_2 > E_1$) is called *anodic scan*. The scan proceeding to more negative potentials ($E_2 < E_1$) is called *cathodic scan*. The voltage applied to the working electrode is positively *forward scan* from E_1 to E_s (known as switching potential and preselected) (Figure 16a) where the direction of the scan is reversed (*reverse scan*) and swept to E_2.

Cyclic voltammetry shows a current-voltage curve (Figure 16b) (or voltam mogram). The current respond is plotted as a function of applied potential. (Figure 16c) shows that the potential is scanned in the positive direction until it reaches the switching potential. The electrode is now positive and sufficiently to oxidize the

species at the electrode surface. The anodic current (I_{pa}) of the oxidation potential (E_{pa}) is observed. The scan direction is switched to negative potential for the reverse scan. The electrode becomes more negative and sufficiently to reduce the oxidant at the reduction potential (E_{pc}). The cathodic current (I_{pc}) is monitored.

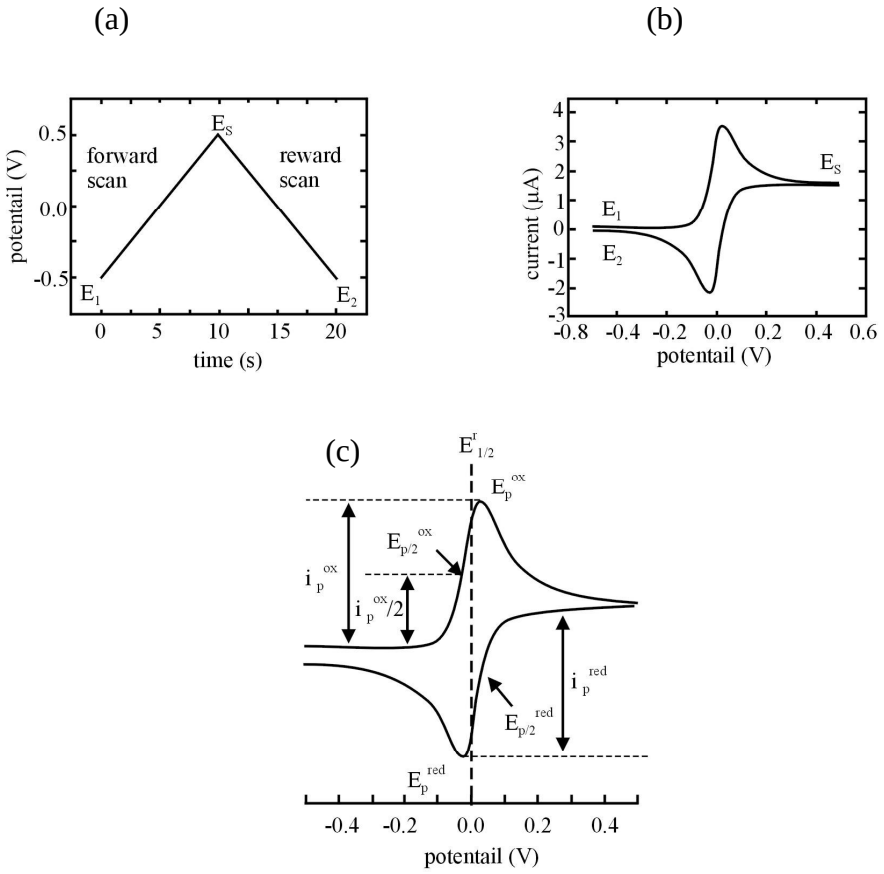

Figure 16 (a) one cycle of triangular potential waveform . E_1, E_s and E_2 are starting potential, switching potential and end potential (b) cyclic voltammogram relative to the triangular potential waveform, and (c) cyclic voltammogram of reversible couple.

A redox couple in which both species rapidly exchange electrons with the working electrode is called an electrochemically reversible couple. The reduction potential (E^o) for a reversible couple is centered between E_{pa} and E_{pc}.

$$E^o = \frac{E_{pa} + E_{pc}}{2} \qquad (27)$$

The number of electrons transferred in the electrode reaction (*n*) for a reversible couple can be determined from the separation between the peak potentials (ΔE_p) which is 0.059 V. The value of I_{pa} and I_{pc} should be identical for a simple reversible couple. Then I_{pa}/I_{pc} is unity.

Cyclic voltammetry measurement was measured by MacLab (4e AD Instruments with potentiostat/Serial No. p068). Software of the MacLab is ECHEM program version 1.5. Three types of electrodes are

- working electrode : glassy carbon
- reference electrode : platinum wire
- counter electrode : platinum wire (flag).

Ferrocenemethanol (Fc-MeOH) was used as an internal standard. The measured potential was comparable versus saturated calomel electrode (SCE) in DMF -0.382 V.

2.3 Sample preparations

2.3.1 Sample preparation for testing photo-physical properties and quenching reaction.

The fresh stock solutions of all chemicals were prepared in various organic solvents. Chlorophyll a stock solution was prepared in the concentration of 5.00×10^{-5} M. Chlorophyll a is a dark light solid with a very tiny amount in a commercial bottle. In order to weigh the chlorophyll a cannot be done directly. The molar extinction coefficient of chlorophyll a at the maximum wavelength (λ_{440}) was taken into account in Lambert-Beer law; $A = \varepsilon c l$ when A is absorbance, *l* is path length (cm), c is concentration (mol L^{-1}) and ε is molar absorptivity (L mol^{-1} cm^{-1}). Stock solution of tris(acetylacetonato)Iron(III), $Fe(acac)_3$ was the quencher in our experiment. $Fe(acac)_3$ was prepared at 1 mM by weighting $Fe(acac)_3$ 0.0048 g (molecular weight = 479.02 $g.mol^{-1}$) and diluted to be 10 mL in each solvent. Both compounds were measured absorption and emission spectra. It was found that $Fe(acac)_3$ was non emissive compound while chlorophyll a gave an enormous emitting fluorescence around 650 nm. The chlorophyll a solutions in each solvent were measured the lifetimes by

modulation technique. All chlorophyll a solutions were removed O_2 by purging Ar before measuring (Figure 17).

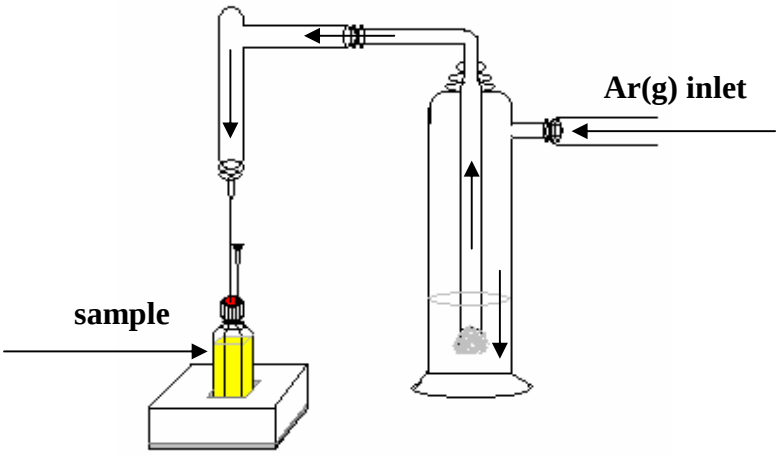

Figure 17 Set-up of purging Ar into the samples for lifetime and quenching experiments.

For quenching experiment, the absorbance of chlorophyll a was fixed at 0.05 in each solvent in order to prevent the re-absorption and self quenching reaction. Then the certain amount of chlorophyll a stock solution was added into 10 mL volumetric flask (see from the Table 3-10). The concentration of chlorophyll a was 1 μM at 0.05 absorbance. This concentration was used for all samples. There were 15-20 samples for each solvent. Concentrations of $Fe(acac)_3$ were varied from $1.00x10^{-5}$ to $2.00x10^{-4}$ M (see from the Table 3-10). The stock solution of $Fe(acac)_3$ was quantitatively added to chlorophyll a solution. The solvent was adjusted to 10 mL and mixed. Later the solution was filled into a clean luminescence cuvette equipped with a septum. Solutions were deaerated with argon gas (Ar) by penetrating the syringe (connected with the Ar gas line) and slowly bubbling Ar through the solution for 10 minutes. After that the surface outside the cuvettes were cleaned carefully with acetone before measuring the fluorescence intensity. The integrated areas under the fluorescence intensity profiles of each sample were recorded.

Table 3 Preparation of chlorophyll a - $Fe(acac)_3$ in benzene.

Chlorophyll a (mL)	**$Fe(acac)_3$ (mL)**
0.2	0.0
0.2	0.1
0.2	0.2
0.2	0.25
0.2	0.3
0.2	0.35
0.2	0.4
0.2	0.5
0.2	0.6
0.2	0.7
0.2	0.8
0.2	0.9
0.2	1.0
0.2	1.1
0.2	1.2
0.2	1.3
0.2	1.4
0.2	1.5
0.2	1.6
0.2	1.7
0.2	1.8

Table 4 Preparation of chlorophyll a - $Fe(acac)_3$ in toluene.

Chlorophyll a (mL)	**$Fe(acac)_3$ (mL)**
0.15	0.0
0.15	0.2
0.15	0.3
0.15	0.4
0.15	0.5
0.15	0.6
0.15	0.7
0.15	0.8
0.15	1.0
0.15	1.2
0.15	1.3
0.15	1.35
0.15	1.4
0.15	1.5
0.15	1.7
0.15	1.8

Table 5 Preparation of chlorophyll a - $Fe(acac)_3$ in ethanol.

Chlorophyll a (mL)	**$Fe(acac)_3$ (mL)**
1.5	0.0
1.5	0.2
1.5	0.3
1.5	0.4
1.5	0.5
1.5	0.6
1.5	0.7
1.5	0.8
1.5	1.0
1.5	1.2
1.5	1.4
1.5	1.6
1.5	1.8
1.5	2.0

Table 6 Preparation of chlorophyll a - $Fe(acac)_3$ in methanol.

Chlorophyll a (mL)	**$Fe(acac)_3$ (mL)**
1.0	0.0
1.0	0.2
1.0	0.3
1.0	0.4
1.0	0.5
1.0	0.6
1.0	0.7
1.0	0.8
1.0	0.9
1.0	1.0
1.0	1.1
1.0	1.2
1.0	1.3
1.0	1.4
1.0	1.5
1.0	1.6
1.0	1.7
1.0	2.0

Table 7 Preparation of chlorophyll a - $Fe(acac)_3$ in DMF.

Chlorophyll a (mL)	**$Fe(acac)_3$ (mL)**
0.15	0.0
0.15	0.1
0.15	0.2
0.15	0.3
0.15	0.4
0.15	0.5
0.15	0.6
0.15	0.7
0.15	0.8
0.15	0.9
0.15	1.0
0.15	1.2
0.15	1.4
0.15	1.6
0.15	1.8

Table 8 Preparation of chlorophyll a - $Fe(acac)_3$ in DMSO.

Chlorophyll a (mL)	**$Fe(acac)_3$ (mL)**
0.8	0.0
0.8	0.1
0.8	0.2
0.8	0.3
0.8	0.4
0.8	0.5
0.8	0.6
0.8	0.7
0.8	0.8
0.8	0.9
0.8	1.0
0.8	1.2
0.8	1.4
0.8	1.7
0.8	2.0

Table 9 Preparation of chlorophyll a - $Fe(acac)_3$ in MeCN.

Chlorophyll a (mL)	**$Fe(acac)_3$ (mL)**
0.15	0.0
0.15	0.1
0.15	0.2
0.15	0.3
0.15	0.4
0.15	0.5
0.15	0.6
0.15	0.7
0.15	0.8
0.15	0.9
0.15	1.0
0.15	1.2
0.15	1.4
0.15	1.6
0.15	1.8
0.15	2.0

Table 10 Preparation of chlorophyll a - $Fe(acac)_3$ in THF.

Chlorophyll a (mL)	**$Fe(acac)_3$ (mL)**
2.0	0.0
2.0	0.1
2.0	0.2
2.0	0.3
2.0	0.4
2.0	0.5
2.0	0.7
2.0	0.8
2.0	1.2

2.3.2 Sample preparation for cyclic voltammetry technique.

The redox potential of $Fe(acac)_3$ was measured by cyclic voltammetry technique. The redox potential of chlorophyll a was taken from the literature. Both redox potentials were taken to calculate the Gibbs free energy of Rehm-Weller equation. The negative value of Gibbs free energy refers to the spontaneous electron transfer which can be studied by quenching reaction.

The preparation of sample for CV experiments can be done by pre paring 0.1 M of tetrabutylammoniumhexafluorophosphate (TBAP) used as supporting electrolyte. The TBAP (Molecular weight = 387.4 $g.mol^{-1}$) 0.1937 g was added into the CV cell. The 5 mL of solvent was added and stirred with purging Ar for 5 minutes. The working electrode was polished by water and acetone, respectively. The purging of Ar was stopped before measuring. Later then the cyclic voltammograms of supporting electrolyte were scanned from -2 V to +2 V with the scan rate of 50, 100, 250, 500, 1000 and 2000 mV. After we saw the smooth and clean voltammogram, the internal standard, ferrocenemethanol, 0.02 M (0.186 g) was added. The experiment was carried out as it was done with the electrolyte. The redox potential of ferrocenemethanol was obtained. Afterward the sample of $Fe(acac)_3$ was added into

the electrolyte solution. The solution was stirred and purged with Ar again for some few minutes before measuring. In the mean while, the working electrode was cleaned again. The cyclic voltammograms of $Fe(acac)_3$ were recorded at the same parameters as like as electrolyte scaning. The cathodic peak potential (E_{pc}) and anodic peak potential (E_{pa}) were recorded.

2.4 Data analysis

Electron transfer ability was studied via quenching reaction. The parameters of quenching rate constant (k_q) and the apparent association constant (K_A) were calculated. The high k_q values can primarily refer to the good electron transfer. However in order to find out the rate of electron transfer (k_{et}) the diffusion rate constant (k_d) has to be considered very well. The quenching rate constant was obtained from the Stern-Volmer plot as already described in the Chapter 1. The $[I_0/I] - 1$ versus concentrations of $Fe(acac)_3$ in studied solvents were obtained. The intensity was taken from the integrated areas of fluorescence spectra.

CHAPTER 3

RESULTS AND DISCUSSION

3.1 Photo-Physical Properties of chlorophyll a and tris(acetylacetonato)Iron(III), $Fe(acac)_3$ and solvents effect.

3.1.1 Photo-Physical Properties of chlorophyll a

Absorption spectra of chlorophyll a in solutions were recorded in UV and visible region. Various solvents like acetonitrile, ethanol, methanol, DMF, DMSO, THF, benzene and toluene were used as solvents. Effect of solvents was investigated. Absorption spectra of chlorophyll a in different solvents can be shown in figure 18. Chlorophyll a shows two major absorption bands in visible range. It is due to extended π-delocalization at the edge of cyclic tetrapyrole (porphyrin) part. These two bands are a Q band (red band) in visible region and a soret band (blue or B band) in Ultraviolet-Visible (Zvezdanovic and Markovic, 2008). The soret Q band shows intense absorption around 430 nm ($\varepsilon = 1.5x10^5\ M^{-1}cm^{-1}$) which is π-π* transition. The absorption Q band locates around 669 nm with extremely high molar extinction coefficient (10^4-$10^5\ M^{-1}cm^{-1}$). This band is expected to be charge transfer band. Both transitions become spin allow upon selection rule. Chlorophyll a contains a network of alternating single and double bonds. The orbital can delocalize electrons stabilizing the structure. Such delocalized polyenes give an enormous absorption in visible region. In chlorophyll a, the central magnesium coordinates with four nitrogen atoms of the pyrrole rings. It can be both electron donor due to presence of ketone (C=O) groups and electron acceptor via its central Mg atom (Trifunac and Katz, 1974). Absorption spectra of chlorophyll a in studied solvents can be shown in figure 23. Absorption data were collected in table 11. There is an interesting behavior of soret absorption bands of chlorophyll a in different polarity of solvents like benzene, methanol, acetonitrile, DMF and DMSO. The maximum wavelengths of absorption

show the red shifting toward higher solvent polarities (Figure 19a). However, the Q bands are independent from the solvent property (Figure 19b).

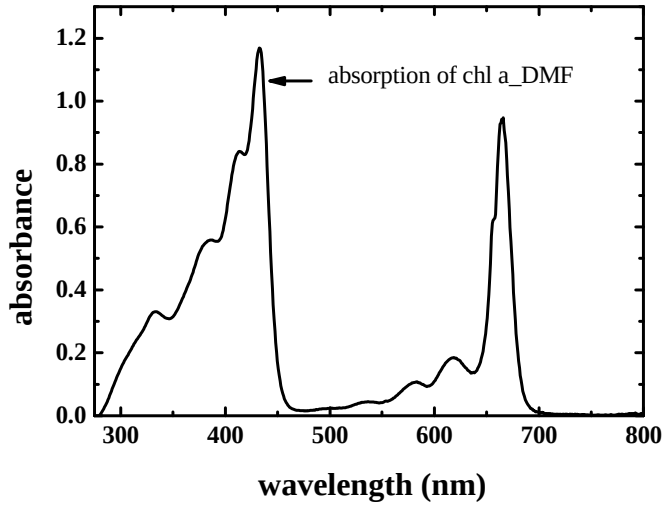

Figure 18 Absorption spectrum of chlorophyll a

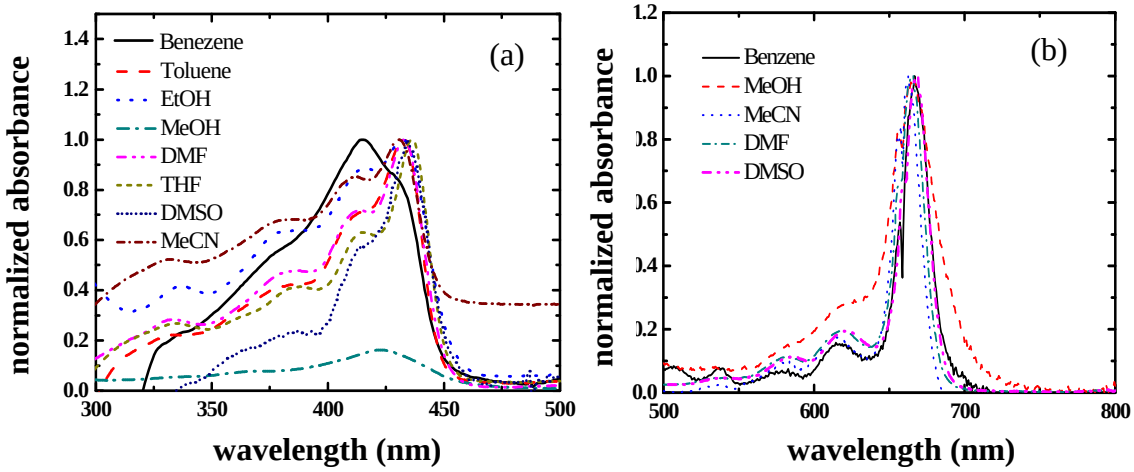

Figure 19 Normalized (a) absorption soret bands and (b) absorption Q bands of chlorophyll a in various solvents.

Table 11 Absorption data of chlorophyll a in various solvents.

solvent	polarity	dielectric constant	λ_{max}^{abs} (nm)		ε of Q band ($M^{-1}cm^{-1}$)
			Soret band	Q band	
Toluene	2.4	2.38[a]	432	664	73,000
Benzene	2.7	2.27[a]	415	667	84,600
THF	4.0	7.58[a]	436	664	70,400
Ethanol	5.0	29.60[b]	432	666	67,903
Methanol	5.1	32.70[a]	423	666	12,049
Acetonitrile	5.8	37.50[c]	430	663	194,000
DMF	6.4	36.71[a]	433	666	141,400
DMSO	7.2	46.68[a]	434	666	32,000

[a]Reported at = 25 °C [b]Reported at = 24 °C [c]Reported at = 20 °C

As discussed before the absorption Soret band occurs from π-π* transition and it shows the red shifted maximum wavelengths. It can be suggested that the excited state of π* is stabilized in high polarity of solvents (Figure 20). Therefore, the energy between π and π* decreases. The maxima wavelengths of absorption appear at longer wavelengths with high polarity of solvents. This fact is different from what have seen in the Q band. The Q band is proposed to be charge transfer band. There is no significant shifting of maximum wavelengths. It is due to an unchanging of π-level energy.

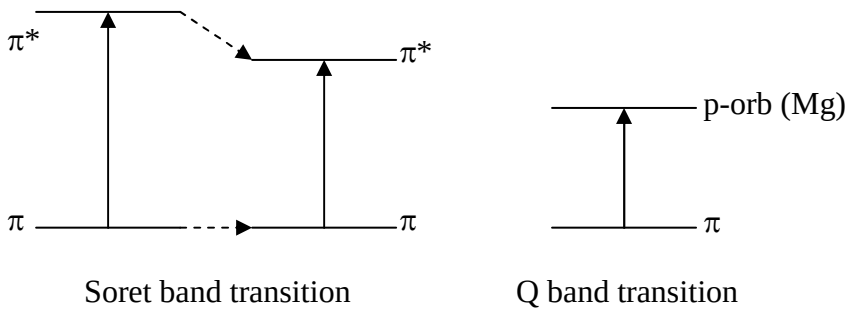

Figure 20 Scheme of π* orbital stabilizing of soret band and unchanged energy level of Q band.

Fluorescence emission of chlorophyll a is observed a strong band with maximum at 670 nm and a shoulder around 720-730 nm in visible and far visible regions (Figure 21). The excitation wavelength is 430 nm which is the Soret band. Following the absorption of chlorophyll a, several processes usually occur. An interesting consequence of emission is typically mirror image. However it is found the emission to be a single broad band with a shoulder at room temperature. The emission spectrum is devoid of vibrational structure. The energy spacing between absorption and emission spectra is illustrated in figure 21.

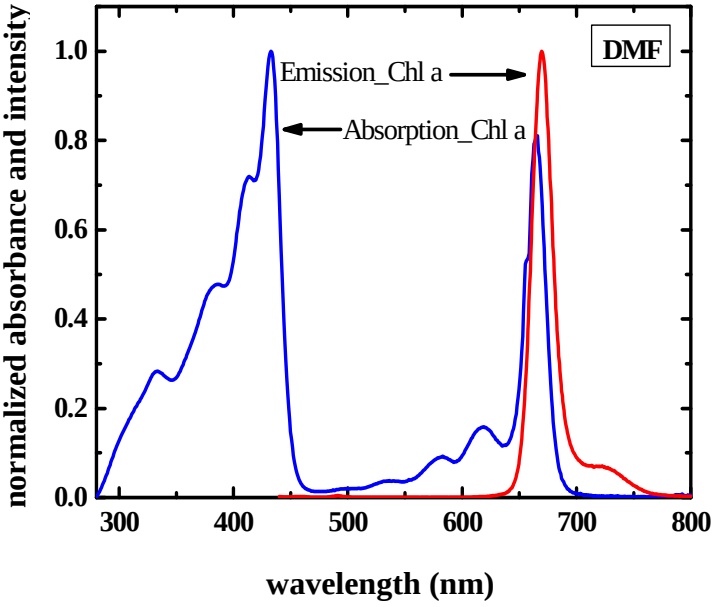

Figure 21 Overlay of absorption and emission spectra of chlorophyll a in DMF solution.

As we have described that there is no significantly shifting of maximum wavelengths of absorption Q band spectra corresponding to the order of viscosity or polarity of all solvents. However, there is an interesting trend showing in emission spectra of the compound. The increasing of viscosity and polarity of solvents leads the emission spectra appear at longer wavelengths as shown in figure 22. The important parameters of fluorescence emission are collected in table 12.

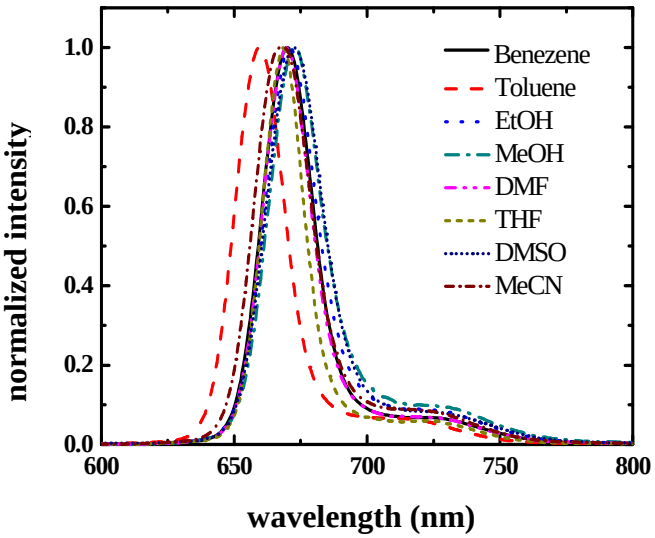

Figure 22 Normalized emission spectra of chlorophyll a in various solvents.

Table 12 Fluorescence emission data with related energies of chlorophyll a in various solvents.

Solvent	**λ^{em}_{max} (nm)**	**Stroke shift (cm^{-1}) (soret band)**	**Stroke shift (cm^{-1}) (Q-band)**	**E_{00} (cm^{-1})**	**τ_0 (nm)**
Benzene	670	23,148.15	15,174.51	19,161.33	5.49±0.29
Toluene	659	24,096.39	14,925.37	19,510.88	7.52±0.07
Ethanol	671	22,935.78	14,947.68	18,941.73	6.13±0.21
Methanol	673	23,148.15	14,903.13	19,025.64	5.54±0.29
DMF	670	23,640.66	14,858.84	19,249.75	7.52±0.07
DMSO	673	23,255.81	14,970.06	19,112.94	6.79±0.13
Acetonitrile	668	23,041.40	14,858.84	18,950.16	6.75±0.12

The photo-physical properties from figure 22 and table 12 show us the small stroke shifts between absorption Q bands and emission spectra. In general for energy transfer to occur, at least partial spectral overlap of the sensitizer emission band and quencher absorption band is required. In this case, we consider the energy transfer

within sensitizer molecule itself. The overlapping of emission and absorption of chlorophyll a displays the homo-energy transfer of chlorophyll a. The Stroke shifts between absorption Soret bands and emission spectra provide large energy values. None of an overlap between these two bands is observed. In this case, the controversy of energy transfer can be neglected. Then the maximum wavelength of Soret band is chosen to be the excitation wavelength instead of Q band. The hetero electron transfer is expected only. The zero-zero (0-0) spectroscopic transition energy gap [E_{00} (D*)] can be estimated from the absorption and emission spectra. In the case of identical symmetry between those two spectra, the E_{00}(D*) can be calculated from the half of the absorption and emission energies as shown here :

$$E_{00}\,(D^*) = \frac{\tilde{\nu}_a^{FC} + \tilde{\nu}_f^{FC}}{2} \qquad (28)$$

where $\tilde{\nu}_a^{FC}$ and $\tilde{\nu}_f^{FC}$ are the Franck-Condon maxima of the donor's absorption and fluorescence spectrum, respectively. The zero-zero transition energies were used to calculate the driving force (ΔG^0) in Rehm-Weller equation. Another important parameter is the excited lifetime which was measured from phase modulation technique with digital storage oscilloscope. In phase modulation technique the sample is excited with a sinussoidally modulated continuous radiation. Hence the observed emission will also be modulated with the same frequency as the excitation. For a monoexponential decay the lifetime can be analyzed to be independent from modulated frequencies. In our case, chlorophyll a has short-lived excited electronic state. First order lifetimes produces a frequency independent lifetime (see Appendix). Then the decay of excited chlorophyll is monoexponential. The lifetimes of the compound in various solvents are in the range of 5.5 to 7.5 ns with no tendency of solvent viscosities as shown in table 12 above.

3.1.2 Photo-Physical Properties of tris(acetylacetonato)Iron(III), $Fe(acac)_3$

Tris(acetylacetonato)Iron(III), $Fe(acac)_3$ complex was chosen to be the quencher in our study. Tris(acetylacetonato)Iron(III) is a good quencher to accept electron from excited chlorophyll a. There are some important criteria to select an appropriate quencher as following :

- The quencher must not interact chemically with the fluorophore.
- The reduction potential E_{red} has to be within a certain range to allow quenching via electron transfer.
- The absorption spectrum of the quencher must not overlap with the emission spectrum of the fluorophore. It can be called re-absorption of the emitted photons by the quencher diminishes the fluorescence intensity and hence results in an apparently higher quenching rate constant.
- The quencher must not absorb in the spectral region where the fluorophore is excited. Else the fluorescence intensity (I_{exp}) is decreased as a consequence of competitive light absorption (so called inner filter effect). The quenching rate constant is higher from realistic value.

From these criteria, the photo-physical properties and electrochemistry behavior have to be investigated carefully. The $Fe(acac)_3$ is non-emissive species. There is no chemical interaction between chlorophyll a and $Fe(acac)_3$. Absorption can be shown in figure 23 and data are summarized in table 13. There are two important bands in UV and Visible occur at 360 and 440 nm, respectively. The transition of these two bands are proposed to allowed transition of π-π^* and MLCT, respectively. There is no significant shifting of maximum absorption wavelength. It means that it is independent of solvent properties.

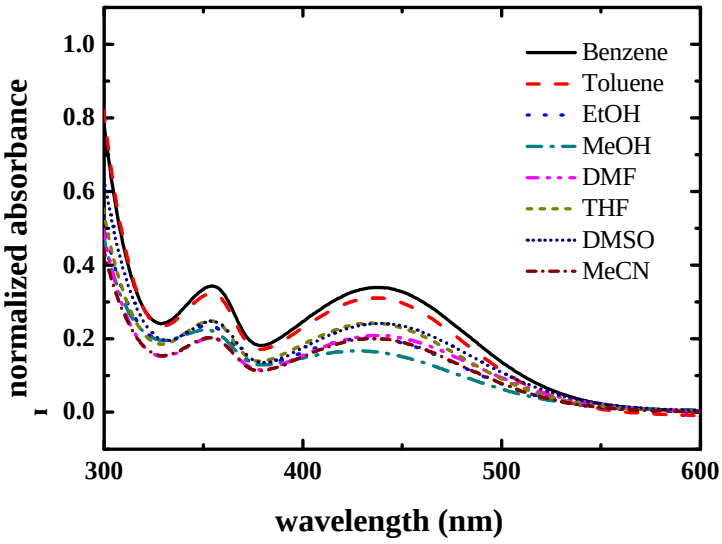

Figure 23 Normalized absorption spectra of $Fe(acac)_3$ in various solvents.

Table 13 Absorption data of $Fe(acac)_3$ in various solvents.

solvent	**polarity**	**dielectric constant**	λ_{max}^{abs} **(nm)**
Toluene	2.4	2.38[a]	437
Benzene	2.7	2.27[a]	438
Ethanol	5.0	29.60[b]	432
Methanol	5.1	32.70[a]	428
Acetonitrile	5.8	37.50[c]	436
DMF	6.4	36.71[a]	438
DMSO	7.2	46.68[a]	438

According to the criteria of being a quencher of $Fe(acac)_3$, the absorption spectrum and emission spectrum of chlorophyll a has to be plotted.

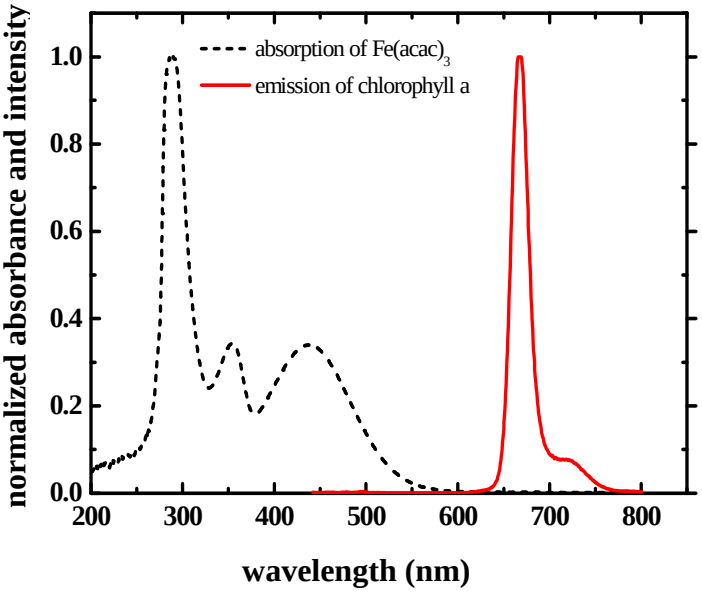

Figure 24 Normalized absorption spectrum of $Fe(acac)_3$ and emission spectrum of chlorophyll a in a solution.

From the figure 24, there is no overlapping among those two spectra. Then there is no hetero-energy transfer between excited chlorophyll a and $Fe(acac)_3$. The re-absorption of the emitted photons by the quencher can be avoided. However, the inner filter effect cannot be neglected. There is a strong overlapping between absorption of chlorophyll a and emission spectrum of $Fe(acac)_3$ (Figure 25). We have to consider the inner filter effect factor and recalculate the corrected emission intensity of chlorophyll a in each quenching reaction. When the solution contains other chromophores that absorb light in the same wavelength range as the fluorescent compound under study. The chromophores act as filters at the excitation wavelength and the fluorescence intensity must be multiplied by a correction factor which will be presented in section 3.3.

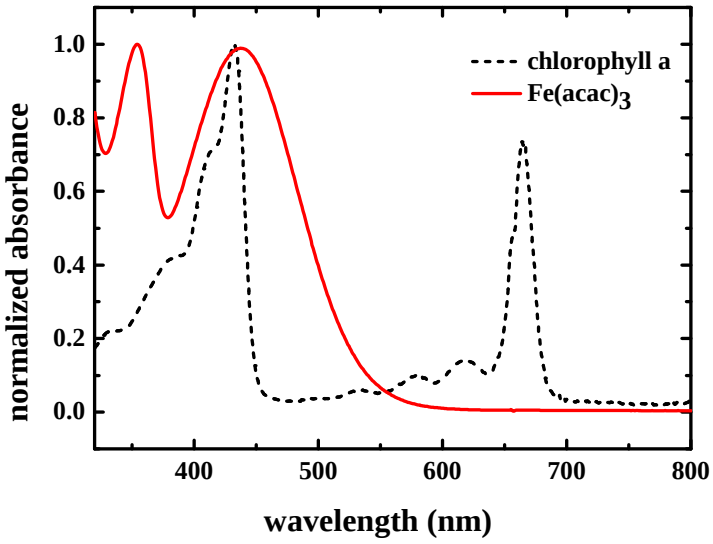

Figure 25 Normalized absorption spectra of $Fe(acac)_3$ and chlorophyll a in a solution.

For electrochemistry behavior of $Fe(acac)_3$, the redox potential of Fe (II/III) was studeied by cyclic voltammetry technique. As it was described before that the reduction potential E_{red} of quencher molecule has to be within a certain range to allow quenching via electron transfer (Rehm-Weller equation). The CV experiments were performed in DMF and compared the reduction potential with the literature (Richert *et al.*, 1989).

The ferrocenemethanol-ferroceniummethanol redox couple was used to estimate junction potential changes upon changing solvents. After each measurement, the redox half wave potentials ($E_{1/2}$) of ferrocenemethanol-ferroceniummethanol were measured as -0.492 V versus SCE. The redox couple for $Fe(acac)_3$ are reversible. The $Fe(acac)_3$ complex can be reversibly reduced to $Fe(acac)_3^-$ as shown in figure 26. The redox potentials are shown in table 14. It has been shown that electron transfer reaction is ligand-centered and brought the redox potential of metal-centered to be changed from 3+ to 2+. This implies that the transition metal complexes electron transfer reactions are facilitated by stabilization of the ligand-radical product via covalent bond formation with an unpaired d electron of the transition metal center.

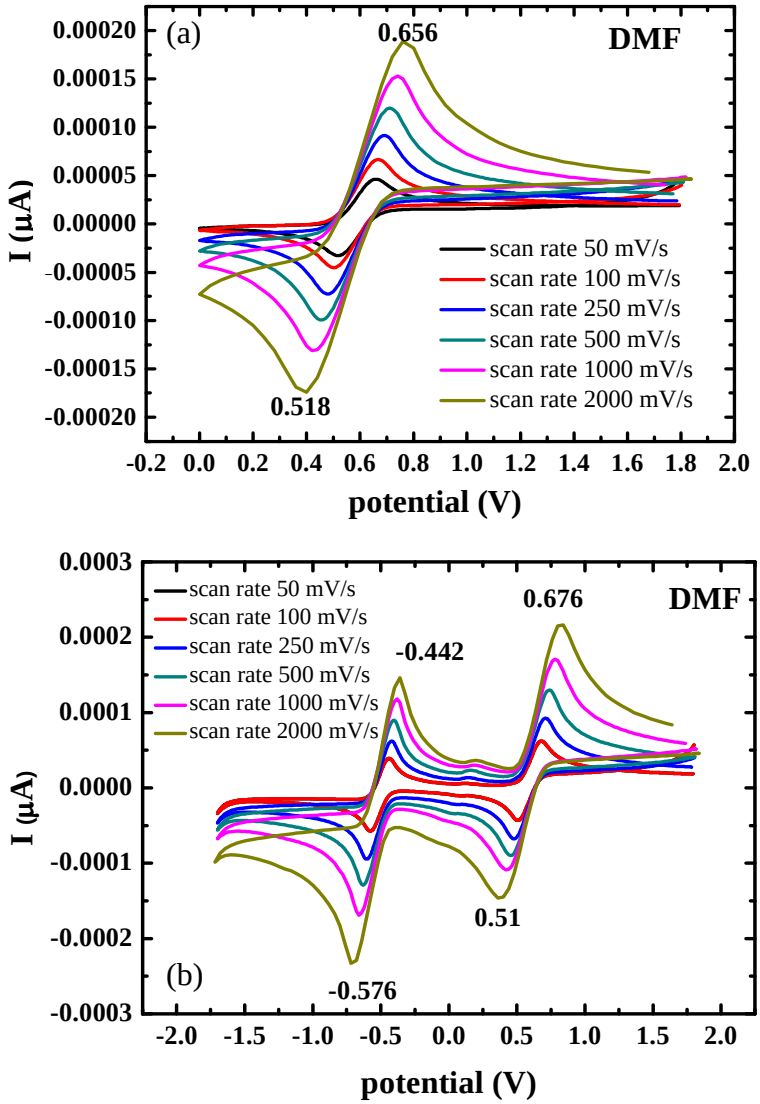

Figure 26 reversible couple of $Fe(acac)_3$ in DMF, (a) cyclic voltammogram of $Fe(acac)_3$ in DMF and (b) cyclic voltammogram of $Fe(acac)_3$ when compare with ferrocene methanol in DMF.

Table 14 Reduction potential for $Fe(acac)_3$ in DMF (0.1 M. Tetrabutylammonium hexafluorophosphate)

Solvent	**$E_{1/2}$ V vs SCE**	
	FeL_3/FeL_3^-	Fc-MeOH/Fc^+-MeOH
DMF	+0.66	-0.492

Table 14 lists the half-wave redox potential $E_{1/2}$ of $Fe(acac)_3$ and ferrocenemethanol at 50 $mV.s^{-1}$ for 10^{-3} M solutions in pure DMF using 0.1 M tetrabutylammoniumhexafluorophosphate electrolyte. Generally, the redox potentials are better expressed by $E_{1/2}$ than by the cathodic (E_{pc}) or anodic (E_{pa}) because both E_{pc} and E_{pa} change with scan rates, whereas $E_{1/2}$ is independent of scan rate. Although, the ΔE_p is broader than the theoretical value of 60 mV of reversible couple, the ΔE_p is similar to what is observed from ferrocene methanol which is well known to be reversible couple. Moreover, the ratio between cathodic peak current and anodic peak current is $I_{pc}/I_{pa} \approx 1$. The cyclic voltammogram of $Fe(acac)_3$ exhibits reversible electrochemical oxidation and reduction for one electron process. Figure 27 shows the plot between peak current and the square root of scan rates. It gives the linear plot which implies that the voltammogram is the reversible couple over increasing of scan rates.

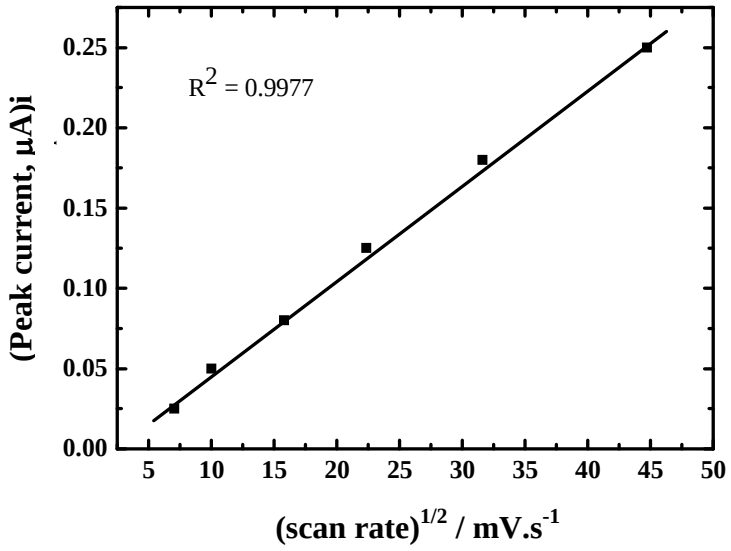

Figure 27 Plot of peak current (I_{pa}) with square root of scan rates

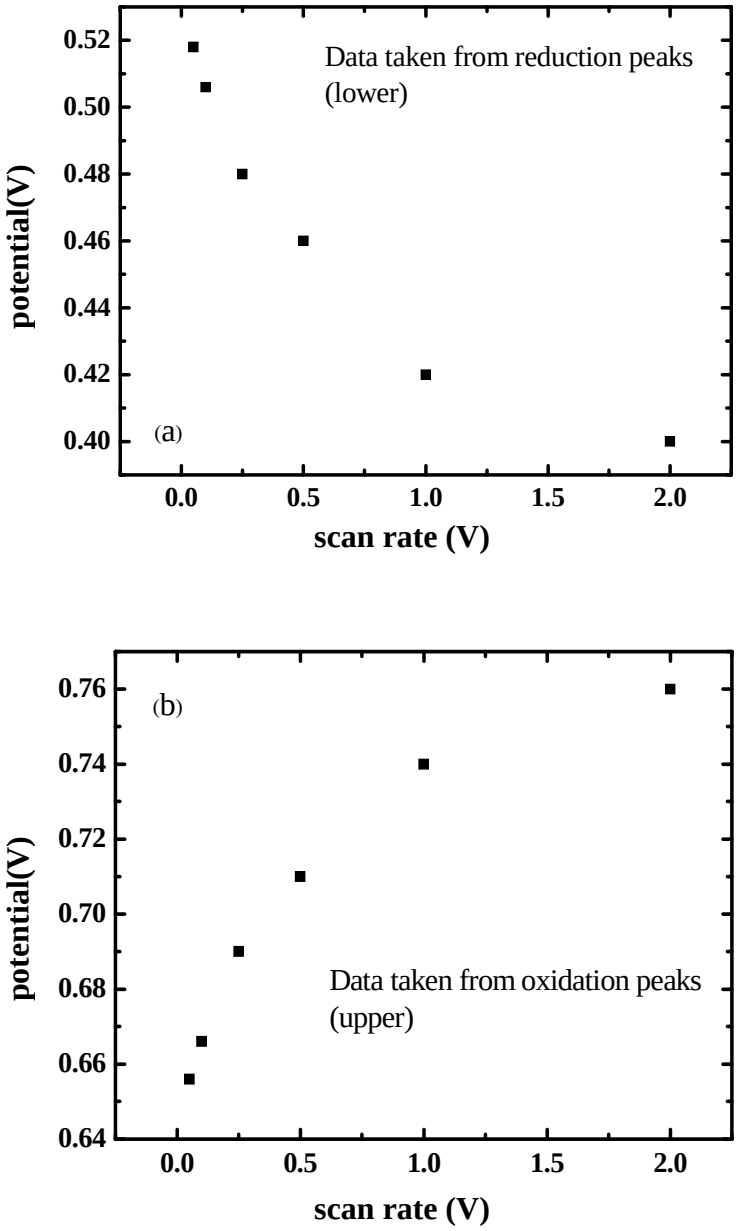

Figure 28 Plot of peak potential (a) E_{pc} and (b) E_{pc} with scan rates

The plot of peak potential both from reduction and oxidation peaks versus scan rate is used to confirm that the cyclic voltammogram of $Fe(acac)_3$ is the reversible couple. When the scan rates increase, the potentials of reduction decreases while the potentials of oxidation are opposite.

3.2 Calculation of free energy change (ΔG^o) for the electron transfer reactions

The thermodynamic driving force of electron transfer can be predicted by Rehm-Weller equation. The driving force of the system must be the fundamental thermodynamic condition for spontaneous electron transfer between neutral reactants, $\Delta G^0 < 0$. Value of ΔG^0 for a photoinduced electron transfer can be estimated by Rhem-Weller equation which is shown in below

$$\Delta G^0 = E_{1/2}(D/D^+) - E_{1/2}(A/A^-) - E_{00}(D^*) + w_p - w_r \quad (29)$$

where $E_{1/2}(D/D^+)$ and $E_{1/2}(A/A^-)$ are the half wave oxidation potential of the ground state donor and the half wave oxidation potential of acceptor couple, respectively. The terms w_p and w_r are the coulombic work terms of the products and reactants, respectively, which correct for the work involved in bringing ionic species together. The coulombic work terms are usually small, and zero for neutral species. The studied system is neutral charge. Then both work term parameters are zero. They can be neglected.

Table 15 The redox potentials (V, vs SCE) of metal-porphyrin (M-Chl a).

Compound	E_{ox}^{II}	E_{ox}^{I}	E_{red}^{I}	E_{red}^{II}	$E_{ox}^{I} - E_{red}^{I}$
H_2-Chl a	1.37(1.38)	0.94(1.00)	-1.01(-0.94)	-1.24(-1.24)	1.95(1.94)
Mg-Chl a	0.86(0.86)	0.58(0.63)	-1.04(-0.94)	-1.29(-1.64)	1.62(1.78)
Fe-Chl a (Cl)	1.03	-	-	-	-
Ni-Chl a	-	-	-1.03(-0.94)	-1.40(-1.3)	-
Cu-Chl a	1.18(1.18)	0.86(0.89)	-1.04 (-0.92)	-1.41(-1.37)	1.90(1.81)
Zn-Chl a	1.00(1.08)	0.64(0.86)	-1.10(-1.10)	-1.44(-1.44)	1.74(1.96)
Zn-PMP a	0.95	0.61	-	-	-
Zn-Chl b	1.11	0.68	-1.06	-	1.74
Zn-Chl e_6 TME	0.93	0.56	-1.30	-1.56	1.86

Nanomura, Y., Igarashi, S., Yoshioka, N., Inoue, H. 1997. Spectroscopic properties of chlorophylls and their derivatives. Influence of molecular structure on the electronic state. Chemical Physics. 220: 155-166.

The oxidation potential of chlorophyll a (Mg is center atom) is taken as the 0.57 V (Nanomura *et al*., 1997; Kathiravan *et al*., 2009) while the reduction potential of $Fe(acac)_3$ is 0.66 V as mentioned in the previous topic. The E_{00} is the excited zero-zero transition of chlorophyll a. The thermodynamic driving force is reported in table 16.

Table 16 Thermodynamic driving force of electron transfer from chlorophyll a by $Fe(acac)_3$ calculated from Rehm-Weller equation. Data reported in DMF solution.

Quencher	**$E_{1/2,ox}$ (chl a)(V)**	**$E_{1/2,red}$ (quench)(V)**	**E_{00}(eV)**	**ΔG^o(eV)**
$Fe(acac)_3$	+0.58[a]	0.66[b]	1.84[a]	-1.93

[a] : data taken from Nanomura**,** Y. Igarashi, S. Yoshioka, N. Inoue, H., Spectroscopic properties of chlorophylls and their derivatives. Influence of molecular structure on the electronic state. Chemical Physics, 220 (1997) 155 – 166.

[b] : our experimental data in DMF calibrated reduction potential versus SCE of ferrocenemethanol with Thander A., Mallik B. Chemical Physics Letters, 330 (2000) 521 – 527.

[c] : data taken from Richert S. A., Tsang P. K. S., Sawyer D. T. Inorg.Chem. 28 (1989) 2471 – 2475.

Gibbs free energy (ΔG^0) was -1.93 eV. The minus value refers that electron transfer from chlorophyll a to $Fe(acac_3)$ can spontaneously occur. The oxidation potentials of chlorophyll a are independent from solvent properties. Nanomura *et al.*, 1997 reported the oxidation potential of chlorophyll a (Mg-Chl a) in DMF at 0.58 V with SCE reference electrode. Similarly with Kathiravan *et al.*, 2009 reported the oxidation potential of chlorophyll a (Mg-Chl a) in MeCN at 0.57 V with SCE reference electrode. One can see that there is just a little different result in both solvents.

3.3 Quenching reaction of chlorophyll a by molecule electron acceptor $Fe(acac)_3$.

The steady-state fluorescence quenching is common experimental method For determining the reaction rate constant. The electron transfer reaction can investigate via observed quenching reaction. The reaction rate constant can be obtained from the Stern-Volmer plot : $I_0/I = K_{sv}.[Q]$. This plot is the relative between I_0/I (y-axis) versus [Q] (x-axis) where I_0 is the intensity with absence of quencher molecule, I is the intensity with presence of quencher molecule and [Q] refers to quencher concentrations. Slope of the linear plot is the Stern-Volmer constant (K_{SV}) which is equal to $k_q.\tau_0$. The quenching rate constant (k_q) is the rate of reaction. The mechanism of quenching reaction is shown below.

$$*\text{Chlorophyll a} + \overset{\text{Fe(III)}}{\text{Fe(acac)}_3} \underset{k_{-d}}{\overset{k_d}{\rightleftharpoons}} [\text{Chlorophyll a-}\overset{\text{Fe(III)}}{\text{Fe(acac)}_3}]$$

$$[\text{Chlorophyll a-}\overset{\text{Fe(III)}}{\text{Fe(acac)}_3}] \xrightarrow{k_{et}} [\text{Chlorophyll}^{+}\text{-}\overset{\text{Fe(II)}}{\text{Fe(acac)}_3^{-}}]$$

Scheme 1 The reaction scheme of photoinduced electron transfer. The rate constants can be applied in the same manner as already described in the introduction part.

Nonetheless, absorbance at the excitation wavelength of 430 nm increased corresponding to the higher concentration of $Fe(acac)_3$ (Figure 29) in quenching experiments of chlorophyll a by $Fe(acac)_3$. In the meanwhile, fluorescence intensity of chlorophyll a decreased when [$Fe(acac)_3$] was more added as shown in figure 30. This behavior implies to inner filter effect (IFE) obviously. In principle, the inner filter effect can be due to high absorption of excitation light by the sample (primary inner filter effect) and/or the re-absorption of emitted light (secondary inner filter effect). In our experiment only the primary inner filter effect was observed. Because there exists only the overlapping of absorption spectrum of $Fe(acac)_3$ in the same range of the absorption of chlorophyll a but there is no overlapping of $Fe(acac)_3$ with emission of chlorophyll a. The competitive of excitation among the fluorophore and quencher

occurs. The excited fluorescence was quenched by quencher molecule but it competitively occurred with inner filter effect.

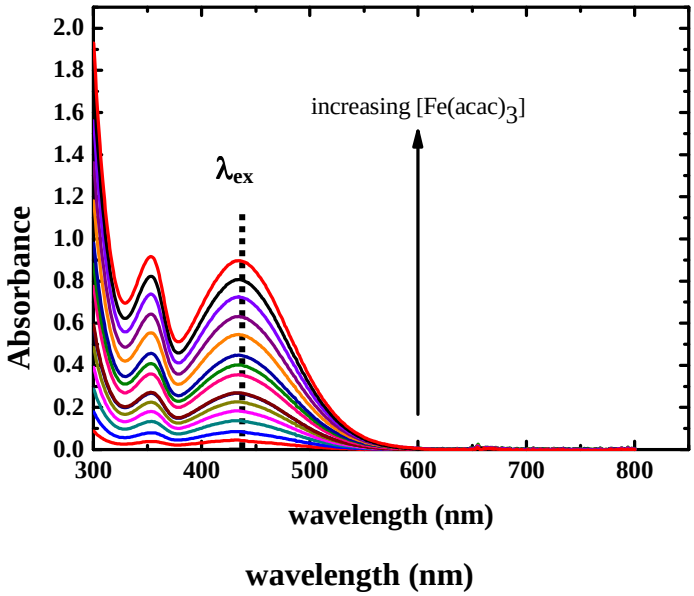

Figure 29 Absorption spectra of chlorophyll a in the presence of $Fe(acac)_3$ is solution.

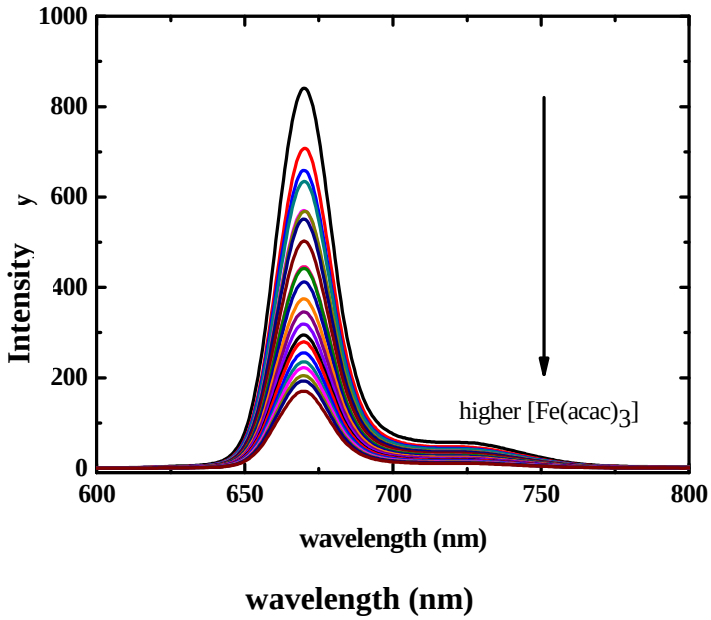

Figure 30 The decreasing of fluorescence intensity of chlorophyll a in the presence of $Fe(acac)_3$.

As described before, the dramatic increasing of absorbance at the excitation wavelength with increasing of quencher concentration significantly attributes to the inner filter effect. The solution contains chromophore of $Fe(acac)_3$ which absorbs light in the same wavelength range as the fluorescent chlorophyll a. The chromophore acts as filters at the excitation wavelength. It causes the decreasing of fluorescence intensity of chlorophyll as a consequence with competitive light absorption. The recorded fluorescence intensity is unreal proportional to the chlorophyll a concentration due to the inner filter effect. The experimental fluorescence intensities from chlorophyll a are lower than that it should be. Therefore, the ratio between I_0/I gets too high as like as the uncorrected k_q value. The measured fluorescence intensity has to be corrected. The observed fluorescence intensity must be multiplied by a correction factor. There are many corrections for inner-filter effect which will be described in detail.

The correction for the primary inner filter effect can be done by many methods(Borissevitch, 1999; Lakowicz, 2006). Lakowicz (Lakowicz, 2006) suggested the correction of primary inner filter effect owing to self-quenching reaction by multiplication the correction factor with each observed intensity based on the idea that the average path length of absorption of the excitation and emission light is ½ of the cuvette length.

$$I_{corr} = I_{\exp}.10^{-(A_{ex}+A_{em})/2} \qquad (30)$$

Where I_{corr} is the corrected intensity, I_{exp} is the experimental intensity, A_{ex} is the absorbance at the excitation wavelength and A_{em} is the absorbance at the emission wavelength. Nevertheless, in our case the self-quenching reaction is protected by using very low concentration of chlorophyll a. The optical density is somewhat around 0.02 (Parker, 1968). It is even lower than the theoretical value of 0.05 (Lakowicz, 1999). The correction of Stern-Volmer constant is not necessary for the solution absorbance $A < 0.02$ in excitation and emission wavelengths (Borissevitch, 1999).

In the present work, there are two methods for correction of inner filter effect. The first method is to correct the real intensity with consider the absorption of quencher, $Fe(acac)_3$. The detection system collects the fluorescence emitted only from the central part of the exciting beam (Figure 31). If the concentration of the sample is low (A<0.02), the incident light will be only slightly attenuated through the cuvette.

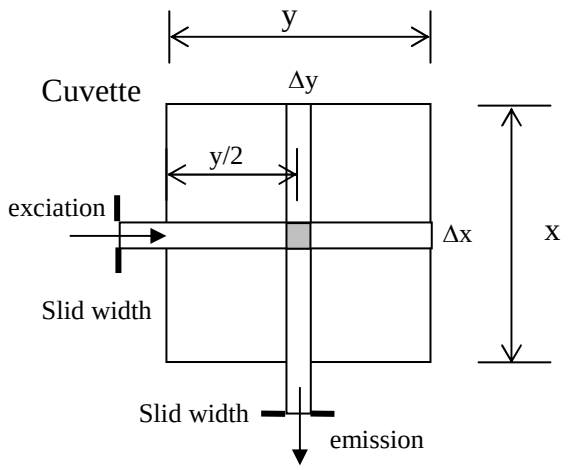

Figure 31 Geometry of fluorescence production in a cuvette cell

Absorption of $Fe(acac)_3$ is treated quantitatively using the Beer-Lambert law. The fraction of monochromatic light transmits through an absorbing system. The relation is expressed through.

$$\frac{I_t}{I_{0,i}} = 10^{-\varepsilon.c.l} \tag{31}$$

where $I_{0,i}$ and I_t are respectively the incident and transmitted light intensities, ε is the molar extinction coefficient ($M^{-1}cm^{-1}$), c is the concentration and l is the path length (cm) of the light beam passed. Likewise in fluorescence measurement, the ideal path length is half of the length of cuvette (Figure 31). The path length (l) is 0.5 cm for the standard of 1 cm^2 cuvette, giving the expression:

$$\frac{I_t}{I_{0,i}} = 10^{-\varepsilon.c.l/2} \quad (32)$$

As we have known that the factor $\varepsilon.c.l$ in above expression is the absorbance of $Fe(acac)_3$ quencher(A_Q). The absorption factor of $Fe(acac)_3$ can be represented below.

$$\frac{I_t}{I_{0,i}} = 10^{-A_Q/2} \quad (33)$$

All measured fluorescence intensities were corrected the inner filter effect by multiplication the fluorescence intensity of chlorophyll a in absence of quencher (I_0) with $10^{-A_Q/2}$ correction factor. Because in the matrix composes of two components. The absorbance of quencher can be calculated from the following equations

$$A_{sample}\,(A_S) = A_{chl}\,(A_F) + A_{Fe(acac)3}\,(A_Q) \quad (34)$$

$$A_Q = A_S - A_F \quad (35)$$

$$A_Q = \Delta A_{abs} \quad (36)$$

where Δ_{Abs} is the different absorbances of sample absorbance (A_S) and fluorophore (A_F) absorbance. The correction factor can be rewritten in term of $10^{-\Delta A_{abs}/2}$. This correction factor was multiplied with the I_0 then it brought the corrected fluorescence intensity, $I_{0,corr}$ for each quencher concentration (Equation 37).

$$I_{0,\,corr} = I_0.10^{-\Delta A_{abs}/2} \quad (37)$$

Then the values of ($I_{0,corr}/I$) were plotted with various [$Fe(acac)_3$] in each solvent. The obtained K_{SV} values were compared with the second method of correction (method of Borissevitch, 1999).

In the year 1999, Borissevitch I.E. published an interesting method to correct the inner filter effect for both primary and secondary types. He demonstrated the necessity of the K_{SV} correction by the quencher absorbance which gave rather high K_{SV} value. His correction factor for both types of inner filter effect represented with η parameter.

$$\eta = \frac{A_{x0}A_{y0}(1-10^{-A_{xi}})(1-10^{-A_{yi}})}{A_{xi}A_{yi}(1-10^{-A_{x0}})(1-10^{-A_{y0}})} \tag{38}$$

Where A_{x0} is the absorbance at the excitation wavelength, A_{y0} is the absorbance of fluorophore at the emission wavelength, A_{xi} is the absorbance of sample at the excitation wavelength and the A_{xi} is the absorbance of sample at the emission wavelength. However in our experiment, the effect causes from only the primary type. The correction factor for excitation only can be deduced to equation 39.

$$\eta = \frac{A_{x0}(1-10^{-A_{xi}})}{A_{xi}(1-10^{-A_{x0}})} \tag{39}$$

The correction factor was multiplication with the ratio of experimental intensities I_0/I as shown in the equation 40. The corrected Stern-Volmer constants were determined.

$$(I_0/I)\eta = 1 + K_{SV}[Q] \tag{40}$$

Absorption characteristic in figure 29 might be also cause from the ground state complex formation of chlorophyll a and $Fe(acac)_3$. The ground state complex formation can be observed from the static quenching mechanism and combination of pseudo-static quenching mechanism. Experimentally, Stern-Volmer plot shows the bend curve upward to the I_0/I axis. Although in the presence of quencher $Fe(acac)_3$ the absorbance at the excitation wavelength (430 nm) is increased without changing in wavelength. It still can imply that there is an interaction of chlorophyll a with

$Fe(acac)_3$. The equilibrium for the formation of the ground state complex is given by equation 41, where K_{app} is the apparent association constant.

$$\text{Chlorophyll a} + Fe(acac)_3 \overset{K_{app}}{\rightleftharpoons} [\text{Chlorophyll a-}Fe(acac)_3]$$

$$K_{app} = \frac{[\text{chlorophyll a} - Fe(acac)_3]}{[\text{chlorophyll a}][Fe(acac)_3]} \qquad (41)$$

There are many ways to calculate the K_{app} as already described in the introduction chapter. A possible way is to calculate K_{app} by using Benesi and Hilderbrand equation (Kathiravan *et al.*, 2009). The apparent association constant (K_{app}) has been calculated according to the following equations :

$$K_{app}\,;\ \frac{1}{I^0 - I} = \frac{1}{I^0 - I'} + \frac{1}{K_{app}(I^0 - I')[Q]} \qquad (42)$$

$$K_{app}\,;\ \frac{1}{A_S - A_F} = \frac{1}{A_c - A_F} + \frac{1}{K_{app}(A_c - A_F)[Q]} \qquad (43)$$

where

K_{app} = the apparent association constant
I_0 = the initial fluorescence intensity of chlorophyll
I' = the fluorescence intensity of quencher adsorbed chlorophyll a
I = the observed fluorescence intensity at its maximum
A_S = the observed absorbance of solution containing different concentrations of $Fe(acac)_3$ [Q]
A_F = the absorbance of chlorophyll a
A_c = the absorbance of ground state complex

Quenching reactions were measured in various solvents. Stern-Volmer plots of uncorrected, corrected with our method and corrected with Borissevitch method will be presented in the next section.

3.3.1 Quenching reaction of chlorophyll a by $Fe(acac)_3$ in benzene

The data of Stern-Volmer plots from experiment with uncorrected IFE, corrected IFE with our method and corrected IFE with Borissevitch method are collected (Appendix Table 9.2). The Stern-Volmer plots of the quenching of chlorophyll a by $Fe(acac)_3$ in benzene is shown in figure 32.

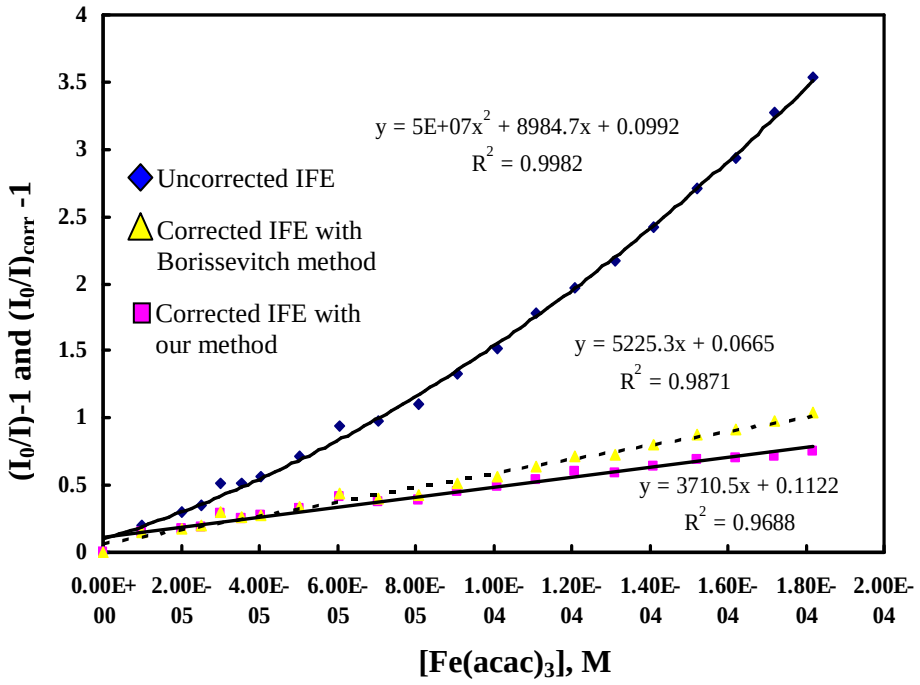

Figure 32 Stern-Volmer plots in benzene solution obtained from experiment with uncorrected IFE, corrected IFE with our method and corrected IFE with Borissevitch method.

The Stern-Volmer plots obtained from the experiment without corrected inner filter effect give the curvature profile bending upward to the y-axis. The K_{SV} of this plot is determined from slope of the linearity part of the curve. The K_{SV} value is very high. In contrast, the corrected Stern-Volmer plots either from our method or Borissevitch method are linear. The K_{SV} values from these two corrections are 4 times less comparing with the uncorrected experimental data. It is owing to inner filter effect. The corrections by our method gives a bit lower K_{SV} value than that of Borissevitch method but gives higher deviation of intercept from unity. No matter what it is, the deviation is still very small within the experimental error of 10 %. The data of K_{SV} and k_q values are collected in table 17. However, the linearity among two methods overlaps in the small concentration range up to $6x10^{-5}$ M which is the most reasonable range.

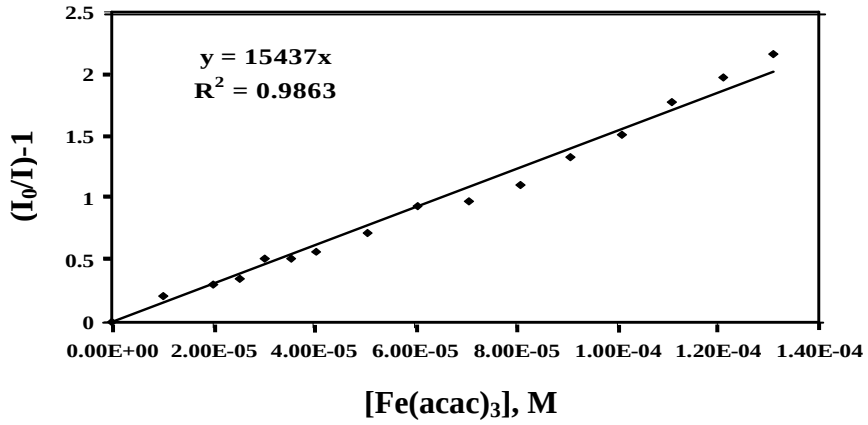

Figure 33 Linearity part of the Stern-Volmer plot in benzene. Data obtained from the experiment with uncorrected inner filter effect.

Table 17 Fluorescence quenching data of chlorophyll a by $Fe(acac)_3$ in benzene

$K_{SV, exp}$ (M^{-1})	$K_{SV,corr/our}$ (M^{-1})	$K_{SV,corr/Boris}$ (M^{-1})	$k_{q,exp}$ ($M^{-1}s^{-1}$)	$k_{q,corr/our}$ ($M^{-1}s^{-1}$)	$k_{q,corr/Boris}$ ($M^{-1}s^{-1}$)
$1.54x10^4$	$3.71x10^3$	$5.22x10^3$	$2.76x10^{12}$	$6.76x10^{11}$	$9.49x10^{11}$

A curvature of Stern-Volmer plot can imply the mechanism of quenching reaction to the combination of static and collisional quenching mechanism. However, after the experimental intensity was corrected. The Stern-Volmer is linear. The ground state complex formation is not supposed to occur. Anyway, the apparent association constant has been calculated in order to determine the possibility of equilibrium for the formation of ground state complex between chlorophyll a and $Fe(acac)_3$ from the curvature of Stern-Volmer plot. The K_{app} was obtained from Benesi and Hildebrand equation as already shown in equation 42-43) (Kathiravan et al., 2009).

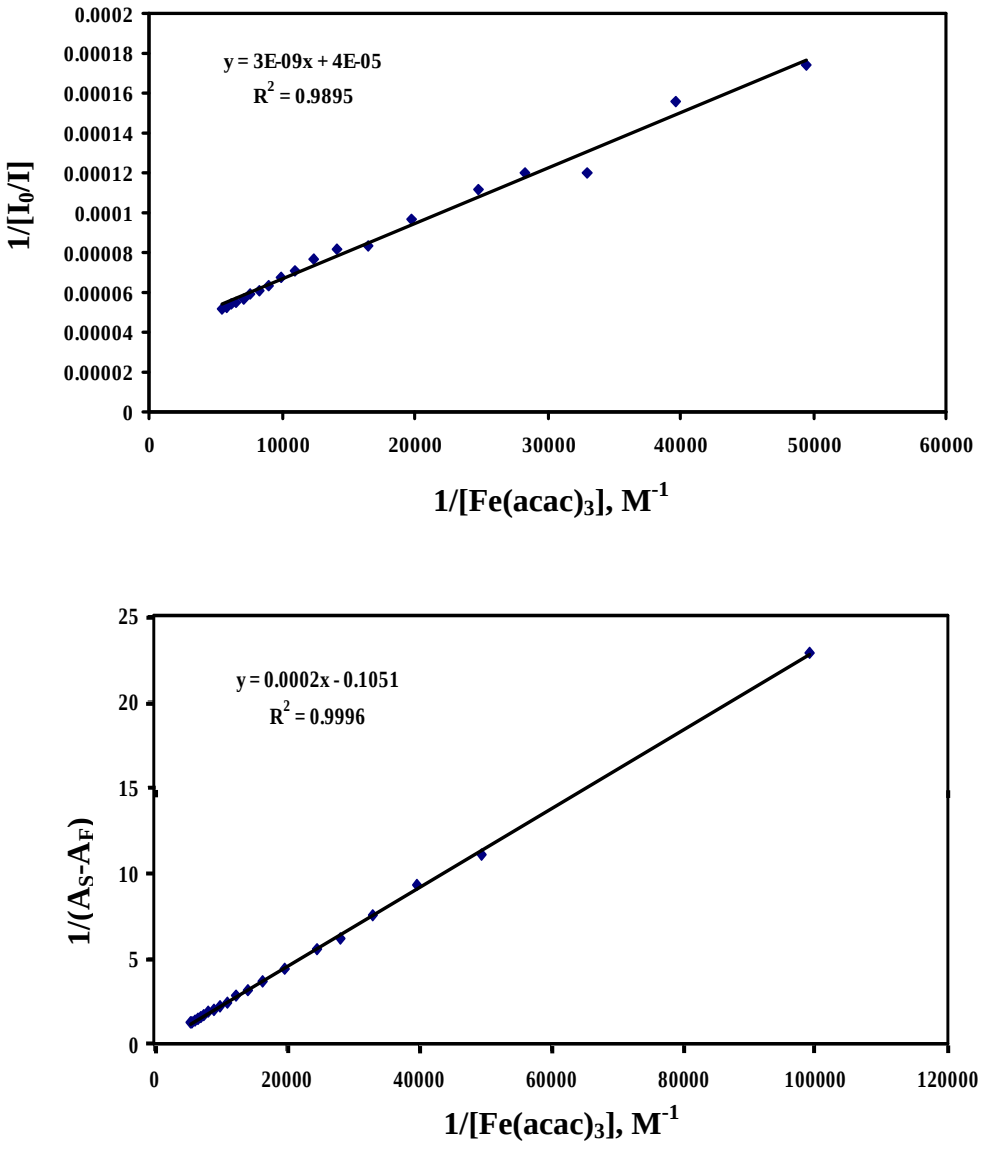

Figure 34 The Benesi and Hildebrand plots for determining K_{app} in benzene.

The value of K_{app} obtained from the data of fluorescence quenching intensity ($1.33x10^4$ M^{-1}) is not in good agreement with the K_{app} from the absorption data ($5.26x10^2$ M^{-1}). The K_{app} obtained from fluorescence intensity gives higher value for 25 times than that of the data from absorbance. It can imply that the assumption of ground state complex formation is not the predominant phenomena to the curvature of Stern-Volmer plot. There might be an effect from inner filter.

3.3.2 Quenching reaction of chlorophyll a by $Fe(acac)_3$ in toluene

The data of Stern-Volmer plots from experiment with uncorrected IFE, corrected IFE with our method and corrected IFE with Borissevitch method are collected (Appendix Table 10.2). The Stern-Volmer plots of the quenching of chlorophyll a by $Fe(acac)_3$ in toluene is shown in figure 35. All types of Stern-Volmer plots give the curvature profiles bending upward to the y-axis. The whole data do not fit well with the linear. The R^2 are somewhat around 0.94. The K_{SV} of this plot was determined from slope of the linearity part of the curves (Figure 36). As like as in benzene solution, the K_{SV} from an uncorrected intensity give much higher value than that of the corrected data. The K_{SV} values from both correction methods are similar. The data of K_{SV} and k_q values are collected in table 18.

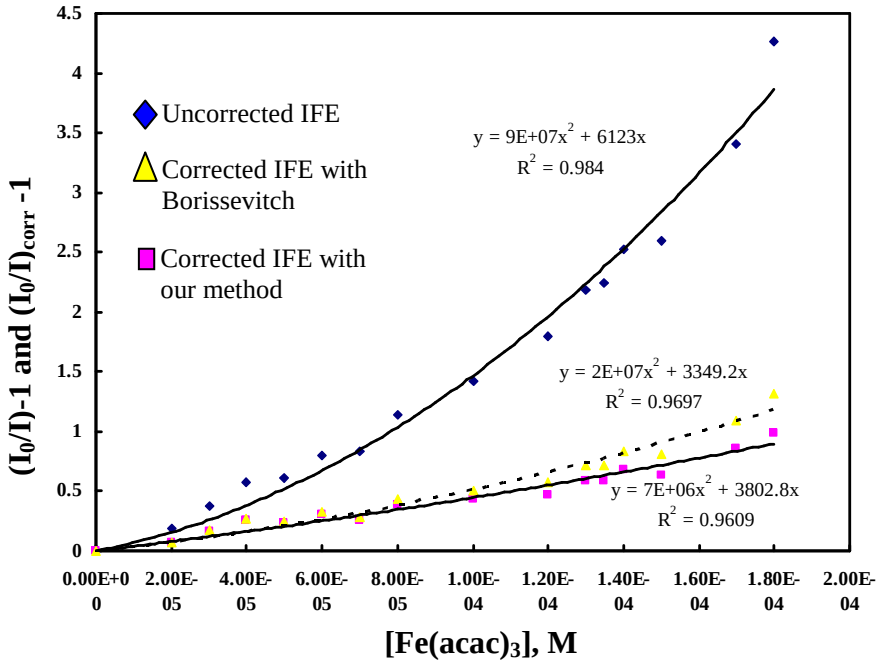

Figure 35 Stern-Volmer plots in toluene solution obtained from experiment with uncorrected IFE, corrected IFE with our method and corrected IFE with Borissevitch method.

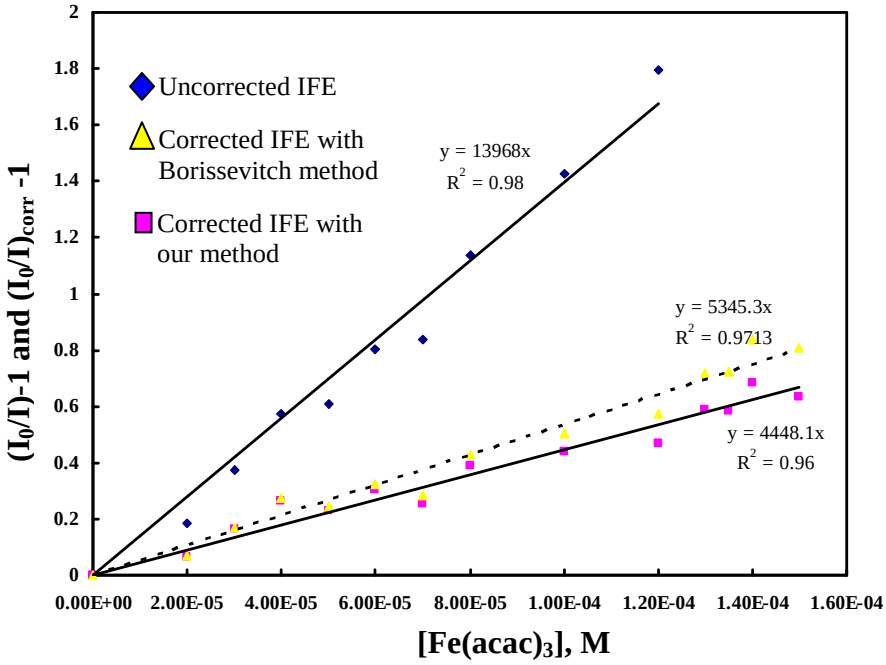

Figure 36 Linearity part of Stern - Volmer plots

Table 18 Fluorescence quenching data of chlorophyll a by $Fe(acac)_3$ in toluene

$K_{SV,\ exp}$ (M^{-1})	$K_{SV,corr/our}$ (M^{-1})	$K_{SV,corr/Boris}$ (M^{-1})	$k_{q,exp}$ ($M^{-1}s^{-1}$)	$k_{q,corr/our}$ ($M^{-1}s^{-1}$)	$k_{q,corr/Boris}$ ($M^{-1}s^{-1}$)
$1.39x10^4$	$4.45x10^3$	$5.34x10^3$	$2.76x10^{12}$	$5.92x10^{11}$	$7.10x10^{11}$

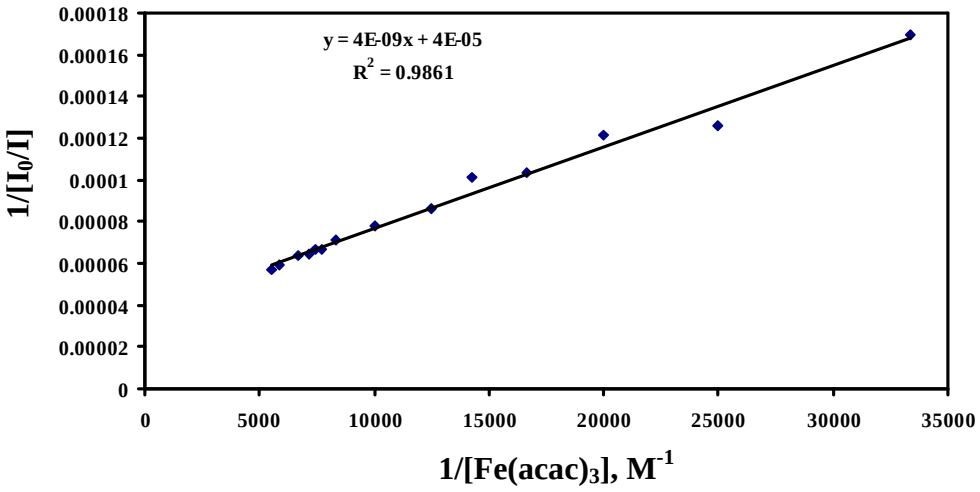

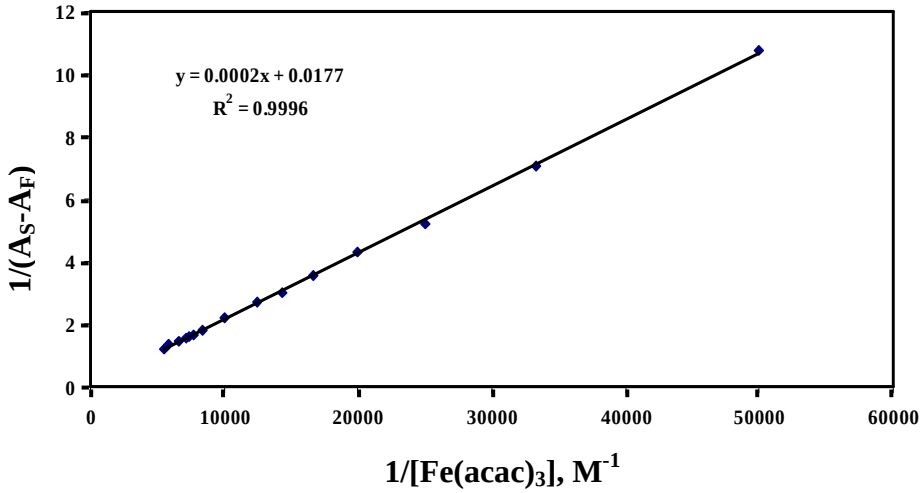

Figure 37 The Benesi and Hildebrand plots for determining K_{app} in toluene

The value of K_{app} obtained from the data of fluorescence quenching intensity ($1.00x10^4$ M^{-1}) does not match with the K_{app} from the absorption data (88.5 M^{-1}). The K_{app} obtained from fluorescence intensity gives higher value for 10^2 times than that of the data from absorbance. The difference of K_{app} is higher than that in benzene for 4 times. The assumption of ground state complex formation is less importance than inner filter effect.

3.3.3 Quenching reaction of chlorophyll a by $Fe(acac)_3$ in ethanol

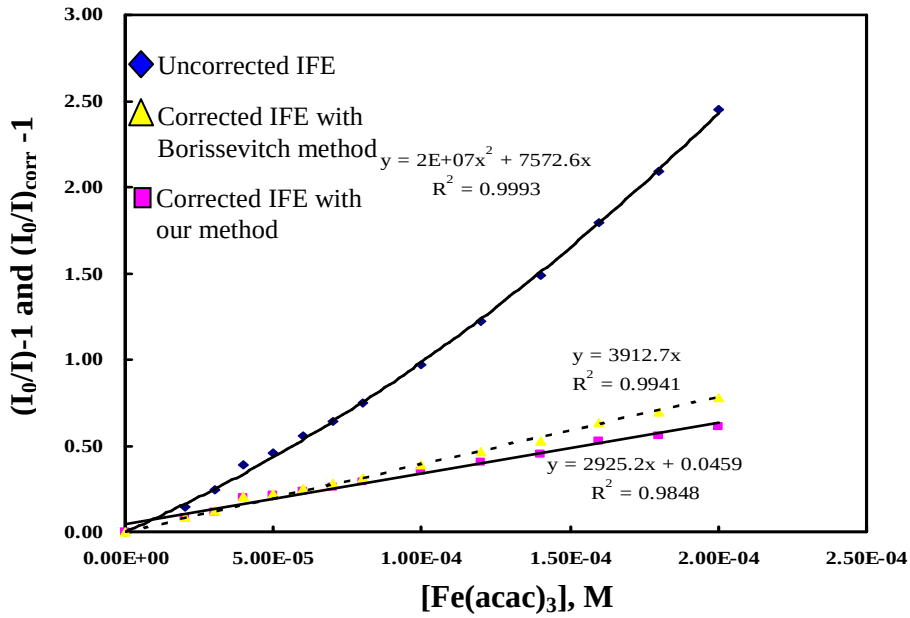

Figure 38 Stern-Volmer plots in ethanol solution obtained from experiment with uncorrected IFE, corrected IFE with our method and corrected IFE with Borissevitch method.

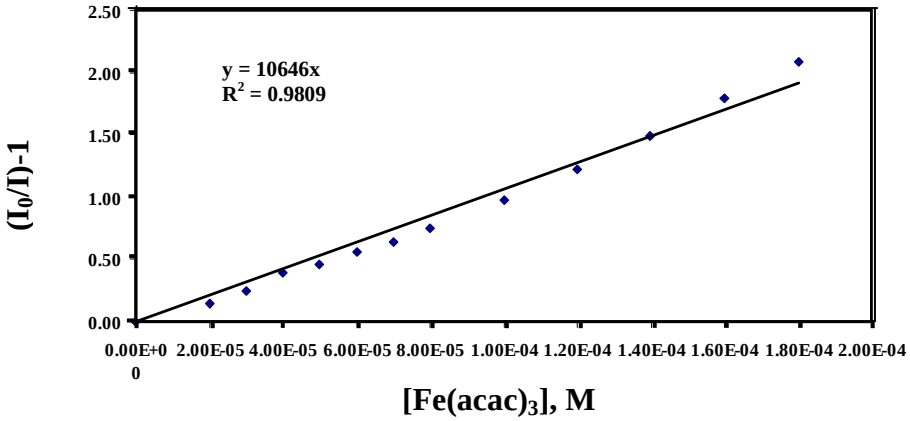

Figure 39 Linearity part of the Stern-Volmer plot in ethanol. Data obtained from the experiment with uncorrected inner filter effect.

Table 19 Fluorescence quenching data of chlorophyll a by $Fe(acac)_3$ in ethanol.

$K_{SV, exp}$ (M^{-1})	$K_{SV,corr/our}$ (M^{-1})	$K_{SV,corr/Boris}$ (M^{-1})	$k_{q,exp}$ ($M^{-1}s^{-1}$)	$k_{q,corr/our}$ ($M^{-1}s^{-1}$)	$k_{q,corr/Boris}$ ($M^{-1}s^{-1}$)
$1.10x10^4$	$2.92x10^3$	$3.91x10^3$	$1.80x10^{12}$	$4.77x10^{11}$	$6.38x10^{11}$

The Stern-Volmer plots obtained from the experiment without corrected inner filter effect obey the same tendency with other solvents. The curvature profile bends upward to the y-axis (Figure 38). The K_{SV} of this plot was determined from slope of the linearity part of the curve as shown in figure 39. The K_{SV} and k_q values from experiment gives higher value than that of the corrected inner filter effect by our method and Borissevitch, respectively. The corrected Stern-Volmer plots from two methods are both linear. The correction by our method gives a small deviation of intercept from unity for 4 %. The linearity of our correction and Borissevitch methods is in the concentration range up to $8x10^{-5}$ M.

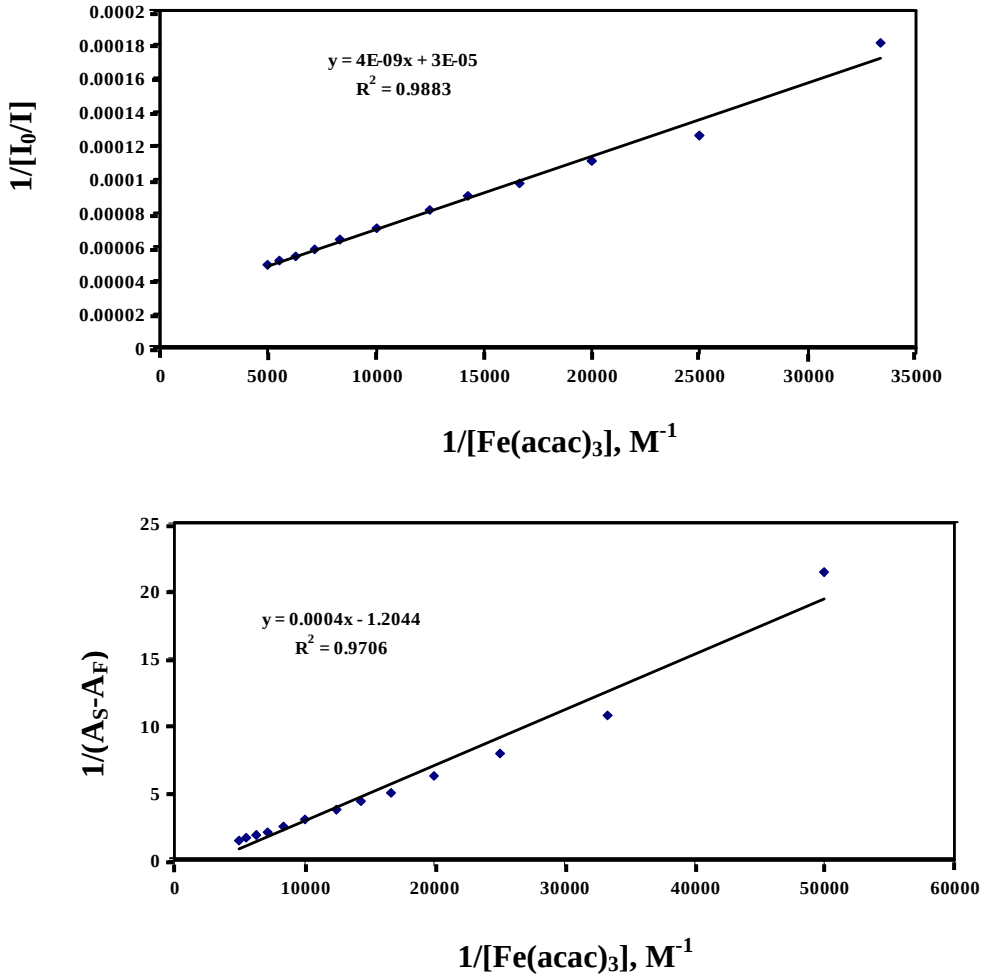

Figure 40 The Benesi and Hildebrand plots for determining K_{app} in ethanol

The difference of K_{app} values obtained from fluorescence intensity and absorbance (7.50×10^3 M^{-1} and 3.01×10^3 M^{-1}, respectively) becomes closer comparing with other solvents. It is possible to form a ground state complex but occurs slightly with a small equilibrium constant ($< 10^6$).

. 3.3.4 Quenching reaction of chlorophyll a by $Fe(acac)_3$ in methanol

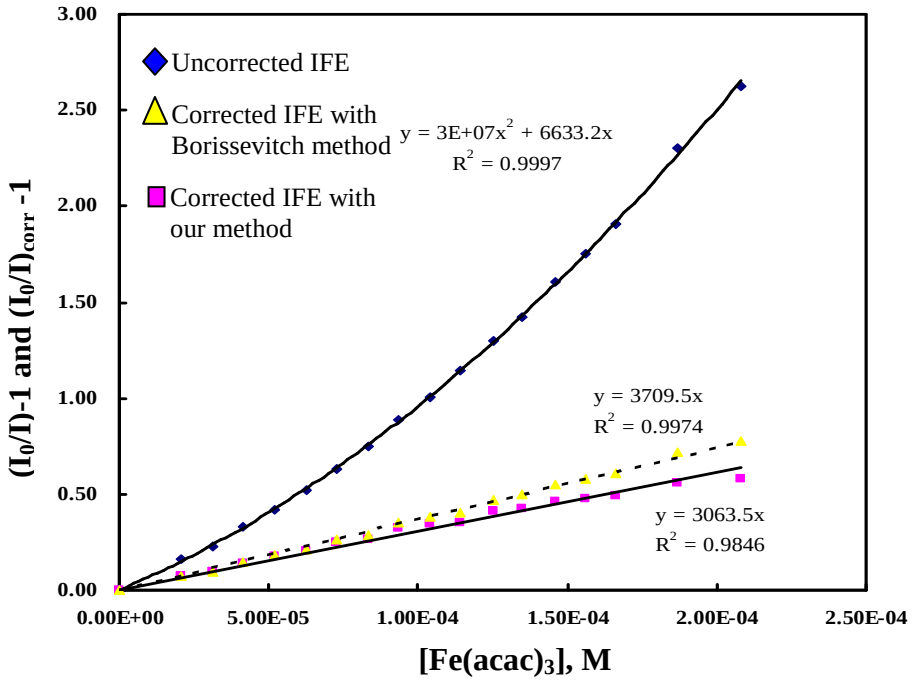

Figure 41 Stern-Volmer plots in methanol solution obtained from experiment with uncorrected IFE, corrected IFE with our method and corrected IFE with Borissevitch method.

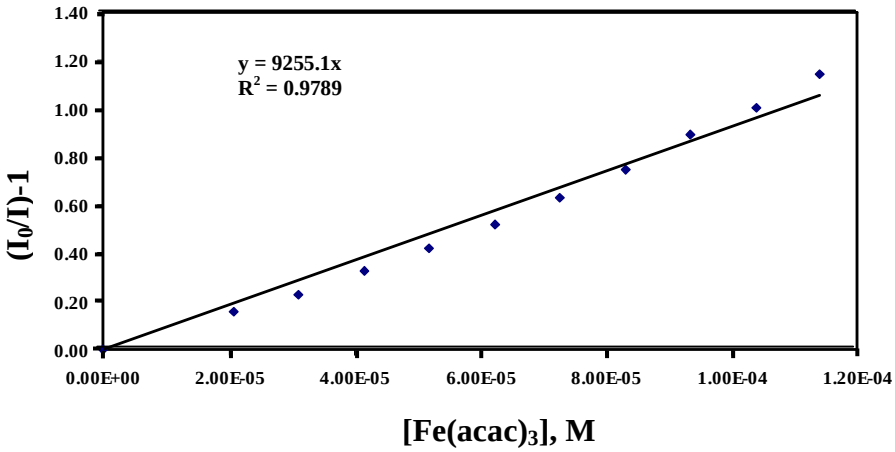

Figure 42 Linearity part of the Stern-Volmer plot in methanol. Data obtained from the experiment with uncorrected inner filter effect.

In methanol, the fitting of Stern-Volmer plots are most reasonable. The intercept is unity with high R^2 value. The behavior of quenching process is as same as that in other solvents. The experimental data gives Stern-Volmer to be a curvature (Figure 41). The K_{SV} and k_q for all data are expressed in table 23. The mechanism of static mechanism would be expected to be found even if the inner filter effect was not concerned. However, the calculated K_{app} from Benesi and Hildebrand plots (Figure 43) show small values. Besides, the K_{app} from intensity and absorbance are different for 10 times ($4.29x10^3$ M^{-1} and $4.37x10^2$ M^{-1}, respectively). The effect of inner filter still influences to make distortion of Stern-Volmer plot.

Table 20 Fluorescence quenching data of chlorophyll a by $Fe(acac)_3$ in methanol

$K_{SV, exp}$ (M^{-1})	$K_{SV,corr/our}$ (M^{-1})	$K_{SV,corr/Boris}$ (M^{-1})	$k_{q,exp}$ ($M^{-1}s^{-1}$)	$k_{q,corr/our}$ ($M^{-1}s^{-1}$)	$k_{q,corr/Boris}$ ($M^{-1}s^{-1}$)
$9.25x10^3$	$3.06x10^3$	$3.91x10^3$	$1.67x10^{12}$	$5.53x10^{11}$	$6.70x10^{11}$

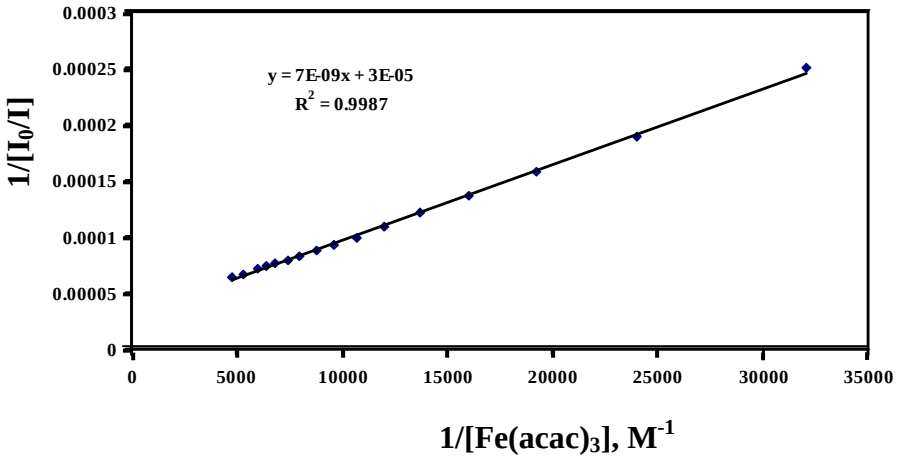

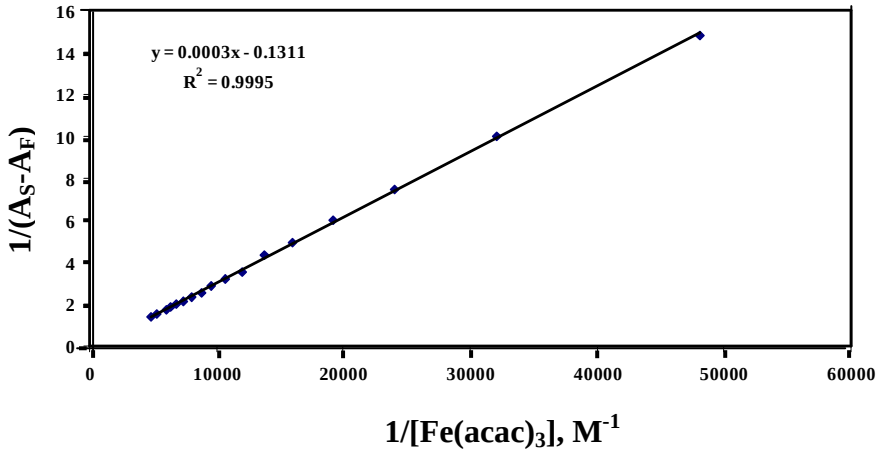

Figure 43 The Benesi and Hildebrand plots for determining K_{app} in methanol

3.3.5 Quenching reaction of chlorophyll a by [Fe(acac)$_3$] in DMF

The Stern-Volmer plots of the quenching of chlorophyll a by Fe(acac)$_3$ in DMF is shown in figure 44. The data of Stern-Volmer plots from experiment with uncorrected IFE, corrected IFE with our method and corrected IFE with Borissevitch method are collected (Appendix Table 13.2). The Stern-Volmer plots obtained from the experiment without corrected inner filter effect give the curvature profile bending upward to the y-axis. The K_{SV} of this plot is determined from slope of the linearity part of the curve (Figure 45). The K_{SV} value is high. In contrast, the corrected Stern-Volmer plots either from our method or Borissevitch method are linear. It is due to inner filter effect. The correction by our method gives lowest K_{SV} value. Our method and Borissevitch method make the deviation of intercept from unity for less than 10%. It is still reasonable within the experimental error. The data of K_{SV} and k_q values are collected in table 21). However, the linearity among two methods overlaps in the small concentration range up to $5x10^{-5}$ M.

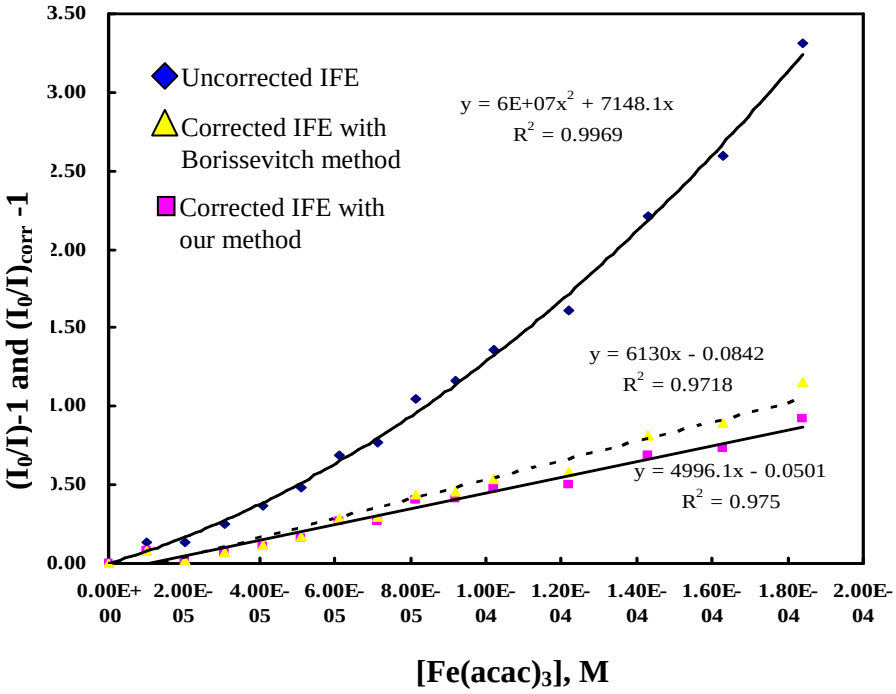

Figure 44 Stern-Volmer plots in DMF solution obtained from experiment with uncorrected IFE, corrected IFE with our method and corrected IFE with Borissevitch method.

Table 21 Fluorescence quenching data of chlorophyll a by $Fe(acac)_3$ in DMF

$K_{SV,\ exp}$ (M^{-1})	$K_{SV,corr/our}$ (M^{-1})	$K_{SV,corr/Boris}$ (M^{-1})	$k_{q,exp}$ ($M^{-1}s^{-1}$)	$k_{q,corr/our}$ ($M^{-1}s^{-1}$)	$k_{q,corr/Boris}$ ($M^{-1}s^{-1}$)
$1.37x10^4$	$5.00x10^3$	$6.13x10^3$	$2.02x10^{12}$	$7.36x10^{11}$	$9.03x10^{11}$

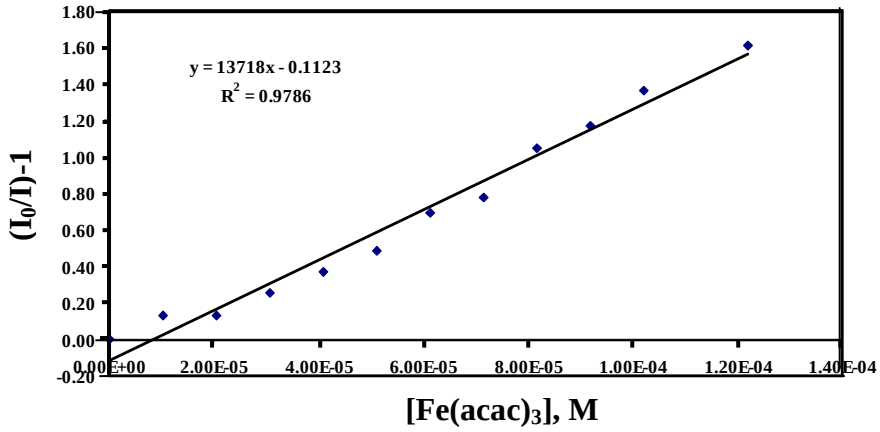

Figure 45 Linearity part of the Stern-Volmer plot in DMF. Data obtained from the experiment with uncorrected inner filter effect.

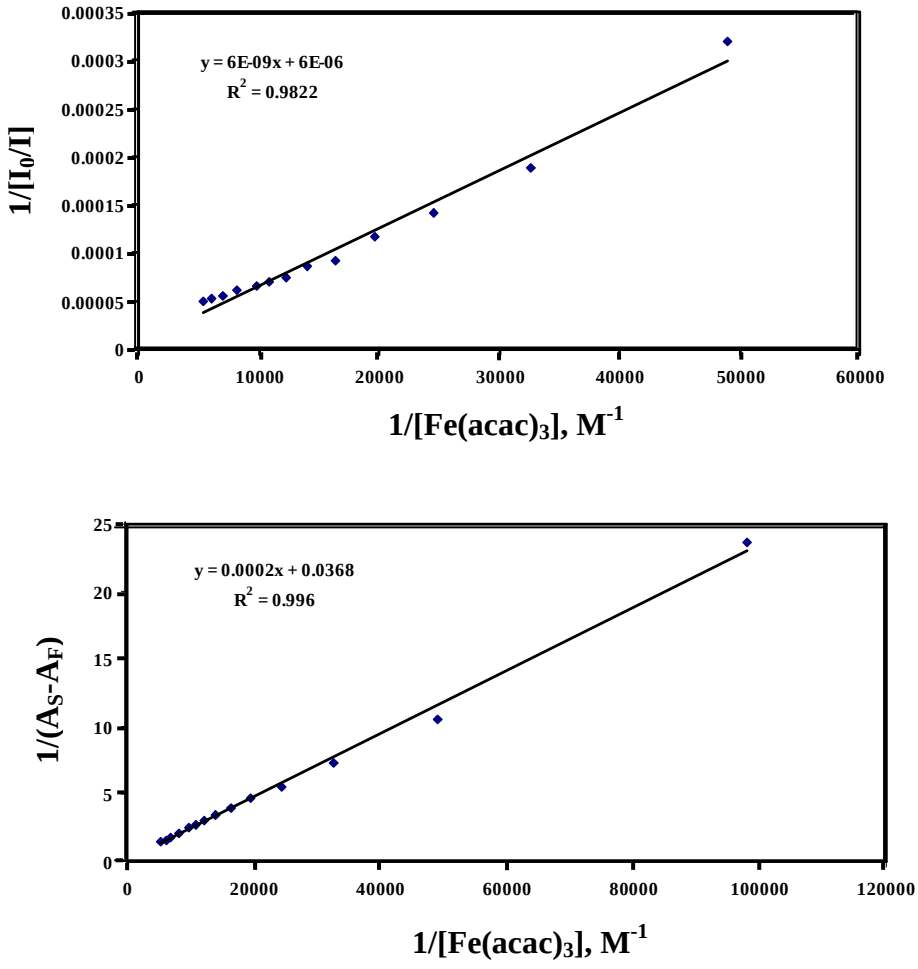

Figure 46 The Benesi and Hildebrand plots for determining K_{app} in DMF

The calculated K_{app} values from both fluorescence intensity and absorbance. Figure 46 are different for 5 times ($1.00x10^3$ M^{-1} and $1.84x10^2$ M^{-1}, respectively).

3.3.6 Quenching reaction of chlorophyll a by $Fe(acac)_3$ in DMSO

The Stern-Volmer plots of all data in DMSO are presented in figure 47. The experimental data gives Stern-Volmer to be a curvature. The k_q can be calculated from the linearity part. The K_{SV} and k_q for all data are expressed in table 22. For obtaining most reasonable R^2 value, the intercept is not unity but slightly deviate for less than 5 % within. The deviation occurs by the experimental error from preparation chlorophyll a concentrations. The behavior of quenching process is as same as that in other solvents.

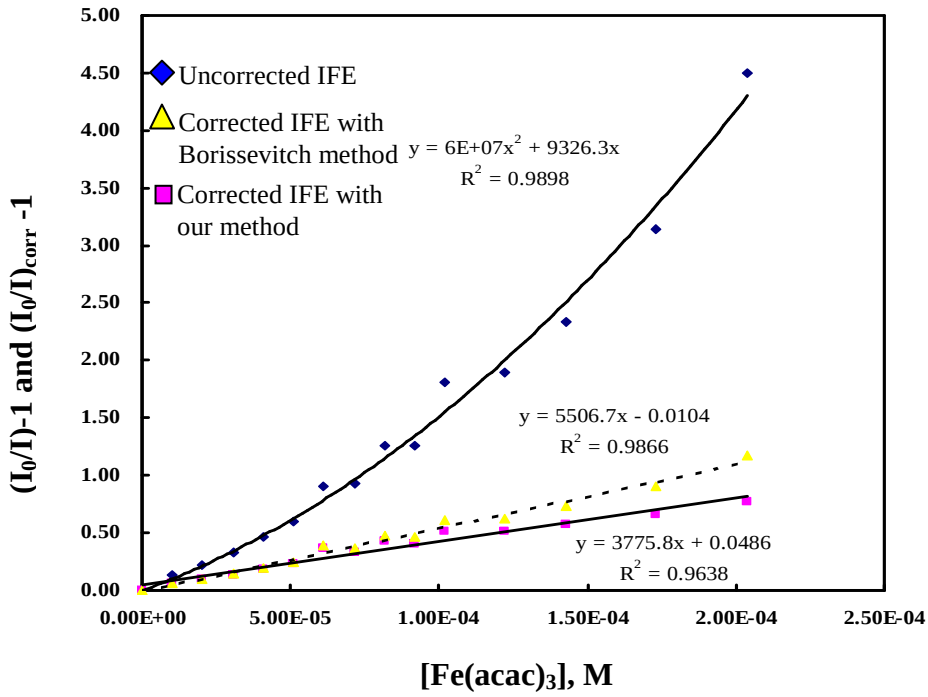

Figure 47 Stern-Volmer plots in DMSO solution obtained from experiment with uncorrected IFE, corrected IFE with our method and corrected IFE with Borissevitch method.

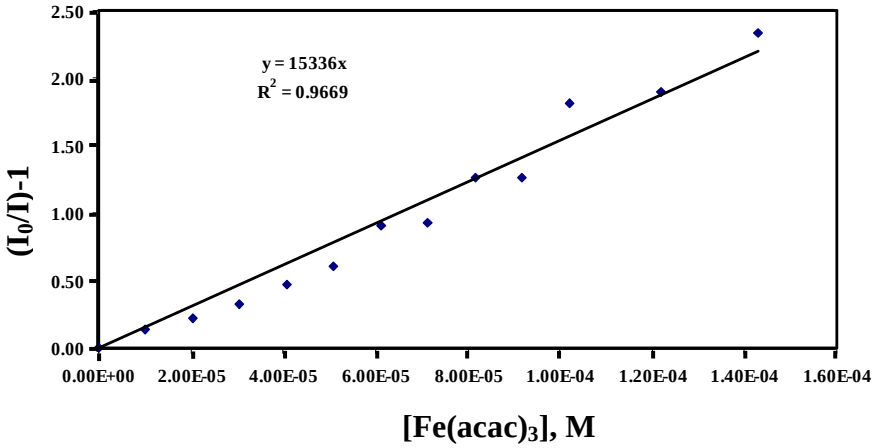

Figure 48 Linearity part of the Stern-Volmer plot in DMSO. Data obtained from the experiment with uncorrected inner filter effect.

Table 22 Fluorescence quenching data of chlorophyll a by $Fe(acac)_3$ in DMSO

$K_{SV,\ exp}$ (M^{-1})	$K_{SV,corr/our}$ (M^{-1})	$K_{SV,corr/Boris}$ (M^{-1})	$k_{q,exp}$ ($M^{-1}s^{-1}$)	$k_{q,corr/our}$ ($M^{-1}s^{-1}$)	$k_{q,corr/Boris}$ ($M^{-1}s^{-1}$)
$1.53x10^4$	$3.78x10^3$	$5.51x10^3$	$2.57x10^{12}$	$6.51x10^{11}$	$9.50x10^{11}$

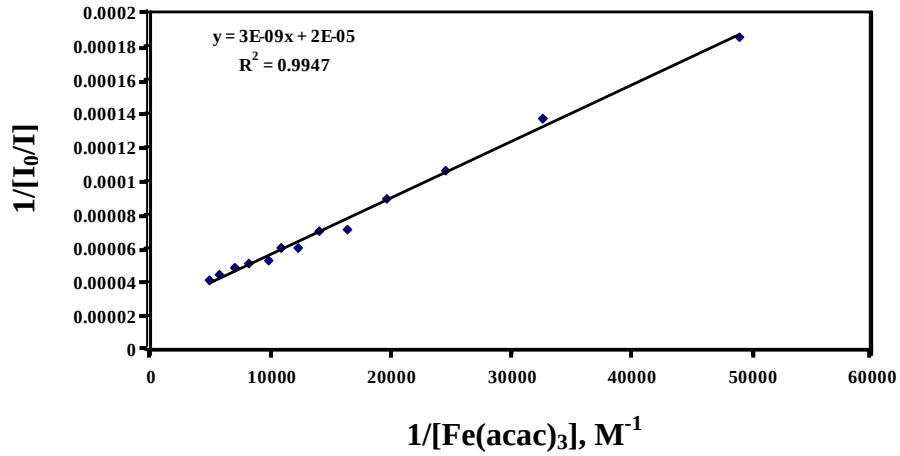

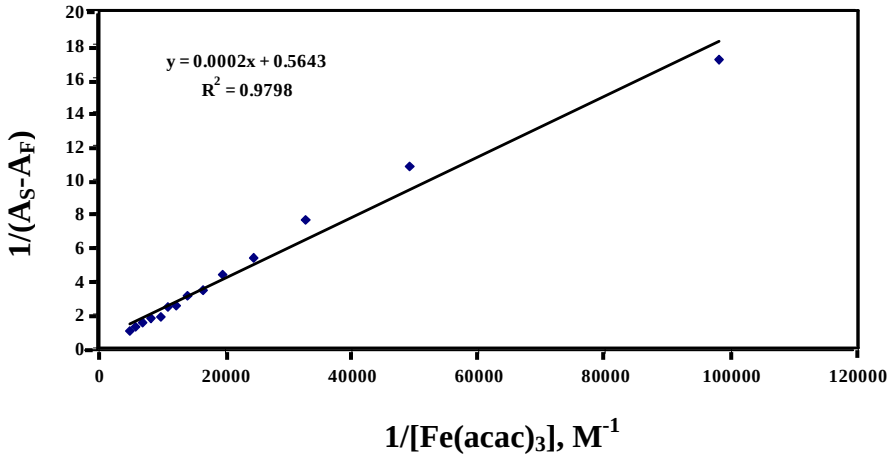

Figure 49 The Benesi and Hildebrand plots for determining K_{app} in DMSO

The calculated K_{app} from Benesi and Hildebrand plots (Figure 49) show small values. Besides, the K_{app} from intensity and absorbance are different for only 3 times (6.67×10^3 M^{-1} and 2.82×10^3 M^{-1}, respectively). The ground state complex formation can occur insignificantly.

. 3.3.7 Quenching reaction of chlorophyll a by $Fe(acac)_3$ in acetonitrile

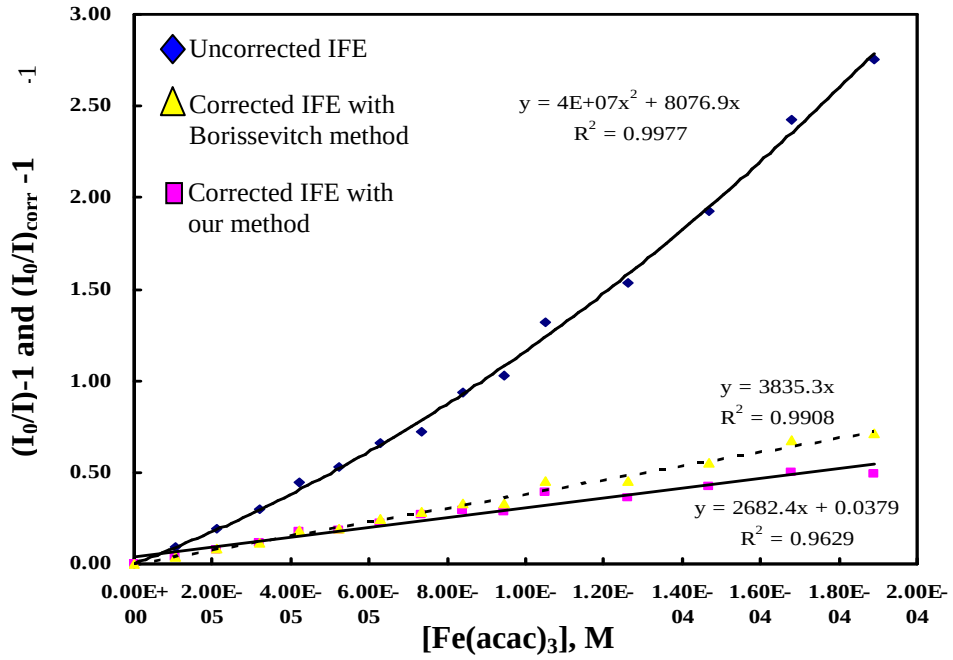

Figure 50 Stern-Volmer plots in acetonitrile solution obtained from experiment with uncorrected IFE, corrected IFE with our method and corrected IFE with Borissevitch method.

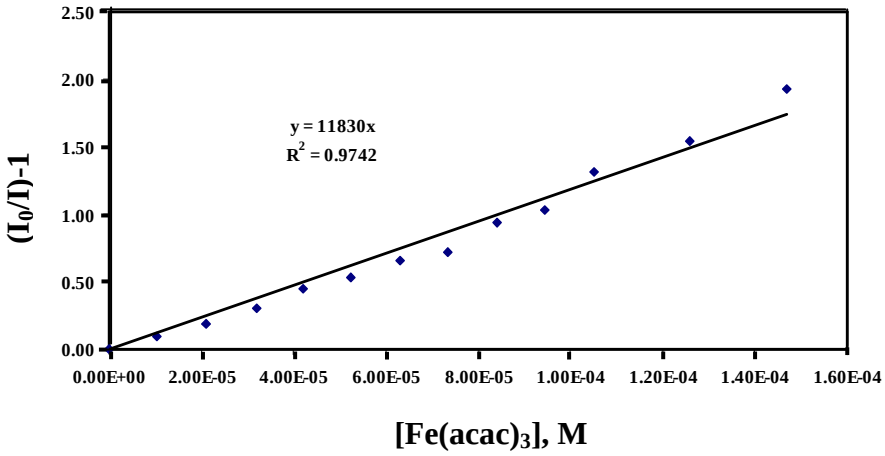

Figure 51 Linearity part of the Stern-Volmer plot in acetonitrile. Data obtained from the experiment with uncorrected inner filter effect.

Table 23 Fluorescence quenching data of chlorophyll a by $Fe(acac)_3$ in acetonitrile

$K_{SV, exp}$ (M^{-1})	$K_{SV,corr/our}$ (M^{-1})	$K_{SV,corr/Boris}$ (M^{-1})	$k_{q,exp}$ ($M^{-1}s^{-1}$)	$k_{q,corr/our}$ ($M^{-1}s^{-1}$)	$k_{q,corr/Boris}$ ($M^{-1}s^{-1}$)
$1.53x10^4$	$2.68x10^3$	$3.84x10^3$	$2.27x10^{12}$	$3.97x10^{11}$	$5.69x10^{11}$

The data of Stern-Volmer plots from experiment with uncorrected IFE, corrected IFE with our method and corrected IFE with Borissevitch method are collected(Appendix Table 15.2). The Stern-Volmer plots of the quenching of chlorophyll a by $Fe(acac)_3$ in acetonitrile is shown in figure 50. All types of Stern-Volmer plots give the curvature profiles bending upward to the y-axis as like as in other solvents. The K_{SV} of this plot was determined from slope of the linearity part of the curve (Figure 51). As like as in other solutions, the K_{SV} from an uncorrected intensity give much higher value than that of the corrected data. The K_{SV} values from both correction methods are similar. The data of K_{SV} and k_q values are collected in table 23.

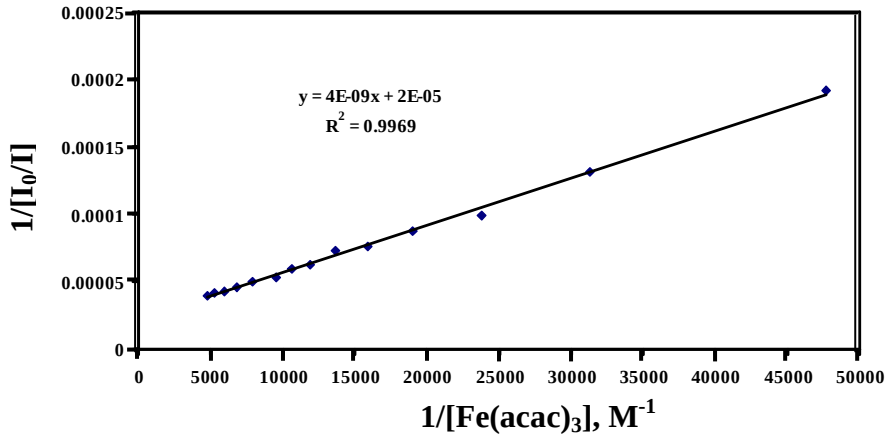

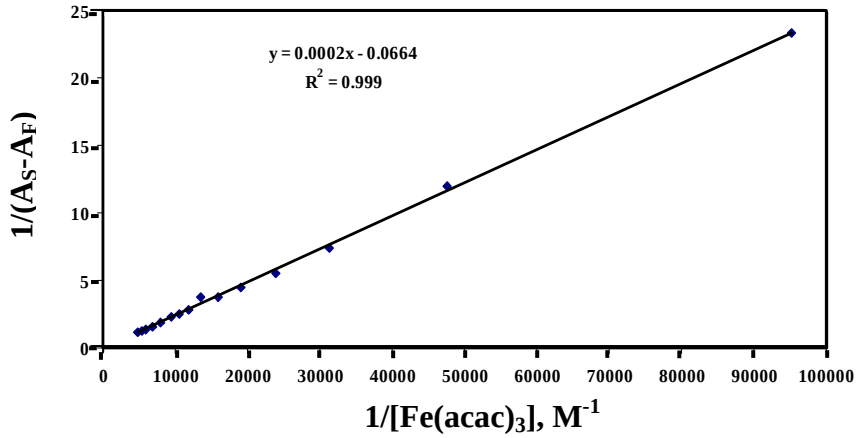

Figure 52 The Benesi and Hildebrand plots for determining K_{app} in acetonitrile

The calculated K_{app} from Benesi and Hildebrand plots (Figure 52) show small values. Besides, the K_{app} from intensity and absorbance are obvious different (5.00×10^3 M^{-1} and 3.32×10^2 M^{-1}, respectively). The effect of inner filter still influences to make distortion of Stern-Volmer plot.

3.4 Solvent effect of Quenching reactions.

Quenching reactions were carried out in various types of solvents. The solvent properties are different. The rate of reactions and the apparent association constants are summarized in table 24. Solvents properties like viscosity are different.

Table 24 Quenching rate constants obtained from Stern-Volmer plots of uncorrected and corrected inner filter effect by our method and Borissevitch method in various solvents.

solvent	[a]Viscosity (cP)	k_q x 10^{-11} ($M^{-1}s^{-1}$)			K_{app} (M^{-1})	
		experiment	Our method	Borissevitch method	Intensity x 10^{-3}	Absorbance x 10^{-2}
MeCN	0.352	22.7	3.97	5.69	5.00	3.32
MeOH	0.544	16.7	5.53	6.70	4.29	4.37
Toluene	0.560	27.6	5.92	7.10	10.0	0.88
Benzene	0.604	27.6	6.76	9.49	13.3	5.26
DMF	0.802	20.2	7.36	9.03	1.00	1.84
EtOH	1.074	18.0	4.77	6.38	7.50	3.01
DMSO	2.140	25.7	6.51	9.50	6.67	28.2

[a] viscosity reported at 25 ^{o}C

Figures 53a to Figure 53c are all the plots between quenching rate constants and solvent viscosities. The quenching rate constants in figure 53a are obtained from the experimental data without correcting inner filter effect. The data in figure 53b and figure 53c are collected from the inner filter effect correction by our method and Borisseivitch method, respectively. It is clearly seen that without correcting of inner filter effect, no tendency of quenching rate constants with viscosities is observed. In contrast with the data in figure 53b, the quenching rate constants show the dependence of quenching rate constants on solvent viscosities from acetonitrile through out DMF. Likewise, the data in figure 53c, the quenching rate constants exhibit the tendency with solvent viscosities from acetonitrile to benzene.

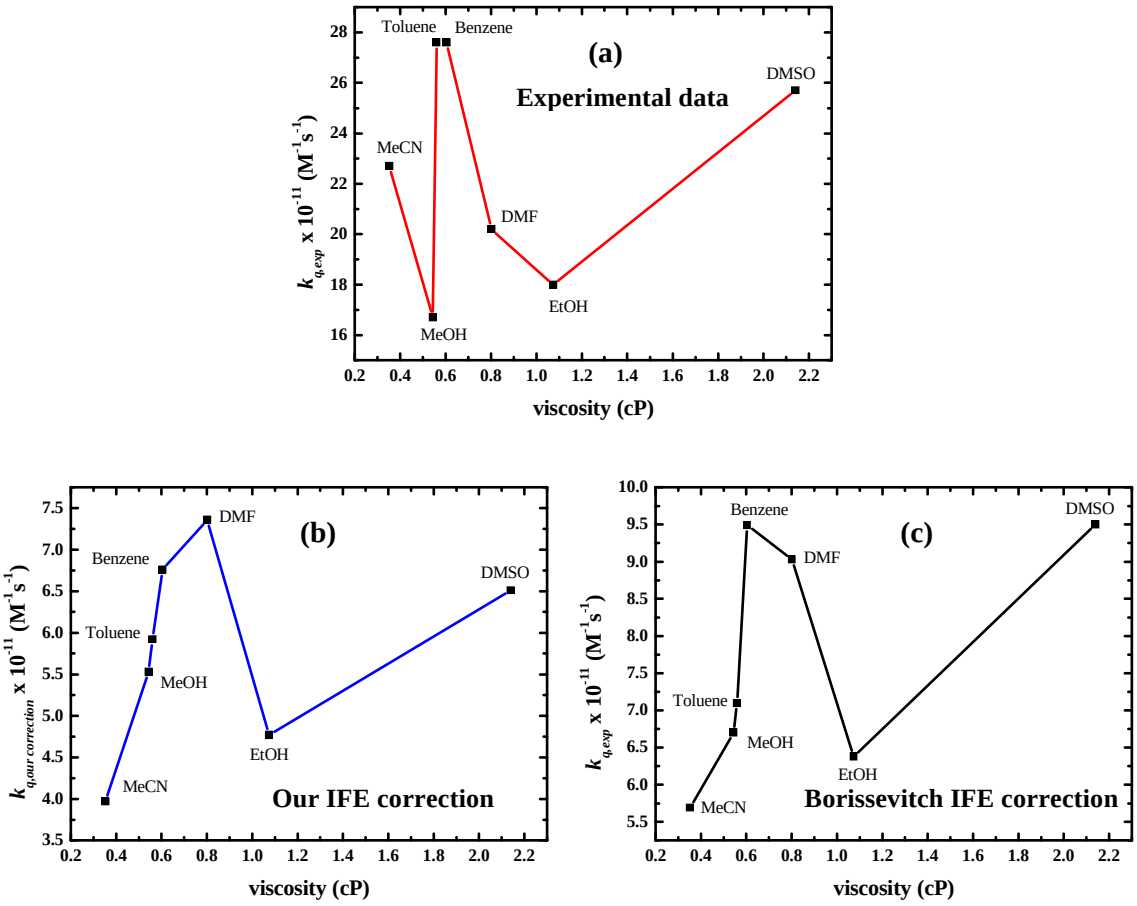

Figure 53 Investigation of effect of solvent viscosities on rates of quenching reactions.

(a) The k_q values obtained from experimental data without correcting of inner filter effect.

(b) The k_q values obtained from the correction of inner filter effect by our method.

(c) The k_q values obtained from the correction of inner filter effect by Borissevitch method.

The viscosity is an important factor for diffusion coefficient in electron transfer system. The viscous solvent can prevent the escape of charge transfer. It can bring donor and acceptor molecules closer to each other and solvate around. In another word, the diffusion rate constant is high. It leads to an increasing of electron transfer ability. However, there is the fluctuation of quenching ability in ethanol which is not obeying the expectation. There might be some other factor occur complexity. The fluctuation of result does not come from an artifact because the experiments were carried out for two times. We still get the same result. Besides, the excellent R^2 obtained from fitting the Stern-Volmer was obtained.

As a result of quenching data the K_{app} tendency can be supposed to depend also on viscosity of solvent in the same manner. It can be seen from the K_{app} which obtained from absorption data. The K_{app} increases with increasing of solvent polarities like the acetonitile, methanol, benzene and DMSO (Figure 54). Nevertheless, it has to be remined that the K_{app} obtained from the experimental data which exists of inner filter effect. It can not consider from the intensity data because the intensity of experimental data is unrealistic. In addition, even if the corrected intensity were used to calculate the K_{app}, the result would be exactly the same with the experimental data without correcting the inner filter effect. We cannot use the equation of Benesi and Hildebrand to see the difference of inner filter effect.

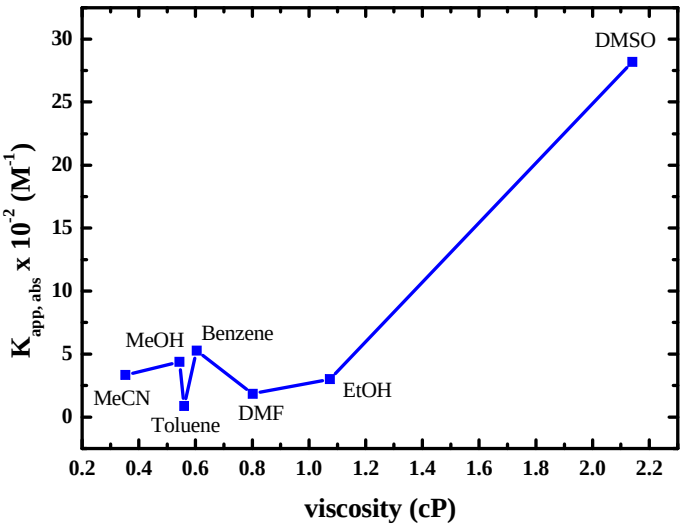

Figure 54 Investigation of effect of solvent viscosities on the apparent association constant.

CHAPTER 4

CONCLUSIONS

This research study about photo-physical properties; absorption, fluorescence emission and lifetimes of chlorophyll a and $Fe(acac)_3$ were investigated. It was clearly that higher viscosity and polarity of solvents. The emission will show at the less energy which means that the wavelength of emission getting longer. The longer emission wavelength shifting or red shift have significant. Because of the excited state is more polar than the ground state, the excited state will be stabilized. While the maximum wavelength of absorption shows no trend at all. It is different from what we obtained from emission spectra. The lifetimes of chlorophyll a in various solvents found that not dependent upon quality is solvents. The lifetimes of chlorophyll a are in the range of 5.5 to 7.5 nanoseconds. There is a monoexponential decay, observe from lifetime measured. There is not dependent frequency of modulate signal of fluorescence by phase modulation technique.

Moreover, there are study about kinetic of electron transfer between chlorophyll a and $Fe(acac)_3$ through quenching reaction in various solvents. The electron transfer occurs in studied reaction fastly. The rate of quenching reaction (k_q) high among range 10^{11}-10^{12} $M^{-1}s^{-1}$. There can be conclude relationship trend about viscosity of solvents higher. The rate of quenching reaction have more higher explain that quenching mechanism in various solvents. When acceptor molecule was different found that quenching mechanism 2 type. That is collisional quenching mechanism and combination of collisional and static quenching mechanism. We are conclude from Stern-Volmer plot. The collisional quenching mechanism it gives the linear plot following the Stern-Volmer plot. The non-linear behavior shows the curvature upward to the Y-axis. There are tells us that the mechanism of quenching is the combination of static and collisional quenching mechanism. The rate of quenching reaction by $Fe(acac)_3$ upon with kind of solvents and viscosity. The viscosity of solvents is lower . Such as acetonitrile and methanol will be electron transfer process is the collisional quenching mechanism. But the viscosity of solvents is higher. Such as DMF, DMSO

and THF will be occurred electron transfer is the static quenching mechanism together.

In this research, there are both of chemicals explain that the rate of quenching reaction (k_q) which have chance electron transfer only. There will be tell us to known the electron transfer correctly. There are study the diffusion rate constant (k_d) combining with that the rate will get k_{et}.

However, In this research was more useful in the exploring research. The possibility of selecting system to electron transfer in basically. This thesis forward ahead to successful and complete. Therefore other thing study method of electron transfer can be used application works. Such as the electron transfer process in dye-sensitized solar cell.

REFERENCES

Amao, Y., Yamada, Y., Aoki, K. 2004. Preparation and properties of dye-sensitized solar cell using chlorophyll derivative immobilized TiO_2 film electrode. *J. Photo. Photobiol. A: Chem*. 164: 47-51.

Borissevitch, I. E. 1999. More about the inner filter effect : corrections of Stern-Volmer fluorescence quenching constants are necessary at very low optical absorption of the quencher. *Journal of Luminescence*. 81: 219-224.

Clark, C. D. and Hoffman, M. Z. 1997. Effect of solution medium on the rate constants of excited-state electron-transfer quenching reactions of ruthenium(II)- diimine photosensitizers. *Coord. Chem. Rev*. 159: 359-373.

Cotton, T. M., Trifunac, A. D. and Katz, J. J. 1974. State of chlorophyll *a* in vitro and in vivo from electronic transition spectra, and the nature of antenna chlorophyll. *Biochimica et Biophysica Acta BBA-Bio energetics*. 181-198.

David, P. R. and Raymond, C. 2007. Lecture Demonstrations of Fluorescence and Phosphorescence. *Chem. Educator*. 12: 279-281.

Diaz-Acosta, I., Baker, J., James, F. H. and Pulay, P. 2002. Calculated and experimental geometries and infrared spectra of metal tris-acetylacetonates: vibrational spectroscopy as a probe of molecular structure for ionic complexes. Part II. *Spectrochimica Acta Part A: Molecular and Biomolecular Spectroscopy*. 59(2): 363-377.

Durrant, J. R., Haque, S. A., Palomares, E. 2004. Towards optimisation of electron transfer processes in dye-sensitized solar cells. *Coord. Chem. Rev*. 248 : 1247-1257.

Flor^encio, M. H., Pires, E., Costa, M., Markovic, D. 2004. Photodegradation of Diquat and Paraquat in aqueous solutions by titanium dioxide: evolution of degradation reactions and characterization of intermediates. *Chemosphere*. 55: 345-355.

Gazdaru, D. 2001. Characterization of the fluorescence quenching of chlorophyll a by 1, 4 benzoquinone using the nonlinear. *Journal of Optoelectronics and Advanced Materials*. 3(1): 145-148.

Jennings, R. C., Zucchelli, G., Garlaschi, F. M. 1989. The influence of reducing the chlorophyll concentration by photobleaching on energy transfer to artificial traps within Photosystem II antenna systems. *Biochim et Biophys. Acta (BBA)-Bioen*. 975: 29-33.

Kathiravan, A., Chandramohan, M., Renganathan, R., Sekar, S. 2009. Cyanobacterial chlorophyll as a sensitizer for colloidal TiO_2. *Spectro chimica Acta Part A : Molecular and Biomolecular Spectroscopy*. 71: 1783-1787.

Kereïche, S., Kouřil, R., Oostergetel, G. T., Fusetti, F., Boekema, E. J., Doust, A. B., van der W.-de W, C. D., Dekker, J. P. 2008. Association of chlorophyll a/c_2 complexes to photosystem I and photosystem II in the cryptophyte Rhodomonas CS24. *Biochimica et Biophysica Acta*. 1777: 1122-1128.

Kobayashi, M., Ohashi, S., Iwamoto, K., Shiraiwa, Y., Kato, Y., Watanabe, T. 2007. Redox potential of Chlorophyll d in vitro. *Biochim. Biophy. Acta*. 596-602.

Kuroiwa, Y., Kato, Y., Watanabe, T. 2009. Negative shift of chlorophyll a oxidation potential by aggregation in acetonitrile/ionic liquid mixed solvents. *Journal of Photochemistry and Photobiology A: Chemistry*. 202(2-3): 191-195.

Landgraf, S. and Grampp, G. 1996. Application of cw-laser diodes for the determination of fluorescence lifetimes. *J. Inf. Rec. Mater*. 23: 203-207.

Landgraf, S. and Grampp, G. 2000. Subnanosecond Time Resolved Fluorescence Lifetime Spectrometer Applying Laser Diodes. *Chemical Monthly*. 131: 839-848.

Landgraf, S. 2004. Use of ultrabright LEDs for the determination of static and time-resolved fluorescence information of liquid and solid crude oil samples *J. Biochem. Biophysics. Methods*. 61: 125-134.

Lakowicz, J. R. 2006. Principles of Fluorescence Spectroscopy, Kluwer Academic/ Plenum Publishers, New York.

Lai, W. H., Su, Y. H., Teoh, L. G., Hon, M. H. 2008. Commercial and natural dyes as photosensitizers for a water-based dye-sensitized solar cell loaded with gold nanoparticles. *J. Photochem. Photobiol A: Chem*. 195: 307-313.

Larsson, T., Wedborg, M., Turner, D. 2007. Correction of inner-filter effect in fluorescence excitation-emission matrix spectrometry using Raman scatter. *Analytica Chimica Acta*. 583: 357–363.

Leesakul, N. 2007. Kinetics of Fast Photo-induced Electron Transfer from Tris(bpy)Ruthenium(II) and Tris(bpy)Osmium(II) Complexes to Iron (III) in water and n-Alcohols.

Li, S. and Inoue, H. 1991. Separation of manganese(II, III) chlorophylls. *Anal. Science*. 7: 121-124.

Liu, B.-Q., Zhao, X.-P., Luo, W. 2008. The synergistic effect of two photosynthetic pigments in dye-sensitized mesoporous TiO_2 solar cells. *Dye and Pigments*. 76: 327-331.

Maciej, G., Patrycja, N., Małgorzata, R. 2004. The action of oxygen on chlorophyll fluorescence quenching and absorption spectra in pea thylakoid membranes under the steady-state conditions. *J.Photochem. Photobiol. B: Biol*. 77: 79-92.

Marcus, R. A. 1997. Electron transfer reactions in chemistry. Theory and experiment *Pure and Applied Chemistry*. 69(1): 13-29.

Maxwell, K. and Johnson, G. N. 2000. Chlorophyll fluorescence-a practical guide. *J. Exp. Bot*. 51: 659-668.

Medforth, C., Muzzi, C. M., Shea, K. M., Smith, K. M., Abraham, R. J., Jia, S., Shelnutt, J. A. 1997. NMR studies of nonplanar porphyrins. Part 2. Effect of nonplanar conformational distortions on the porphyrins ring current. *J. Chem. Soc., Perkin Trans*. 2: 839-844.

Moreira, L. M., Lima, A., Soares, R. R. S., Batistela, V. R., Gerola, A. P., Hioka, N., Bonacin, J. A., Severino, D., Baptista, M. S., da Hora Machado, A. E., Rodrigues, M. R., Codognotoa, L., de Oliveira, H. P. M. 2009. Metallochlorophylls of Magnesium, Copper and Zinc: Evaluation of the Influence of the First Coordination Sphere on their Solvatochromism and Aggregation Properties. *J. Braz. Chem. Soc*. 20(9): 1653-1658.

Nanomura, Y., Hatano, H., Fukuda, K., Inoue, H.1994. Preparation and determination of cobalt(II)chlorophylls by high-performance liquid chromatography. *Anal. Science*. 10: 117-119.

Nanomura, Y., Igarashi, S., Yoshioka, N., Inoue, H. 1997. Spectroscopic properties Of chlorophylls and their derivatives. Influence of molecular structure on the electronic state. *Chemical Physics*. 220: 155-166.

Ngweniform, P., Kusumoto, Y., Ikeda, M., Somekawa, S., Ahmmad, B., Kurawaki, J., Hayakawa, K. 2007. Photophysical and photo chemical studies of chlorophyll a and cobalt(II)tetraphenylporphyrin in poly(l-glutamate)-decylammonium ion complex. *J. Photo. Photobiol. B: Biol*. 87: 154-162.

Rajagopal, S., Egorova, E. A., Bukhov, N. G., Carpentier, R. 2003. Quenching of excited states of chlorophyll molecules in submembrane fractions of Photosystem I by exogenous quinines. *Biochim. et Biophys. Acta (BBA)-Bioen*. 1606: 147-152.

Richert, S. A., Tsang, P. K. S., Sawyer, D. T. 1989. Ligand-Centered Redox Processes for MnL_3, FeL_3, and CoL_3 Complexes (L = Acetylacetonate, 8-Quinolinate, Picolinate, 2,2'-Bipyridyl, 1,10-Phenanthroline) and for Their Tetrakis (2, 6-dichlorophenyl) porphinato Complexes [(Por)]. *Inorg. Chem*. 28: 2471-2475.

Schweitzer, R. H., Melkozernov, A. N., Blankenship, R. E., Brudvig, G. W. 1998. Time-Resolved fluorescence measurements of photosystem II. The effect of quenching by oxidized chlorophyll z. *J. Phys. Chem. B*. 102: 8320-8326.

Sergio, L., David, E. N., Thomas, A. M., Ana, L. M., Devens, G. 1996. Synthesis and Fluorescence Quenching Studies of a Series of Carotenoporphyrins with Carotenoids of Various Lengths. *J. Braz, Chem. Soc*. 7(1): 19-29.

Smestad, G. P. 1998. Education and solar conversion : Demonstrating electron. *Solar Energy Materials and Solar Cells*. 55: 157-178.

Song, Y., Zhang, D. X., Zhang, H. J. 2006. Study of 660 nm laser-induce photo luminescence of chlorophyll a and its applications. *Journal of Physics: Conference Series*. 48: 1488-151.

Teruhiro, T., Hiroshi, I., Satsuki, N., Shigeru, I. 1983. Effects of pH and magnesium on the electron transfer reactions between P700 - chlorophyll a protein complex and plastocyanin. *J. Biochem*. 94: 1901-1911.

Thander, A., Mallik, B. 2000. Photoinduced charge-transfer between ferrocene derivatives and chloroform molecules confined in poly(methyl methacrylate) thin films. *Chem. Phys. Lett*. 330: 521-527.

Wang, X.-F., Matsuda, A., Koyama, Y., Nagae, H., Sasaki, S.-I., Tamiaki, H., Wada, Y. 2006. Effects of plant carotenoid spacers on the performance of a dye-sensitized solar cell using a chlorophyll derivative: Enhancement of photocurrent determined by one electron-oxidation potential of each carotenoid. *Chem. Phys. Lett*. 423: 470-475.

Wang, X.-F., Zhan, C.-H., Maoka, T., Wada, Y., Koyama, Y. 2007. Fabrication of dye – sensitized solar cells using chlorophylls c_1 and c_2 and their oxidized forms and from Undariapinnatifida (Wakame). *Chem. Phys. Lett*. 447: 79-85.

Xiaoqing, L., Mingyu, S., Chao, L., Lu, Z., Wenhui, S., Fashui, H. 2007. Effects of $CeCl_3$ on Energy Transfer and Oxygen Evolution in Spinach Photosystem II. *J. Rare Earths*. 25: 624-630.

Yamashita, H. and Inoue, H. 1991. Determination of Zinc(II)chlorophylls and their derivatives by high performance liquid chromatography with fluorometric detection. *Anal. Science*. 7: 1371-1374.

Zvezdanovic, J., Cvetic, T., Veljovic-Jovanovic´, S., Markovic´, D. 2009. Chlorophyll bleaching by UV-irradiation in vitro and in situ: Absorption and fluorescence studies. *Radiation Physics and Chemistry*. 78: 25-32.

Zvezdanovic, J., Markovic, D. 2008. Bleaching of chlorophylls by UV-irradiation in vitro : the effects on chlorophyll organization in acetone and n-hexane. *J. Serb. Chem. Soc*. 73(3): 271-282.

APPENDIX

1. Photo-Physical Properties of chlorophyll a and $Fe(acac)_3$ in various solvents.

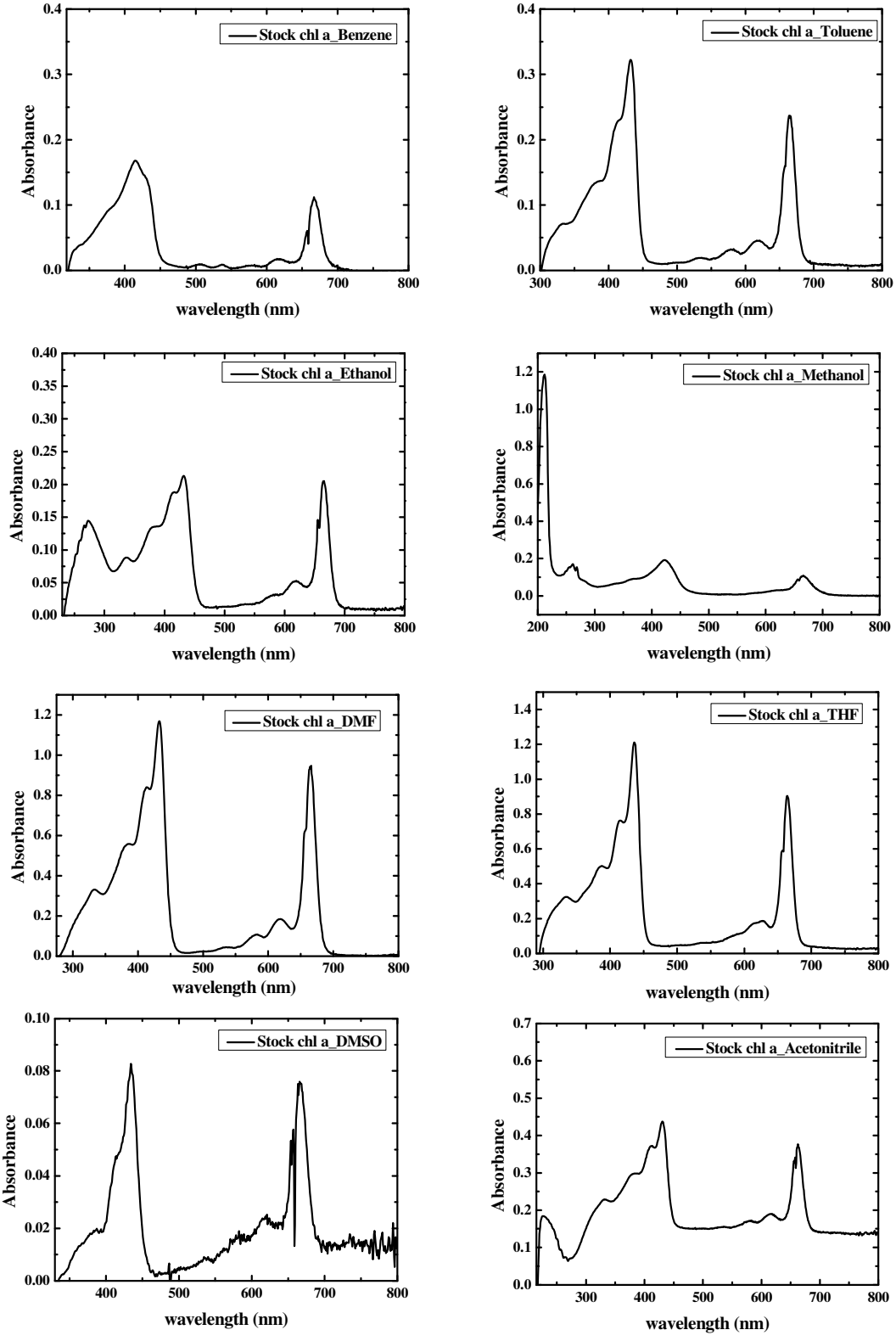

Figure 1 Absorption spectra of chlorophyll a in various solvents.

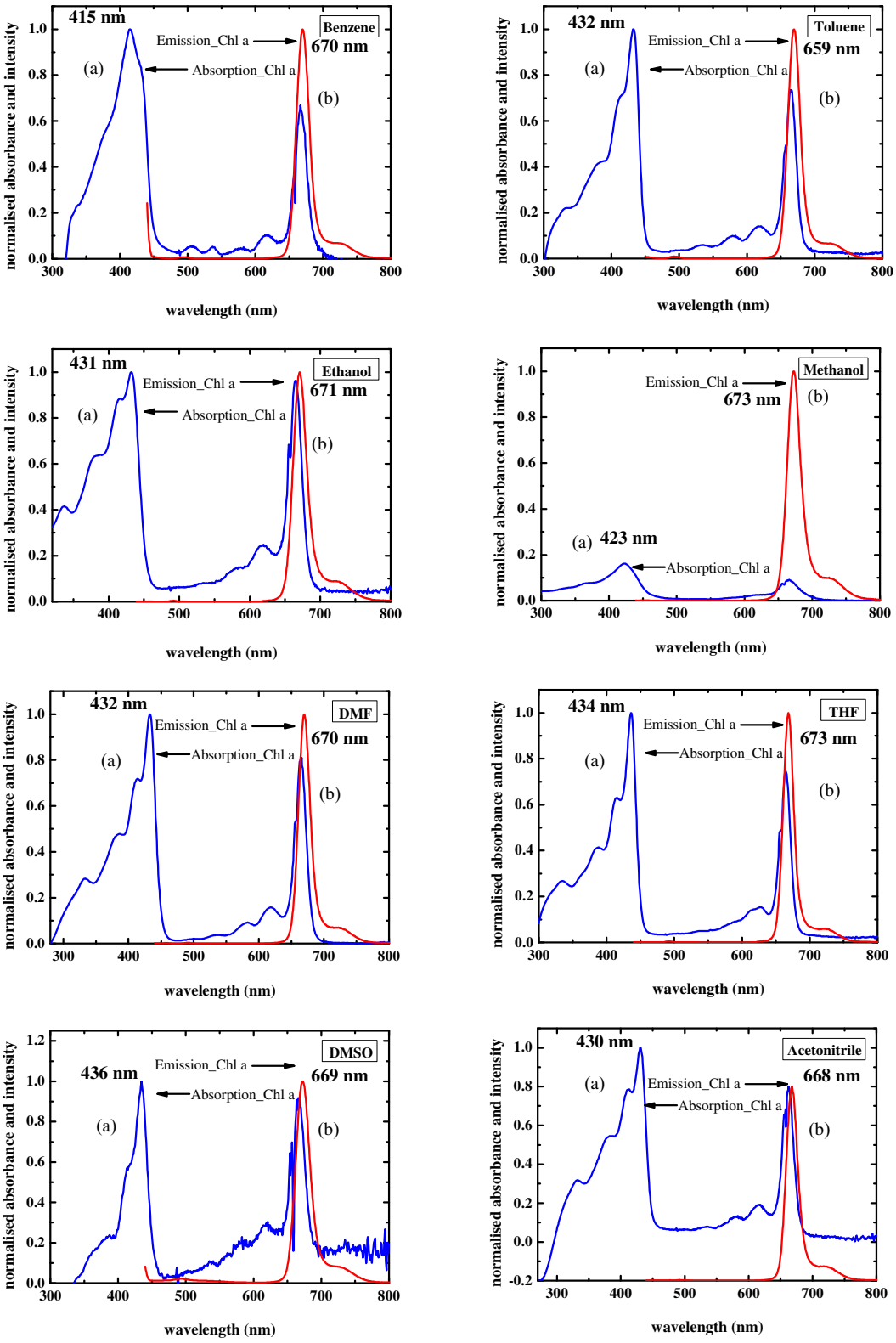

Figure 2 Overlay between normalized (a) absorption spectra of chlorophyll a and (b) emission spectra of chlorophyll a in various solvents.

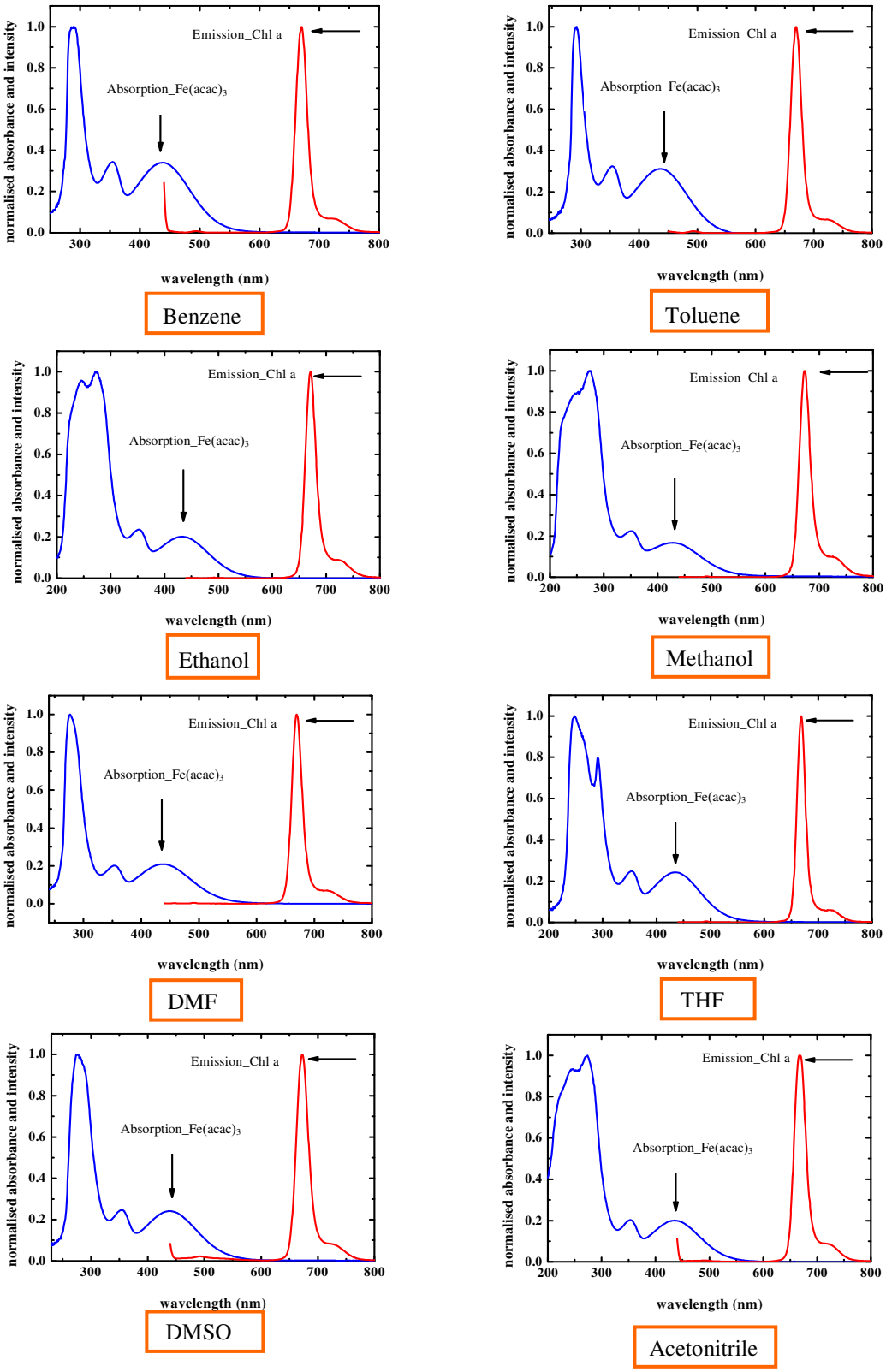

Figure 3 Overlay between normalized absorption spectra of $Fe(acac)_3$ (line blue) and normalized emission spectra of chlorophyll a (line red) in various solvents.

2. The data lifetimes of chlorophyll a in various solvents by changing modulation frequencies.

Table 1 The data lifetime of chlorophyll a in benzene.

Analysis data				Fit data			
f (MHz)	τ (ns)	sig(ns)	phase^0	τ (ns)	sig(ns)	phase^0	mod%
4.9995	5.3200	0.9600	9.4900	5.2292	0.0954	9.3285	38.8668
9.9991	5.4100	0.7500	18.7900	5.5270	0.0954	19.1494	37.2806
14.9985	5.3300	0.6300	26.6900	5.5682	0.0954	27.6880	34.9325
19.9981	5.1600	0.5900	33.0100	5.3282	0.0954	33.8027	32.4023
24.9978	5.6200	0.4200	41.4700	5.8394	0.0954	42.5263	29.7447
29.9974	5.0900	0.3900	43.8800	5.4271	0.0954	45.6485	26.9520
AVG =	5.3216			5.4865			

Table 2 The data lifetime of chlorophyll a in toluene.

Analysis data				Fit data			
f (MHz)	τ (ns)	sig(ns)	phase^0	τ (ns)	sig(ns)	phase^0	mod%
4.9995	7.7700	0.5000	13.7200	7.5477	0.0231	13.3384	86.9770
9.9991	7.6800	0.5600	25.7500	7.4783	0.0231	25.1660	80.3414
14.9985	7.7500	0.4300	36.1400	7.5635	0.0231	35.4804	73.6121
19.9981	7.6300	0.5200	43.8100	7.4353	0.0231	43.0533	65.2665
24.9978	7.5500	0.3500	49.8600	7.5626	0.0231	49.9070	58.2160
29.9974	7.6800	0.3100	55.3500	7.5259	0.0231	54.8170	51.6010
AVG =	7.6766			7.5189			

Table 3 The data lifetime of chlorophyll a in ethanol.

Analysis data				Fit data			
f (MHz)	τ (ns)	sig(ns)	phase^0	τ (ns)	sig(ns)	phase^0	mod%
4.9995	5.4600	0.5600	9.7400	6.0015	0.0692	10.6765	58.7809
9.9991	5.9400	0.6200	20.4700	6.0007	0.0692	20.6567	56.1907
14.9985	5.8600	0.5700	28.9300	6.1071	0.0692	29.9216	52.0052
19.9981	5.9800	0.5800	36.9900	6.0287	0.0692	37.1448	48.0504
24.9978	6.4000	0.3800	45.1600	6.3487	0.0692	44.9185	43.8731
29.9972	6.3400	0.3100	50.0800	6.2976	0.0692	49.8865	39.6942
AVG =	5.9966			6.1307			

Table 4 The data lifetime of chlorophyll a in THF.

Analysis data				Fit data			
f (MHz)	τ (ns)	sig(ns)	phase^0	τ (ns)	sig(ns)	phase^0	mod%
4.9995	7.7700	0.5000	13.7200	7.5477	0.0231	13.3384	86.9770
9.9991	7.6800	0.5600	25.7500	7.4783	0.0231	25.1660	80.3414
14.9985	7.7500	0.4300	36.1400	7.5635	0.0231	35.4804	73.6121
19.9981	7.6300	0.5200	43.8100	7.4353	0.0231	43.0533	65.2665
24.9978	7.5500	0.3500	49.8600	7.5626	0.0231	49.9070	58.2160
29.9974	7.6800	0.3100	55.3500	7.5259	0.0231	54.8170	51.6010
AVG =	7.6766			7.5189			

Table 5 The data lifetime of chlorophyll a in DMF.

Analysis data				Fit data			
f (MHz)	τ (ns)	sig(ns)	phase^0	τ (ns)	sig(ns)	phase^0	mod%
4.9995	7.1100	0.5300	12.5900	6.8294	0.0431	12.1085	85.7127
9.9991	7.0600	0.5300	23.9200	6.7925	0.0431	23.1104	80.9227
14.9985	7.2000	0.5000	34.1600	6.8601	0.0431	32.8822	74.1940
19.9981	6.8700	0.4500	40.8000	6.6589	0.0431	39.9194	66.8334
24.9978	7.0300	0.3100	47.8500	6.8977	0.0431	47.2924	59.9779
29.9972	6.6300	0.3300	51.3300	6.6841	0.0431	51.5584	51.5066
AVG =	6.9833			6.7871			

Table 6 The data lifetime of chlorophyll a in DMSO.

Analysis data				Fit data			
f (MHz)	τ (ns)	sig(ns)	phase^0	τ (ns)	sig(ns)	phase^0	mod%
4.9995	4.1000	2.4800	7.4500	5.9258	0.0996	10.5449	20.2558
9.9991	3.3800	2.2300	15.1300	5.7634	0.0996	19.9052	19.3354
14.9985	5.3800	0.8200	26.9200	5.6615	0.0996	28.0811	19.2180
19.9981	6.5200	1.7500	38.6800	5.3839	0.0996	34.0784	17.9141
24.9978	7.5400	1.3800	49.5500	5.9195	0.0996	42.9150	16.1611
29.9972	0.9700	10.8800	10.1300	5.4900	0.0996	45.9785	14.1347
AVG =	5.9500			5.6907			

Table 7 The data lifetime of chlorophyll a in acetonitrile.

Analysis data				Fit data			
f (MHz)	τ (ns)	sig(ns)	phase^0	τ (ns)	sig(ns)	phase^0	mod%
4.9995	7.2000	0.7500	12.7500	6.6626	0.0389	11.8212	70.5814
9.9991	7.0100	0.5600	23.7800	6.7577	0.0389	23.0045	65.5318
14.9985	6.6800	0.5600	32.2000	6.6913	0.0389	32.2346	60.2451
19.9981	6.8400	0.5300	40.7000	6.7030	0.0389	40.1058	54.2952
24.9978	6.8100	0.3600	46.9500	6.8956	0.0389	47.2836	48.9929
29.9972	7.0300	0.3700	52.9800	6.8088	0.0389	52.0730	44.1423
AVG =	6.9283			6.7532			

Table 8 The data lifetime of chlorophyll a in methanol.

Analysis data				Fit data			
f (MHz)	τ (ns)	sig(ns)	phase^0	τ (ns)	sig(ns)	phase^0	mod%
4.9995	5.7200	0.7000	10.1900	5.6493	0.0958	10.0633	46.7232
9.9991	5.4800	0.8500	19.0000	5.6127	0.0958	19.4240	33.0202
14.9985	3.8700	1.3000	14.6900	5.5985	0.0958	27.8158	30.7986
19.9981	5.1200	0.6900	32.7900	5.3639	0.0958	33.9796	28.5894
24.9978	6.0600	0.5500	43.6300	5.7958	0.0958	42.3127	26.4840
29.9974	-1.8100	0.0000	-18.4700	5.2044	0.0958	44.4480	23.4363
AVG =	5.5950			5.5374			

3. Quenching reaction

Table 9 Quenching reaction data of Chlorophyll a by $Fe(acac)_3$ in benzene.

Table 9.1 Stern-Volmer plot data.

V. of stock Chl a (mL)	V. of stock $Fe(acac)_3$ (mL)	$[Fe(acac)_3]$ (M)	I	I_0/I	$(I_0/I)-1$
0.2	0.0	0	2.48×10^4	1.00	0.00
0.2	0.1	1.01×10^{-5}	2.05×10^4	1.20	0.20
0.2	0.2	2.02×10^{-5}	1.90×10^4	1.30	0.30
0.2	0.25	2.52×10^{-5}	1.83×10^4	1.35	0.35
0.2	0.3	3.03×10^{-5}	1.64×10^4	1.51	0.51
0.2	0.35	3.54×10^{-5}	1.63×10^4	1.51	0.51
0.2	0.4	4.04×10^{-5}	1.58×10^4	1.56	0.56
0.2	0.5	5.05×10^{-5}	1.44×10^4	1.72	0.72
0.2	0.6	6.06×10^{-5}	1.28×10^4	1.94	0.94
0.2	0.7	7.07×10^{-5}	1.25×10^4	1.97	0.97
0.2	0.8	8.08×10^{-5}	1.17×10^4	2.11	1.11
0.2	0.9	9.09×10^{-5}	1.06×10^4	2.33	1.33
0.2	1.0	1.01×10^{-4}	9.85×10^3	2.51	1.51
0.2	1.1	1.11×10^{-4}	8.92×10^3	2.78	1.78
0.2	1.2	1.21×10^{-4}	8.34×10^3	2.97	1.97
0.2	1.3	1.31×10^{-4}	7.82×10^3	3.16	2.16
0.2	1.4	1.41×10^{-4}	7.23×10^3	3.42	2.42
0.2	1.5	1.52×10^{-4}	6.66×10^3	3.71	2.71
0.2	1.6	1.62×10^{-4}	6.30×10^3	3.93	2.93
0.2	1.7	1.72×10^{-4}	5.80×10^3	4.27	3.27
0.2	1.8	1.82×10^{-4}	5.46×10^3	4.531	3.53

Table 9.2 Inner filter effect correction for Stern-Volmer plot data.

Fe^{3+}, M	abs 430	Δabs	Δabs/2	(Δabs/2)*-1	$10^{-(\Delta abs/2)}$	I_{exp}	$I_{0,corr}$	$I_{0,corr}/I_{exp}$	$(I_0/I)-1$
0	1.29×10^{-2}	0	0	0	1.00	2.48×10^{4}	2.48×10^{4}	1.00	0.00
1.01×10^{-5}	5.67×10^{-2}	4.38×10^{-2}	2.19×10^{-2}	-2.19×10^{-2}	0.95	2.06×10^{4}	2.35×10^{4}	1.15	0.15
2.02×10^{-5}	1.03×10^{-1}	9.04×10^{-2}	4.52×10^{-2}	-4.52×10^{-2}	0.90	1.90×10^{4}	2.23×10^{4}	1.17	0.17
2.52×10^{-5}	1.20×10^{-1}	1.08×10^{-1}	5.39×10^{-2}	-5.39×10^{-2}	0.88	1.83×10^{4}	2.19×10^{4}	1.19	0.19
3.03×10^{-5}	1.46×10^{-1}	1.33×10^{-1}	6.67×10^{-2}	-6.67×10^{-2}	0.86	1.64×10^{4}	2.12×10^{4}	1.29	0.29
3.54×10^{-5}	1.74×10^{-1}	1.62×10^{-1}	8.09×10^{-2}	-8.09×10^{-2}	0.83	1.64×10^{4}	2.05×10^{4}	1.25	0.25
4.04×10^{-5}	1.93×10^{-1}	1.81×10^{-1}	9.04×10^{-2}	-9.04×10^{-2}	0.81	1.58×10^{4}	2.01×10^{4}	1.27	0.27
5.05×10^{-5}	2.39×10^{-1}	2.26×10^{-1}	1.13×10^{-1}	-1.13×10^{-1}	0.77	1.44×10^{4}	1.91×10^{4}	1.33	0.33
6.06×10^{-5}	2.87×10^{-1}	2.74×10^{-1}	1.37×10^{-1}	-1.37×10^{-1}	0.73	1.28×10^{4}	1.81×10^{4}	1.41	0.41
7.07×10^{-5}	3.32×10^{-1}	3.20×10^{-1}	1.60×10^{-1}	-1.60×10^{-1}	0.69	1.25×10^{4}	1.71×10^{4}	1.37	0.37
8.08×10^{-5}	3.74×10^{-1}	3.62×10^{-1}	1.81×10^{-1}	-1.81×10^{-1}	0.66	1.17×10^{4}	1.63×10^{4}	1.39	0.39
9.09×10^{-5}	4.24×10^{-1}	4.11×10^{-1}	2.05×10^{-1}	-2.05×10^{-1}	0.62	1.06×10^{4}	1.54×10^{4}	1.45	0.45
1.01×10^{-4}	4.68×10^{-1}	4.55×10^{-1}	2.27×10^{-1}	-2.27×10^{-1}	0.59	9.85×10^{3}	1.47×10^{4}	1.49	0.49
1.11×10^{-4}	5.23×10^{-1}	5.10×10^{-1}	2.55×10^{-1}	-2.55×10^{-1}	0.56	8.92×10^{3}	1.38×10^{4}	1.54	0.54
1.21×10^{-4}	5.51×10^{-1}	5.38×10^{-1}	2.69×10^{-1}	-2.69×10^{-1}	0.54	8.34×10^{3}	1.33×10^{4}	1.60	0.60
1.31×10^{-4}	6.08×10^{-1}	5.95×10^{-1}	2.98×10^{-1}	-2.98×10^{-1}	0.50	7.83×10^{3}	1.25×10^{4}	1.59	0.59
1.41×10^{-4}	6.49×10^{-1}	6.36×10^{-1}	3.18×10^{-1}	-3.18×10^{-1}	0.48	7.23×10^{3}	1.19×10^{4}	1.64	0.64
1.52×10^{-4}	6.96×10^{-1}	6.83×10^{-1}	3.42×10^{-1}	-3.42×10^{-1}	0.46	6.66×10^{3}	1.13×10^{4}	1.69	0.69
1.62×10^{-4}	7.42×10^{-1}	7.29×10^{-1}	3.64×10^{-1}	-3.64×10^{-1}	0.43	6.30×10^{3}	1.07×10^{4}	1.70	0.70
1.72×10^{-4}	8.02×10^{-1}	7.89×10^{-1}	3.95×10^{-1}	-3.95×10^{-1}	0.40	5.80×10^{3}	9.98×10^{3}	1.72	0.72
1.82×10^{-4}	8.40×10^{-1}	8.26×10^{-1}	4.13×10^{-1}	-4.13×10^{-1}	0.39	5.46×10^{3}	9.56×10^{3}	1.75	0.75

Table 9.3 Inner filter effect correction of Borissevitch for Stern-Volmer plot data.

$[Fe(acac)_3]$,M	A_{ex}	$1\text{-}10^{-Aex0}$	$1\text{-}10^{-Aex}$	IFE_{corr}	I_{exp}	I_0/I_{exp}	$(I_0/I_{exp})_{corr}$	$(I_0/I_{exp})_{corr}$-1
0	1.29×10^{-2}	2.94×10^{-2}	2.94×10^{-2}	1.00	2.48×10^{4}	1.00	1.00	0.00
1.01×10^{-5}	5.67×10^{-2}	2.94×10^{-2}	1.22×10^{-1}	0.95	2.06×10^{4}	1.20	1.15	0.15
2.02×10^{-5}	1.03×10^{-1}	2.94×10^{-2}	2.12×10^{-1}	0.90	1.90×10^{4}	1.30	1.18	0.18
2.52×10^{-5}	1.20×10^{-1}	2.94×10^{-2}	2.43×10^{-1}	0.89	1.83×10^{4}	1.35	1.20	0.20
3.03×10^{-5}	1.46×10^{-1}	2.94×10^{-2}	2.86×10^{-1}	0.86	1.64×10^{4}	1.51	1.30	0.30
3.54×10^{-5}	1.74×10^{-1}	2.94×10^{-2}	3.31×10^{-1}	0.84	1.64×10^{4}	1.51	1.26	0.26
4.04×10^{-5}	1.93×10^{-1}	2.94×10^{-2}	3.60×10^{-1}	0.82	1.58×10^{4}	1.56	1.28	0.28
5.05×10^{-5}	2.39×10^{-1}	2.94×10^{-2}	4.23×10^{-1}	0.78	1.44×10^{4}	1.72	1.34	0.34
6.06×10^{-5}	2.87×10^{-1}	2.94×10^{-2}	4.84×10^{-1}	0.74	1.28×10^{4}	1.94	1.44	0.44
7.07×10^{-5}	3.32×10^{-1}	2.94×10^{-2}	5.35×10^{-1}	0.71	1.25×10^{4}	1.97	1.40	0.40
8.08×10^{-5}	3.74×10^{-1}	2.94×10^{-2}	5.78×10^{-1}	0.68	1.17×10^{4}	2.11	1.43	0.43
9.09×10^{-5}	4.24×10^{-1}	2.94×10^{-2}	6.23×10^{-1}	0.65	1.06×10^{4}	2.33	1.51	0.51
1.01×10^{-4}	4.68×10^{-1}	2.94×10^{-2}	6.59×10^{-1}	0.62	9.85×10^{4}	2.51	1.56	0.56
1.11×10^{-4}	5.23×10^{-1}	2.94×10^{-2}	7.00×10^{-1}	0.59	8.92×10^{4}	2.78	1.64	0.64
1.21×10^{-4}	5.51×10^{-1}	2.94×10^{-2}	7.19×10^{-1}	0.58	8.34×10^{4}	2.97	1.71	0.71
1.31×10^{-4}	6.08×10^{-1}	2.94×10^{-2}	7.53×10^{-1}	0.55	7.83×10^{4}	3.16	1.73	0.73
1.41×10^{-4}	6.49×10^{-1}	2.94×10^{-2}	7.76×10^{-1}	0.53	7.23×10^{4}	3.42	1.80	0.80
1.52×10^{-4}	6.96×10^{-1}	2.94×10^{-2}	7.99×10^{-1}	0.50	6.66×10^{4}	3.71	1.88	0.88
1.62×10^{-4}	7.42×10^{-1}	2.94×10^{-2}	8.19×10^{-1}	0.49	6.30×10^{4}	3.93	1.91	0.91
1.72×10^{-4}	8.02×10^{-1}	2.94×10^{-2}	8.42×10^{-1}	0.46	5.80×10^{4}	4.27	1.98	0.98
1.82×10^{-4}	8.40×10^{-1}	2.94×10^{-2}	8.55×10^{-1}	0.45	5.46×10^{4}	4.53	2.04	1.04

Table 9.4 The apparent association constant (K_{app}) data.

$[Fe(acac)_3]$	**(I_0-I)**	**$1/(I_0-I)$**	**$1/[Fe(acac)_3]$**
0	0	-	-
1.00×10^{-5}	4.20×10^{3}	2.38×10^{-4}	9.90×10^{4}
2.00×10^{-5}	5.74×10^{3}	1.74×10^{-4}	4.95×10^{4}
2.50×10^{-5}	6.43×10^{3}	1.56×10^{-4}	3.97×10^{4}
3.00×10^{-5}	8.35×10^{3}	1.20×10^{-4}	3.30×10^{4}
3.50×10^{-5}	8.36×10^{3}	1.20×10^{-4}	2.82×10^{4}
4.00×10^{-5}	8.93×10^{3}	1.12×10^{-4}	2.48×10^{4}
5.00×10^{-5}	1.04×10^{4}	9.64×10^{-5}	1.98×10^{4}
6.00×10^{-5}	1.20×10^{4}	8.35×10^{-5}	1.65×10^{4}
7.00×10^{-5}	1.22×10^{4}	8.19×10^{-5}	1.41×10^{4}
8.00×10^{-5}	1.30×10^{4}	7.69×10^{-5}	1.24×10^{4}
9.00×10^{-5}	1.41×10^{4}	7.08×10^{-5}	1.10×10^{4}
1.01×10^{-4}	1.49×10^{4}	6.71×10^{-5}	9.90×10^{3}
1.11×10^{-4}	1.58×10^{4}	6.32×10^{-5}	9.01×10^{3}
1.21×10^{-4}	1.64×10^{4}	6.09×10^{-5}	8.26×10^{3}
1.31×10^{-4}	1.69×10^{4}	5.91×10^{-5}	7.63×10^{3}
1.41×10^{-4}	1.75×10^{4}	5.71×10^{-5}	7.09×10^{3}
1.52×10^{-4}	1.81×10^{4}	5.53×10^{-5}	6.58×10^{3}
1.62×10^{-4}	1.84×10^{4}	5.42×10^{-5}	6.17×10^{3}
1.72×10^{-4}	1.89×10^{4}	5.28×10^{-5}	5.81×10^{3}
1.82×10^{-4}	1.93×10^{4}	5.18×10^{-5}	5.49×10^{3}

Table 10 Quenching reaction Data of Chlorophyll a by $Fe(acac)_3$ in toluene.

Table 10.1 Stern-Volmer plot data.

V. of stock Chl a (mL)	**V. of stock $Fe(acac)_3$ (mL)**	**[$Fe(acac)_3$] (M)**	**I**	**I_0/I**	**$(I_0/I)-1$**
0.15	0.0	0	2.17×10^4	1	0
0.15	0.2	2×10^{-5}	1.83×10^4	1.19	0.19
0.15	0.3	3×10^{-5}	1.58×10^4	1.38	0.38
0.15	0.4	4×10^{-5}	1.38×10^4	1.58	0.58
0.15	0.5	5×10^{-5}	1.35×10^4	1.61	0.61
0.15	0.6	6×10^{-5}	1.20×10^4	1.80	0.80
0.15	0.7	7×10^{-5}	1.18×10^4	1.84	0.84
0.15	0.8	8×10^{-5}	1.02×10^4	2.14	1.13
0.15	1.0	1×10^{-4}	8.96×10^3	2.43	1.43
0.15	1.2	1.2×10^{-4}	7.77×10^3	2.80	1.80
0.15	1.3	1.3×10^{-4}	6.83×10^3	3.18	2.18
0.15	1.35	1.35×10^{-4}	6.70×10^3	3.24	2.24
0.15	1.4	1.4×10^{-4}	6.16×10^3	3.53	2.53
0.15	1.5	1.5×10^{-4}	6.04×10^3	3.60	2.60
0.15	1.7	1.7×10^{-4}	4.94×10^3	4.40	3.40
0.15	1.8	1.8×10^{-4}	4.13×10^3	5.26	4.26

Table 10.2 Inner filter effect correction for Stern-Volmer plot data.

Fe^{3+}, M	abs 430	Δabs	Δabs/2	(Δabs/2)*-1	$10^{-(\Delta abs/2)}$	I_{exp}	$I_{0,corr}$	$I_{0,corr}/I_{exp}$	$(I_0/I)-1$
0	-5.51×10^{-3}	0	0	0	1.00	2.17×10^{4}	2.17×10^{4}	1.00	0.00
2.00×10^{-5}	8.73×10^{-2}	9.28×10^{-2}	4.64×10^{-2}	-4.64×10^{-2}	0.90	1.83×10^{4}	1.95×10^{4}	1.07	0.07
3.00×10^{-5}	1.36×10^{-1}	1.42×10^{-1}	7.09×10^{-2}	-7.09×10^{-2}	0.85	1.58×10^{4}	1.85×10^{4}	1.17	0.17
4.00×10^{-5}	1.86×10^{-1}	1.91×10^{-1}	9.57×10^{-2}	-9.57×10^{-2}	0.80	1.38×10^{4}	1.74×10^{4}	1.26	0.26
5.00×10^{-5}	2.27×10^{-1}	2.32×10^{-1}	1.16×10^{-1}	-1.16×10^{-1}	0.76	1.35×10^{4}	1.66×10^{4}	1.23	0.23
6.00×10^{-5}	2.76×10^{-1}	2.82×10^{-1}	1.41×10^{-1}	-1.41×10^{-1}	0.72	1.20×10^{4}	1.57×10^{4}	1.30	0.30
7.00×10^{-5}	3.25×10^{-1}	3.31×10^{-1}	1.65×10^{-1}	-1.65×10^{-1}	0.68	1.18×10^{4}	1.49×10^{4}	1.26	0.26
8.00×10^{-5}	3.68×10^{-1}	3.74×10^{-1}	1.87×10^{-1}	-1.87×10^{-1}	0.65	1.02×10^{4}	1.41×10^{4}	1.39	0.39
1.00×10^{-5}	4.48×10^{-1}	4.53×10^{-1}	2.27×10^{-1}	-2.27×10^{-1}	0.59	8.96×10^{3}	1.29×10^{4}	1.44	0.44
1.20×10^{-5}	5.53×10^{-1}	5.59×10^{-1}	2.79×10^{-1}	-2.79×10^{-1}	0.52	7.77×10^{3}	1.14×10^{4}	1.47	0.47
1.30×10^{-5}	5.97×10^{-1}	6.02×10^{-1}	3.01×10^{-1}	-3.01×10^{-1}	0.50	6.83×10^{3}	1.09×10^{4}	1.59	0.59
1.35×10^{-4}	6.17×10^{-1}	6.22×10^{-1}	3.11×10^{-1}	-3.11×10^{-1}	0.49	6.70×10^{3}	1.06×10^{4}	1.59	0.59
1.40×10^{-4}	6.38×10^{-1}	6.43×10^{-1}	3.22×10^{-1}	-3.22×10^{-1}	0.48	6.16×10^{3}	1.04×10^{4}	1.68	0.68
1.50×10^{-4}	6.81×10^{-1}	6.87×10^{-1}	3.43×10^{-1}	-3.43×10^{-1}	0.45	6.04×10^{3}	9.86×10^{3}	1.63	0.63
1.70×10^{-4}	7.45×10^{-1}	7.51×10^{-1}	3.75×10^{-1}	-3.75×10^{-1}	0.42	4.94×10^{3}	9.16×10^{3}	1.86	0.86
1.80×10^{-4}	8.40×10^{-1}	8.45×10^{-1}	4.22×10^{-1}	-0.4225685	0.38	4.13×10^{3}	8.22×10^{3}	1.99	0.99

Table 10.3 Inner filter effect correction of Borissevitch for Stern-Volmer plot data.

$[Fe(acac)_3]$,M	A_{ex}	$1\text{-}10^{-Aex0}$	$1\text{-}10^{-Aex}$	IFE_{corr}	I_{exp}	I_0/I_{exp}	$(I_0/I_{exp})_{corr}$	$(I_0/I_{exp})_{corr}$-1
0	-5.51×10^{-3}	-1.28×10^{-2}	-1.28×10^{-2}	1.00	2.17×10^{4}	1.00	1.00	0.00
2.00×10^{-5}	8.73×10^{-2}	-1.28×10^{-2}	1.82×10^{-1}	0.90	1.83×10^{4}	1.19	1.07	0.07
3.00×10^{-5}	1.36×10^{-1}	-1.28×10^{-2}	2.69×10^{-1}	0.85	1.58×10^{4}	1.37	1.17	0.17
4.00×10^{-5}	1.86×10^{-1}	-1.28×10^{-2}	3.48×10^{-1}	0.80	1.38×10^{4}	1.58	1.27	0.27
5.00×10^{-5}	2.27×10^{-1}	-1.28×10^{-2}	4.07×10^{-1}	0.77	1.35×10^{4}	1.61	1.25	0.25
6.00×10^{-5}	2.76×10^{-1}	-1.28×10^{-2}	4.71×10^{-1}	0.74	1.20×10^{4}	1.80	1.33	0.33
7.00×10^{-5}	3.25×10^{-1}	-1.28×10^{-2}	5.27×10^{-1}	0.70	1.18×10^{4}	1.84	1.28	0.28
8.00×10^{-5}	3.68×10^{-1}	-1.28×10^{-2}	5.72×10^{-1}	0.67	1.02×10^{4}	2.14	1.43	0.43
1.00×10^{-4}	4.48×10^{-1}	-1.28×10^{-2}	6.43×10^{-1}	0.62	8.96×10^{3}	2.43	1.50	0.50
1.20×10^{-4}	5.53×10^{-1}	-1.28×10^{-2}	7.20×10^{-1}	0.56	7.77×10^{3}	2.80	1.57	0.57
1.30×10^{-4}	5.97×10^{-1}	-1.28×10^{-2}	7.47×10^{-1}	0.54	6.83×10^{3}	3.18	1.72	0.72
1.35×10^{-4}	6.17×10^{-1}	-1.28×10^{-2}	7.58×10^{-1}	0.53	6.70×10^{3}	3.25	1.72	0.72
1.40×10^{-4}	6.38×10^{-1}	-1.28×10^{-2}	7.70×10^{-1}	0.52	6.16×10^{3}	3.53	1.84	0.84
1.50×10^{-4}	6.81×10^{-1}	-1.28×10^{-2}	7.79×10^{-1}	0.50	6.04×10^{3}	3.60	1.81	0.81
1.70×10^{-4}	7.45×10^{-1}	-1.28×10^{-2}	8.20×10^{-1}	0.47	4.94×10^{3}	4.40	2.09	1.09
1.80×10^{-4}	8.40×10^{-1}	-1.28×10^{-2}	8.55×10^{-1}	0.44	4.13×10^{3}	5.26	2.31	1.31

Table 10.4 The apparent association constant (K_{app}) data.

$[Fe(acac)_3]$	**(I_0-I)**	**$1/(I_0-I)$**	**$1/[Fe(acac)_3]$**
0	0	-	-
2.00×10^{-5}	3.42×10^{3}	2.92×10^{-4}	5.00×10^{4}
3.00×10^{-5}	5.91×10^{3}	1.69×10^{-4}	3.33×10^{4}
4.00×10^{-5}	7.94×10^{3}	1.26×10^{-4}	2.50×10^{4}
5.00×10^{-5}	8.23×10^{3}	$1.22x\ 10^{-4}$	2.00×10^{4}
6.00×10^{-5}	9.69×10^{3}	1.03×10^{-4}	1.67×10^{4}
7.00×10^{-5}	9.91×10^{3}	1.01×10^{-4}	1.43×10^{4}
8.00×10^{-5}	1.16×10^{4}	8.65×10^{-5}	1.25×10^{4}
1.00×10^{-4}	1.28×10^{4}	8.65×10^{-5}	1.00×10^{4}
1.20×10^{-4}	1.40×10^{4}	7.83×10^{-5}	8.33×10^{3}
1.30×10^{-4}	1.49×10^{4}	7.16×10^{-5}	7.69×10^{3}
1.35×10^{-4}	1.50×10^{4}	6.71×10^{-5}	7.41×10^{3}
1.40×10^{-4}	1.56×10^{4}	6.65×10^{-5}	7.14×10^{3}
1.50×10^{-4}	1.57×10^{4}	6.42×10^{-5}	6.67×10^{3}
1.70×10^{-4}	1.68×10^{4}	5.95×10^{-5}	5.88×10^{3}
1.80×10^{-4}	1.76×10^{4}	5.68×10^{-5}	5.56×10^{3}

Table 11 Quenching reaction Data of Chlorophyll a by $Fe(acac)_3$ in ethanol.

Table 11.1 Stern-Volmer plot data.

V. of stock Chl a (mL)	V. of stock $Fe(acac)_3$ (mL)	$[Fe(acac)_3]$ (M)	I	I_0/I	$(I_0/I)-1$
1.5	0.0	0	2.85×10^4	1.00	0
1.5	0.2	2×10^{-5}	2.50×10^4	1.14	0.14
1.5	0.3	3×10^{-5}	2.30×10^4	1.24	0.24
1.5	0.4	4×10^{-5}	2.06×10^4	1.39	0.39
1.5	0.5	5×10^{-5}	1.95×10^4	1.46	0.46
1.5	0.6	6×10^{-5}	1.83×10^4	1.56	0.56
1.5	0.7	7×10^{-5}	1.74×10^4	1.64	0.64
1.5	0.8	8×10^{-5}	1.63×10^4	1.75	0.75
1.5	1.0	1×10^{-4}	1.45×10^4	1.97	0.97
1.5	1.2	1.2×10^{-4}	1.28×10^4	2.22	1.22
1.5	1.4	1.4×10^{-4}	1.15×10^4	2.49	1.49
1.5	1.6	1.6×10^{-4}	1.02×10^4	2.80	1.80
1.5	1.8	1.8×10^{-4}	9.23×10^3	3.09	2.09
1.5	2.0	2.0×10^{-4}	8.26×10^3	3.45	2.45

Table 11.2 Inner filter effect correction for Stern-Volmer plot data.

Fe^{3+}, M	abs 430	Δabs	Δabs/2	(Δabs/2)*-1	$10^{-(\Delta abs/2)}$	I_{exp}	$I_{0,corr}$	$I_{0,corr}/I_{exp}$	$(I_0/I)-1$
0	2.72×10^{-2}	0	0	0	1.00	2.85×10^{4}	2.85×10^{4}	1.00	0.00
2.00×10^{-5}	7.40×10^{-2}	4.69×10^{-2}	2.34×10^{-2}	-2.34×10^{-2}	0.95	2.50×10^{4}	2.70×10^{4}	1.08	0.08
3.00×10^{-5}	1.20×10^{-1}	9.28×10^{-2}	4.64×10^{-2}	-4.64×10^{-2}	0.90	2.30×10^{4}	2.56×10^{4}	1.12	0.12
4.00×10^{-5}	1.53×10^{-1}	1.26×10^{-1}	6.28×10^{-2}	-6.28×10^{-2}	0.86	2.06×10^{4}	2.47×10^{4}	1.20	0.20
5.00×10^{-5}	1.87×10^{-1}	1.60×10^{-1}	8.00×10^{-2}	-8.00×10^{-2}	0.83	1.95×10^{4}	2.37×10^{4}	1.22	0.22
6.00×10^{-5}	2.27×10^{-1}	2.00×10^{-1}	9.99×10^{-2}	-9.99×10^{-2}	0.79	1.83×10^{4}	2.27×10^{4}	1.24	0.24
7.00×10^{-5}	2.54×10^{-1}	2.26×10^{-1}	1.13×10^{-1}	-1.13×10^{-1}	0.77	1.74×10^{4}	2.20×10^{4}	1.26	0.26
8.00×10^{-5}	2.91×10^{-1}	2.64×10^{-1}	1.32×10^{-1}	-1.32×10^{-1}	0.74	1.63×10^{4}	2.10×10^{4}	1.29	0.29
1.00×10^{-4}	3.55×10^{-1}	3.28×10^{-1}	1.64×10^{-1}	-1.64×10^{-1}	0.68	1.45×10^{4}	1.96×10^{4}	1.35	0.35
1.20×10^{-4}	4.24×10^{-1}	3.97×10^{-1}	1.99×10^{-1}	-1.99×10^{-1}	0.63	1.28×10^{4}	1.81×10^{4}	1.41	0.41
1.40×10^{-4}	4.97×10^{-1}	4.70×10^{-1}	2.35×10^{-1}	-2.35×10^{-1}	0.58	1.15×10^{4}	1.66×10^{4}	1.45	0.45
1.60×10^{-4}	5.53×10^{-1}	5.26×10^{-1}	2.63×10^{-1}	-2.63×10^{-1}	0.54	1.02×10^{4}	1.56×10^{4}	1.53	0.53
1.80×10^{-4}	6.23×10^{-1}	5.96×10^{-1}	2.98×10^{-1}	-2.98×10^{-1}	0.50	9.23×10^{3}	1.44×10^{4}	1.56	0.56
2.00×10^{-4}	6.91×10^{-1}	6.64×10^{-1}	3.32×10^{-1}	-3.32×10^{-1}	0.46	8.26×10^{3}	1.33×10^{4}	1.61	0.61

Table 10.3 Inner filter effect correction of Borissevitch for Stern-Volmer plot data.

$[Fe(acac)_3]$,M	A_{ex}	$1\text{-}10^{-Aex0}$	$1\text{-}10^{-Aex}$	IFE_{corr}	I_{exp}	I_0/I_{exp}	$(I_0/I_{exp})_{corr}$	$(I_0/I_{exp})_{corr}$-1
0	2.72×10^{-2}	6.06×10^{-2}	6.06×10^{-2}	1.00	2.85×10^{4}	1.00	1.00	0.00
2.00×10^{-5}	7.40×10^{-2}	6.06×10^{-2}	1.57×10^{-1}	0.94	2.50×10^{4}	1.14	1.08	0.08
3.00×10^{-5}	1.20×10^{-1}	6.06×10^{-2}	2.41×10^{-1}	0.90	2.30×10^{4}	1.24	1.12	0.12
4.00×10^{-5}	1.53×10^{-1}	6.06×10^{-2}	2.97×10^{-1}	0.87	2.06×10^{4}	1.39	1.21	0.21
5.00×10^{-5}	1.87×10^{-1}	6.06×10^{-2}	3.50×10^{-1}	0.84	1.95×10^{4}	1.46	1.22	0.22
6.00×10^{-5}	2.27×10^{-1}	6.06×10^{-2}	4.07×10^{-1}	0.80	1.83×10^{4}	1.56	1.25	0.25
7.00×10^{-5}	2.54×10^{-1}	6.06×10^{-2}	4.42×10^{-1}	0.78	1.74×10^{4}	1.64	1.28	0.28
8.00×10^{-5}	2.91×10^{-1}	6.06×10^{-2}	4.89×10^{-1}	0.75	1.63×10^{4}	1.75	1.31	0.31
1.00×10^{-4}	3.55×10^{-1}	6.06×10^{-2}	5.58×10^{-1}	0.70	1.45×10^{4}	1.97	1.39	0.39
1.20×10^{-4}	4.24×10^{-1}	6.06×10^{-2}	6.24×10^{-1}	0.66	1.28×10^{4}	2.22	1.46	0.46
1.40×10^{-4}	4.97×10^{-1}	6.06×10^{-2}	6.82×10^{-1}	0.61	1.15×10^{4}	2.49	1.53	0.53
1.60×10^{-4}	5.53×10^{-1}	6.06×10^{-2}	7.20×10^{-1}	0.58	1.02×10^{4}	2.80	1.63	0.63
1.80×10^{-4}	6.23×10^{-1}	6.06×10^{-2}	7.62×10^{-1}	0.55	9.23×10^{3}	3.09	1.69	0.69
2.00×10^{-4}	6.91×10^{-1}	6.06×10^{-2}	7.96×10^{-1}	0.52	8.26×10^{3}	3.45	1.78	0.78

Table 11.4 The apparent association constant (K_{app}) data.

[Fe(acac)$_3$]	**(I_0-I)**	**1/(I_0-I)**	**1/[Fe(acac)$_3$]**
0	0	-	-
2.00×10^{-5}	3.55×10^{3}	2.82×10^{-4}	5.00×10^{4}
3.00×10^{-5}	5.54×10^{3}	1.80×10^{-4}	3.33×10^{4}
4.00×10^{-5}	7.96×10^{3}	1.26×10^{-4}	2.50×10^{4}
5.00×10^{-5}	9.00×10^{3}	1.11×10^{-4}	2.00×10^{4}
6.00×10^{-5}	1.02×10^{4}	9.77×10^{-5}	1.67×10^{4}
7.00×10^{-5}	1.11×10^{4}	8.99×10^{-5}	1.43×10^{4}
8.00×10^{-5}	1.22×10^{4}	8.20×10^{-5}	1.25×10^{4}
1.00×10^{-4}	1.40×10^{4}	7.12×10^{-5}	1.00×10^{4}
1.20×10^{-4}	1.57×10^{4}	6.38×10^{-5}	8.33×10^{3}
1.40×10^{-4}	1.71×10^{4}	5.86×10^{-5}	7.14×10^{3}
1.60×10^{-4}	1.83×10^{4}	5.46×10^{-5}	6.25×10^{3}
1.80×10^{-4}	1.93×10^{4}	5.18×10^{-5}	5.56×10^{3}
2.00×10^{-4}	2.03×10^{4}	4.94×10^{-5}	5.00×10^{3}

Table 12 Quenching reaction Data of Chlorophyll a by $Fe(acac)_3$ in methanol.

Table 12.1 Stern-Volmer plot data.

V. of stock Chl a (mL)	**V. of stock $Fe(acac)_3$ (mL)**	**[$Fe(acac)_3$] (M)**	**I**	**I_0/I**	**$(I_0/I)-1$**
1.0	0.0	0	2.14×10^4	1.00	0
1.0	0.2	2.08×10^{-5}	1.85×10^4	1.16	0.16
1.0	0.3	3.12×10^{-5}	1.74×10^4	1.23	0.23
1.0	0.4	4.16×10^{-5}	1.62×10^4	1.33	0.33
1.0	0.5	5.2×10^{-5}	1.51×10^4	1.42	0.42
1.0	0.6	6.24×10^{-5}	1.41×10^4	1.52	0.52
1.0	0.7	7.28×10^{-5}	1.32×10^4	1.63	0.63
1.0	0.8	8.32×10^{-5}	1.23×10^4	1.74	0.74
1.0	0.9	9.36×10^{-4}	1.14×10^4	1.89	0.89
1.0	1.0	1.04×10^{-4}	1.07×10^4	2.00	1.00
1.0	1.1	1.14×10^{-4}	1.01×10^4	2.14	1.14
1.0	1.2	1.25×10^{-4}	9.34×10^3	2.30	1.30
1.0	1.3	1.35×10^{-4}	8.85×10^3	2.42	1.42
1.0	1.4	1.46×10^{-4}	8.24×10^3	2.60	1.60
1.0	1.5	1.56×10^{-4}	7.79×10^3	2.76	1.76
1.0	1.6	1.66×10^{-4}	7.39×10^3	2.90	1.90
1.0	1.7	1.87×10^{-4}	6.50×10^3	3.30	2.30
1.0	2.0	2.08×10^{-4}	5.91×10^3	3.63	2.63

Table 12.2 Inner filter effect correction for Stern-Volmer plot data.

Fe^{3+}, M	abs 430	Δabs	Δabs/2	(Δabs/2)*-1	$10^{-(\Delta abs/2)}$	I_{exp}	$I_{0,corr}$	$I_{0,corr}/I_{exp}$	$(I_0/I)-1$
0	1.61×10^{-2}	0	0	0	1.00	2.15×10^{4}	2.15×10^{4}	1.00	0.00
2.08×10^{-5}	8.37×10^{-2}	6.76×10^{-2}	3.38×10^{-2}	-3.38×10^{-2}	0.92	1.85×10^{4}	1.99×10^{4}	1.07	0.07
3.12×10^{-5}	1.16×10^{-1}	1.00×10^{-1}	5.00×10^{-2}	-5.00×10^{-2}	0.89	1.75×10^{4}	1.91×10^{4}	1.10	0.10
4.16×10^{-5}	1.50×10^{-1}	1.34×10^{-1}	6.70×10^{-2}	-6.70×10^{-2}	0.86	1.62×10^{4}	1.84×10^{4}	1.14	0.14
5.20×10^{-5}	1.82×10^{-1}	1.66×10^{-1}	8.30×10^{-2}	-8.30×10^{-2}	0.82	1.51×10^{4}	1.77×10^{4}	1.17	0.17
6.24×10^{-5}	2.19×10^{-1}	2.03×10^{-1}	1.01×10^{-1}	-1.01×10^{-1}	0.79	1.41×10^{4}	1.70×10^{4}	1.20	0.20
7.28×10^{-5}	2.47×10^{-1}	2.30×10^{-1}	1.15×10^{-1}	-1.15×10^{-1}	0.77	1.32×10^{4}	1.65×10^{4}	1.25	0.25
8.32×10^{-5}	2.97×10^{-1}	2.81×10^{-1}	1.40×10^{-1}	-1.40×10^{-1}	0.72	1.23×10^{4}	1.55×10^{4}	1.26	0.26
9.36×10^{-5}	3.28×10^{-1}	3.12×10^{-1}	1.56×10^{-1}	-1.56×10^{-1}	0.70	1.14×10^{4}	1.50×10^{4}	1.32	0.32
1.04×10^{-4}	3.64×10^{-1}	3.48×10^{-1}	1.74×10^{-1}	-1.74×10^{-1}	0.67	1.07×10^{4}	1.44×10^{4}	1.34	0.34
1.14×10^{-4}	4.16×10^{-1}	4.00×10^{-1}	2.00×10^{-1}	-2.00×10^{-1}	0.63	1.00×10^{4}	1.35×10^{4}	1.35	0.35
1.25×10^{-4}	4.42×10^{-1}	4.26×10^{-1}	2.13×10^{-1}	-2.13×10^{-1}	0.61	9.34×10^{3}	1.31×10^{4}	1.41	0.41
1.35×10^{-4}	4.78×10^{-1}	4.62×10^{-1}	2.31×10^{-1}	-2.31×10^{-1}	0.59	8.85×10^{3}	1.26×10^{4}	1.42	0.42
1.46×10^{-4}	5.18×10^{-1}	5.02×10^{-1}	2.51×10^{-1}	-2.51×10^{-1}	0.56	8.25×10^{3}	1.20×10^{4}	1.46	0.46
1.56×10^{-4}	5.57×10^{-1}	5.40×10^{-1}	2.70×10^{-1}	-2.70×10^{-1}	0.54	7.79×10^{3}	1.15×10^{4}	1.48	0.48
1.66×10^{-4}	5.95×10^{-1}	5.79×10^{-1}	2.90×10^{-1}	-2.90×10^{-1}	0.51	7.39×10^{3}	1.10×10^{4}	1.49	0.49
1.87×10^{-4}	6.68×10^{-1}	6.52×10^{-1}	3.26×10^{-1}	-3.26×10^{-1}	0.47	6.50×10^{3}	1.01×10^{4}	1.56	0.56
2.08×10^{-4}	7.39×10^{-1}	7.23×10^{-1}	3.62×10^{-1}	-3.62×10^{-1}	0.43	5.91×10^{3}	9.34×10^{3}	1.58	0.58

Table 11.3 Inner filter effect correction of Borissevitch for Stern-Volmer plot data.

$[Fe(acac)_3]$,M	A_{ex}	$1\text{-}10^{-Aex0}$	$1\text{-}10^{-Aex}$	IFE_{corr}	I_{exp}	I_0/I_{exp}	$(I_0/I_{exp})_{corr}$	$(I_0/I_{exp})_{corr}$-1
0	1.61×10^{-2}	3.64×10^{-2}	3.64×10^{-2}	1.00	2.15×10^{4}	1.00	1.00	0.00
2.08×10^{-5}	8.37×10^{-2}	3.64×10^{-2}	1.75×10^{-1}	0.93	1.85×10^{4}	1.16	1.07	0.07
3.12×10^{-5}	1.16×10^{-1}	3.64×10^{-2}	2.35×10^{-1}	0.89	1.75×10^{4}	1.23	1.10	0.10
4.16×10^{-5}	1.50×10^{-1}	3.64×10^{-2}	2.92×10^{-1}	0.86	1.62×10^{4}	1.33	1.14	0.14
5.20×10^{-5}	1.82×10^{-1}	3.64×10^{-2}	3.43×10^{-1}	0.83	1.51×10^{4}	1.42	1.18	0.18
6.24×10^{-5}	2.19×10^{-1}	3.64×10^{-2}	3.96×10^{-1}	0.80	1.41×10^{4}	1.52	1.21	0.21
7.28×10^{-5}	2.47×10^{-1}	3.64×10^{-2}	4.33×10^{-1}	0.78	1.32×10^{4}	1.63	1.27	0.27
8.32×10^{-5}	2.97×10^{-1}	3.64×10^{-2}	4.95×10^{-1}	0.74	1.23×10^{4}	1.75	1.29	0.29
9.36×10^{-5}	3.28×10^{-1}	3.64×10^{-2}	5.30×10^{-1}	0.71	1.14×10^{4}	1.89	1.35	0.35
1.04×10^{-4}	3.64×10^{-1}	3.64×10^{-2}	5.67×10^{-1}	0.69	1.07×10^{4}	2.01	1.38	0.38
1.14×10^{-4}	4.16×10^{-1}	3.64×10^{-2}	6.16×10^{-1}	0.66	1.00×10^{4}	2.15	1.41	0.41
1.25×10^{-4}	4.42×10^{-1}	3.64×10^{-2}	6.38×10^{-1}	0.64	9.34×10^{3}	2.30	1.47	0.47
1.35×10^{-4}	4.78×10^{-1}	3.64×10^{-2}	6.67×10^{-1}	0.62	8.85×10^{3}	2.42	1.50	0.50
1.46×10^{-4}	5.18×10^{-1}	3.64×10^{-2}	6.97×10^{-1}	0.59	8.25×10^{3}	2.60	1.55	0.55
1.56×10^{-4}	5.57×10^{-1}	3.64×10^{-2}	7.22×10^{-1}	0.57	7.79×10^{3}	2.76	1.58	0.58
1.66×10^{-4}	5.95×10^{-1}	3.64×10^{-2}	7.46×10^{-1}	0.55	7.39×10^{3}	2.90	1.61	0.61
1.87×10^{-4}	6.68×10^{-1}	3.64×10^{-2}	7.85×10^{-1}	0.52	6.50×10^{3}	3.30	1.72	0.72
2.08×10^{-4}	7.39×10^{-1}	3.64×10^{-2}	8.18×10^{-1}	0.49	5.91×10^{3}	3.63	1.78	0.78

Table 12.4 The apparent association constant (K_{app}) data.

[Fe(acac)$_3$]	**(I_0-I)**	**1/(I_0-I)**	**1/[Fe(acac)$_3$]**
0	0	-	-
2.10×10^{-5}	2.94×10^{3}	3.40×10^{-4}	4.81×10^{4}
3.12×10^{-5}	4.01×10^{3}	2.49×10^{-4}	3.20×10^{4}
4.16×10^{-5}	5.31×10^{3}	1.88×10^{-4}	$2..40 \times 10^{4}$
5.20×10^{-5}	6.36×10^{3}	1.57×10^{-4}	1.92×10^{4}
6.24×10^{-5}	7.32×10^{3}	1.36×10^{-4}	1.60×10^{4}
7.28×10^{-5}	8.28×10^{3}	1.20×10^{-4}	1.37×10^{4}
8.32×10^{-5}	9.17×10^{3}	1.09×10^{-4}	1.20×10^{4}
9.36×10^{-5}	1.01×10^{4}	9.89×10^{-5}	1.07×10^{4}
1.04×10^{-4}	1.08×10^{4}	9.29×10^{-5}	9.62×10^{3}
1.14×10^{-4}	1.14×10^{4}	8.72×10^{-5}	8.77×10^{3}
1.25×10^{-4}	1.21×10^{4}	8.24×10^{-5}	8.00×10^{3}
1.35×10^{-4}	1.26×10^{4}	7.93×10^{-5}	7.41×10^{3}
1.46×10^{-4}	1.32×10^{4}	7.56×10^{-5}	6.85×10^{3}
1.56×10^{-4}	1.37×10^{4}	7.31×10^{-5}	6.41×10^{3}
1.66×10^{-4}	1.41×10^{4}	7.10×10^{-5}	6.02×10^{3}
1.87×10^{-4}	1.50×10^{4}	6.68×10^{-5}	5.35×10^{3}
2.08×10^{-4}	1.56×10^{4}	6.43×10^{-5}	4.81×10^{3}

Table 13 Quenching reaction Data of Chlorophyll a by $Fe(acac)_3$ in DMF.

Table 13.1 Stern-Volmer plot data.

V. of stock Chl a (mL)	**V. of stock $Fe(acac)_3$ (mL)**	**[$Fe(acac)_3$] (M)**	**I**	**I_0/I**	**$(I_0/I)-1$**
0.15	0.0	0	2.64×10^4	1	0
0.15	0.1	1.02×10^{-5}	2.33×10^4	1.13	0.13
0.15	0.2	2.04×10^{-5}	2.33×10^4	1.13	0.13
0.15	0.3	3.06×10^{-5}	2.11×10^4	1.25	0.25
0.15	0.4	4.08×10^{-5}	1.93×10^4	1.37	0.37
0.15	0.5	5.10×10^{-5}	1.78×10^4	1.48	0.48
0.15	0.6	6.12×10^{-5}	1.56×10^4	1.69	0.69
0.15	0.7	7.14×10^{-5}	1.49×10^4	1.77	0.77
0.15	0.8	8.16×10^{-4}	1.29×10^4	2.05	1.05
0.15	0.9	9.18×10^{-4}	1.22×10^4	2.17	1.17
0.15	1.0	1.02×10^{-4}	1.12×10^4	2.36	1.36
0.15	1.2	1.22×10^{-4}	1.01×10^4	2.61	1.61
0.15	1.4	1.43×10^{-4}	8.24×10^3	3.21	2.21
0.15	1.6	1.63×10^{-4}	7.36×10^3	3.59	2.59
0.15	1.8	1.84×10^{-4}	6.13×10^3	4.31	3.31

Table 13.2 Inner filter effect correction for Stern-Volmer plot data.

Fe^{3+}, M	abs 430	Δabs	Δabs/2	(Δabs/2)*-1	$10^{-(\Delta abs/2)}$	I_{exp}	$I_{0,corr}$	$I_{0,corr}/I_{exp}$	$(I_0/I)-1$
0	1.49×10^{-2}	0	0	0	1.00	2.64×10^{4}	2.64×10^{4}	1.00	0.00
1.02×10^{-5}	5.72×10^{-2}	4.23×10^{-2}	2.12×10^{-2}	-2.12×10^{-2}	0.95	2.33×10^{4}	2.52×10^{4}	1.08	0.08
2.04×10^{-5}	1.10×10^{-1}	9.54×10^{-2}	4.77×10^{-2}	-4.77×10^{-2}	0.90	2.33×10^{4}	2.37×10^{4}	1.02	0.02
3.06×10^{-5}	1.51×10^{-1}	1.36×10^{-1}	6.82×10^{-2}	-6.82×10^{-2}	0.85	2.11×10^{4}	2.26×10^{4}	1.07	0.07
4.08×10^{-5}	1.95×10^{-1}	1.80×10^{-1}	8.99×10^{-2}	-8.99×10^{-2}	0.81	1.93×10^{4}	2.15×10^{4}	1.11	0.11
5.10×10^{-5}	2.27×10^{-1}	2.12×10^{-1}	1.06×10^{-1}	-1.06×10^{-1}	0.78	1.78×10^{4}	2.07×10^{4}	1.16	0.16
6.12×10^{-5}	2.66×10^{-1}	2.51×10^{-1}	1.26×10^{-1}	-1.26×10^{-1}	0.75	1.56×10^{4}	1.98×10^{4}	1.27	0.27
7.14×10^{-5}	3.09×10^{-1}	2.94×10^{-1}	1.47×10^{-1}	-1.47×10^{-1}	0.71	1.49×10^{4}	1.88×10^{4}	1.26	0.26
8.16×10^{-5}	3.44×10^{-1}	3.30×10^{-1}	1.65×10^{-1}	-1.65×10^{-1}	0.68	1.29×10^{4}	1.81×10^{4}	1.40	0.40
9.18×10^{-5}	3.86×10^{-1}	3.71×10^{-1}	1.86×10^{-1}	-1.86×10^{-1}	0.65	1.22×10^{4}	1.72×10^{4}	1.41	0.41
1.02×10^{-4}	4.23×10^{-1}	4.08×10^{-1}	2.04×10^{-1}	-2.04×10^{-1}	0.62	1.12×10^{4}	1.65×10^{4}	1.48	0.48
1.22×10^{-4}	4.98×10^{-1}	4.83×10^{-1}	2.42×10^{-1}	-2.42×10^{-1}	0.57	1.01×10^{4}	1.52×10^{4}	1.50	0.50
1.43×10^{-4}	5.70×10^{-1}	5.55×10^{-1}	2.78×10^{-1}	-2.78×10^{-1}	0.53	8.24×10^{3}	1.39×10^{4}	1.69	0.69
1.63×10^{-4}	6.49×10^{-1}	6.34×10^{-1}	3.17×10^{-1}	-3.17×10^{-1}	0.48	7.36×10^{3}	1.27×10^{4}	1.73	0.73
1.84×10^{-4}	7.14×10^{-1}	7.00×10^{-1}	3.50×10^{-1}	-3.50×10^{-1}	0.45	6.13×10^{3}	1.18×10^{4}	1.93	0.93

Table 13.3 Inner filter effect correction of Borissevitch for Stern-Volmer plot data.

$[Fe(acac)_3]$,M	A_{ex}	$1\text{-}10^{-Aex0}$	$1\text{-}10^{-Aex}$	IFE_{corr}	I_{exp}	I_0/I_{exp}	$(I_0/I_{exp})_{corr}$	$(I_0/I_{exp})_{corr}$-1
0	1.49×10^{-2}	3.37×10^{-2}	3.37×10^{-2}	1.00	2.64×10^{4}	1.00	1.00	0.00
1.02×10^{-5}	5.72×10^{-2}	3.37×10^{-2}	1.23×10^{-1}	0.95	2.33×10^{4}	1.13	1.08	0.08
2.04×10^{-5}	1.10×10^{-1}	3.37×10^{-2}	2.24×10^{-1}	0.90	2.33×10^{4}	1.13	1.02	0.02
3.06×10^{-5}	1.51×10^{-1}	3.37×10^{-2}	2.94×10^{-1}	0.86	2.11×10^{4}	1.25	1.07	0.07
4.08×10^{-5}	1.95×10^{-1}	3.37×10^{-2}	3.61×10^{-1}	0.82	1.93×10^{4}	1.37	1.12	0.12
5.10×10^{-5}	2.27×10^{-1}	3.37×10^{-2}	4.07×10^{-1}	0.79	1.78×10^{4}	1.48	1.17	0.17
6.12×10^{-5}	2.66×10^{-1}	3.37×10^{-2}	4.58×10^{-1}	0.76	1.56×10^{4}	1.69	1.29	0.29
7.14×10^{-5}	3.09×10^{-1}	3.37×10^{-2}	5.09×10^{-1}	0.73	1.49×10^{4}	1.77	1.29	0.29
8.16×10^{-5}	3.44×10^{-1}	3.37×10^{-2}	5.48×10^{-1}	0.70	1.29×10^{4}	2.05	1.44	0.44
9.18×10^{-5}	3.86×10^{-1}	3.37×10^{-2}	5.89×10^{-1}	0.67	1.22×10^{4}	2.17	1.46	0.46
1.02×10^{-4}	4.23×10^{-1}	3.37×10^{-2}	6.22×10^{-1}	0.65	1.12×10^{4}	2.36	1.54	0.54
1.22×10^{-4}	4.98×10^{-1}	3.37×10^{-2}	6.82×10^{-1}	0.60	1.01×10^{4}	2.61	1.58	0.58
1.43×10^{-4}	5.70×10^{-1}	3.37×10^{-2}	7.31×10^{-1}	0.57	8.24×10^{3}	3.21	1.82	0.82
1.63×10^{-4}	6.49×10^{-1}	3.37×10^{-2}	7.76×10^{-1}	0.53	7.36×10^{3}	3.59	1.90	0.90
1.84×10^{-4}	7.14×10^{-1}	3.37×10^{-2}	8.07×10^{-1}	0.50	6.13×10^{3}	4.31	2.15	1.15

Table 13.4 The apparent association constant (K_{app}) data.

[Fe(acac)$_3$]	**(I_0-I)**	**1/(I_0-I)**	**1/[Fe(acac)$_3$]**
0	0	-	-
1.02×10^{-5}	3.13×10^{3}	3.19×10^{-4}	9.80×10^{4}
2.04×10^{-5}	3.13×10^{3}	3.19×10^{-4}	4.90×10^{4}
3.06×10^{-5}	5.31×10^{3}	1.88×10^{-4}	3.27×10^{4}
4.08×10^{-5}	7.10×10^{3}	1.41×10^{-4}	2.45×10^{4}
5.10×10^{-5}	8.59×10^{3}	1.16×10^{-4}	1.96×10^{4}
6.12×10^{-5}	1.08×10^{4}	9.25×10^{-5}	1.63×10^{4}
7.14×10^{-5}	1.15×10^{4}	8.67×10^{-5}	1.40×10^{4}
8.16×10^{-5}	1.35×10^{4}	7.39×10^{-5}	1.22×10^{4}
9.18×10^{-5}	1.42×10^{4}	7.02×10^{-5}	1.09×10^{4}
1.02×10^{-4}	1.52×10^{4}	6.56×10^{-5}	9.80×10^{3}
1.22×10^{-4}	1.63×10^{4}	6.13×10^{-5}	8.20×10^{3}
1.43×10^{-4}	1.82×10^{4}	5.49×10^{-5}	6.99×10^{3}
1.63×10^{-4}	1.91×10^{4}	5.24×10^{-5}	6.13×10^{3}
1.84×10^{-4}	2.03×10^{4}	4.93×10^{-5}	5.43×10^{3}

Table 14 Quenching reaction Data of Chlorophyll a by $Fe(acac)_3$ in DMSO.

Table 14.1 Stern-Volmer plot data.

V. of stock Chl a (mL)	**V. of stock $Fe(acac)_3$ (mL)**	**[$Fe(acac)_3$] (M)**	**I**	**I_0/I**	**$(I_0/I)-1$**
0.8	0.0	0	2.98×10^4	1.00	0
0.8	0.1	1.02×10^{-5}	2.63×10^4	1.13	0.13
0.8	0.2	2.04×10^{-5}	2.44×10^4	1.22	0.22
0.8	0.3	3.06×10^{-5}	2.25×10^4	1.32	0.32
0.8	0.4	4.08×10^{-5}	2.03×10^4	1.47	0.47
0.8	0.5	5.10×10^{-5}	1.86×10^4	1.60	0.60
0.8	0.6	6.12×10^{-5}	1.56×10^4	1.91	0.91
0.8	0.7	7.14×10^{-5}	1.54×10^4	1.93	0.93
0.8	0.8	8.16×10^{-4}	1.32×10^4	2.26	1.26
0.8	0.9	9.18×10^{-4}	1.31×10^4	2.26	1.26
0.8	1.0	1.02×10^{-4}	1.06×10^4	2.81	1.81
0.8	1.2	1.22×10^{-4}	1.03×10^4	2.90	1.90
0.8	1.4	1.43×10^{-4}	8.94×10^3	3.33	2.33
0.8	1.7	1.73×10^{-4}	7.20×10^3	4.14	3.14
0.8	2.0	2.04×10^{-4}	5.42×10^3	5.49	4.49

Table 14.2 Inner filter effect correction for Stern-Volmer plot data.

Fe^{3+}, M	abs 430	Δabs	Δabs/2	(Δabs/2)*-1	$10^{-(\Delta abs/2)}$	I_{exp}	$I_{0,corr}$	$I_{0,corr}/I_{exp}$	$(I_0/I)-1$
0	9.10×10^{-4}	0	0	0	1.00	2.98×10^{4}	2.98×10^{4}	1.00	0.00
1.02×10^{-5}	5.95×10^{-2}	5.86×10^{-2}	2.93×10^{-2}	-2.93×10^{-2}	0.93	2.63×10^{4}	2.78×10^{4}	1.06	0.06
2.04×10^{-5}	9.39×10^{-2}	9.30×10^{-2}	4.65×10^{-2}	-4.65×10^{-2}	0.89	2.44×10^{4}	2.68×10^{4}	1.10	0.10
3.06×10^{-5}	1.33×10^{-1}	1.32×10^{-1}	6.62×10^{-2}	-6.62×10^{-2}	0.86	2.25×10^{4}	2.56×10^{4}	1.14	0.14
4.08×10^{-5}	1.88×10^{-1}	1.87×10^{-1}	9.34×10^{-2}	-9.34×10^{-2}	0.81	2.03×10^{4}	2.40×10^{4}	1.18	0.18
5.10×10^{-5}	2.30×10^{-1}	2.30×10^{-1}	1.15×10^{-1}	-1.15×10^{-1}	0.77	1.86×10^{4}	2.29×10^{4}	1.23	0.23
6.12×10^{-5}	2.92×10^{-1}	2.91×10^{-1}	1.46×10^{-1}	-1.46×10^{-1}	0.71	1.56×10^{4}	2.13×10^{4}	1.36	0.36
7.14×10^{-5}	3.23×10^{-1}	3.22×10^{-1}	1.61×10^{-1}	-1.61×10^{-1}	0.69	1.54×10^{4}	2.06×10^{4}	1.33	0.33
8.16×10^{-5}	4.00×10^{-1}	3.99×10^{-1}	2.00×10^{-1}	-2.00×10^{-1}	0.63	1.32×10^{4}	1.88×10^{4}	1.43	0.43
9.18×10^{-5}	4.15×10^{-1}	4.14×10^{-1}	2.07×10^{-1}	-2.07×10^{-1}	0.62	1.32×10^{4}	1.85×10^{4}	1.41	0.41
1.02×10^{-4}	5.42×10^{-1}	5.41×10^{-1}	2.70×10^{-1}	-2.70×10^{-1}	0.54	1.06×10^{4}	1.60×10^{4}	1.51	0.51
1.22×10^{-4}	5.64×10^{-1}	5.63×10^{-1}	2.81×10^{-1}	-2.81×10^{-1}	0.52	1.03×10^{4}	1.56×10^{4}	1.52	0.52
1.43×10^{-4}	6.50×10^{-1}	6.49×10^{-1}	3.25×10^{-1}	-3.25×10^{-1}	0.47	8.94×10^{3}	1.41×10^{4}	1.58	0.58
1.73×10^{-4}	7.91×10^{-1}	7.90×10^{-1}	3.95×10^{-1}	-3.95×10^{-1}	0.40	7.20×10^{3}	1.20×10^{4}	1.66	0.66
2.04×10^{-4}	9.85×10^{-1}	9.84×10^{-1}	4.92×10^{-1}	-4.92×10^{-1}	0.32	5.42×10^{4}	9.59×10^{3}	1.77	0.77

Table 14.3 Inner filter effect correction of Borissevitch for Stern-Volmer plot data.

$[Fe(acac)_3]$,M	A_{ex}	$1\text{-}10^{-Aex0}$	$1\text{-}10^{-Aex}$	IFE_{corr}	I_{exp}	I_0/I_{exp}	$(I_0/I_{exp})_{corr}$	$(I_0/I_{exp})_{corr}$-1
0	9.10×10^{-4}	2.09×10^{-3}	2.09×10^{-3}	1.00	2.98×10^{4}	1.00	1.00	0.00
1.02×10^{-5}	5.95×10^{-2}	2.09×10^{-3}	1.28×10^{-1}	0.94	2.63×10^{4}	1.13	1.06	0.06
2.04×10^{-5}	9.39×10^{-2}	2.09×10^{-3}	1.94×10^{-1}	0.90	2.44×10^{4}	1.22	1.10	0.10
3.06×10^{-5}	1.33×10^{-1}	2.09×10^{-3}	2.64×10^{-1}	0.86	2.25×10^{4}	1.32	1.14	0.14
4.08×10^{-5}	1.88×10^{-1}	2.09×10^{-3}	3.51×10^{-1}	0.81	2.03×10^{4}	1.47	1.19	0.19
5.10×10^{-5}	2.30×10^{-1}	2.09×10^{-3}	4.12×10^{-1}	0.78	1.86×10^{4}	1.60	1.24	0.24
6.12×10^{-5}	2.92×10^{-1}	2.09×10^{-3}	4.90×10^{-1}	0.73	1.56×10^{4}	1.91	1.39	0.39
7.14×10^{-5}	3.23×10^{-1}	2.09×10^{-3}	5.24×10^{-1}	0.71	1.54×10^{4}	1.93	1.36	0.36
8.16×10^{-5}	4.00×10^{-1}	2.09×10^{-3}	6.02×10^{-1}	0.65	1.32×10^{4}	2.26	1.48	0.48
9.18×10^{-5}	4.15×10^{-1}	2.09×10^{-3}	6.16×10^{-1}	0.64	1.32×10^{4}	2.26	1.46	0.46
1.02×10^{-4}	5.42×10^{-1}	2.09×10^{-3}	7.13×10^{-1}	0.57	1.06×10^{4}	2.81	1.61	0.61
1.22×10^{-4}	5.64×10^{-1}	2.09×10^{-3}	7.27×10^{-1}	0.56	1.03×10^{4}	2.90	1.62	0.62
1.43×10^{-4}	6.50×10^{-1}	2.09×10^{-3}	7.76×10^{-1}	0.52	8.94×10^{3}	3.33	1.73	0.73
1.73×10^{-4}	7.91×10^{-1}	2.09×10^{-3}	8.38×10^{-1}	0.46	7.20×10^{3}	4.14	1.90	0.90
2.04×10^{-4}	9.85×10^{-1}	2.09×10^{-3}	8.96×10^{-1}	0.40	5.42×10^{3}	5.49	2.17	1.17

Table 14.4 The apparent association constant (K_{app}) data.

[Fe(acac)$_3$]	**(I_0-I)**	**1/(I_0-I)**	**1/[Fe(acac)$_3$]**
0	0	-	-
1.02×10^{-5}	3.51×10^{3}	2.85×10^{-4}	9.80×10^{4}
2.04×10^{-5}	5.41×10^{3}	1.85×10^{-4}	4.90×10^{4}
3.06×10^{-5}	7.30×10^{3}	1.37×10^{-4}	3.27×10^{4}
4.08×10^{-5}	9.48×10^{3}	1.05×10^{-4}	2.45×10^{4}
5.10×10^{-5}	1.12×10^{4}	8.94×10^{-5}	1.96×10^{4}
6.12×10^{-5}	1.42×10^{4}	7.06×10^{-5}	1.63×10^{4}
7.14×10^{-5}	1.44×10^{4}	6.96×10^{-5}	1.40×10^{4}
8.16×10^{-5}	1.65×10^{4}	6.03×10^{-5}	1.22×10^{4}
9.18×10^{-5}	1.66×10^{4}	6.01×10^{-5}	1.09×10^{4}
1.02×10^{-4}	1.92×10^{4}	5.21×10^{-5}	9.80×10^{3}
1.22×10^{-4}	1.95×10^{4}	5.12×10^{-5}	8.20×10^{3}
1.43×10^{-4}	2.08×10^{4}	4.80×10^{-5}	6.99×10^{3}
1.73×10^{-4}	2.26×10^{4}	4.43×10^{-5}	5.78×10^{3}
2.04×10^{-4}	2.44×10^{4}	4.10×10^{-5}	4.90×10^{3}

Table 15 Quenching reaction Data of Chlorophyll a by $Fe(acac)_3$ in acetonitrile.

Table 15.1 Stern-Volmer plot data.

V. of stock Chl a (mL)	**V. of stock $Fe(acac)_3$ (mL)**	**[$Fe(acac)_3$] (M)**	**I**	**I_0/I**	**$(I_0/I)-1$**
0.15	0.0	0	3.30×10^4	1.00	0
0.15	0.1	1.05×10^{-5}	3.01×10^4	1.09	0.09
0.15	0.2	2.10×10^{-5}	2.77×10^4	1.19	0.19
0.15	0.3	3.20×10^{-5}	2.54×10^4	1.30	0.30
0.15	0.4	4.20×10^{-5}	2.28×10^4	1.44	0.44
0.15	0.5	5.25×10^{-5}	2.16×10^4	1.53	0.53
0.15	0.6	6.30×10^{-5}	1.99×10^4	1.66	0.66
0.15	0.7	7.35×10^{-5}	1.92×10^4	1.72	0.72
0.15	0.8	8.40×10^{-4}	1.70×10^4	1.93	0.93
0.15	0.9	9.45×10^{-4}	1.62×10^4	2.03	1.03
0.15	1.0	1.05×10^{-4}	1.42×10^4	2.32	1.32
0.15	1.2	1.26×10^{-4}	1.30×10^4	2.54	1.54
0.15	1.4	1.47×10^{-4}	1.13×10^4	2.92	1.92
0.15	1.6	1.68×10^{-4}	9.63×10^3	3.42	2.42
0.15	1.8	1.89×10^{-4}	8.78×10^3	3.76	2.76
0.15	2.0	2.10×10^{-4}	7.76×10^3	4.25	3.25

Table 15.2 Inner filter effect correction for Stern-Volmer plot data.

Fe^{3+}, M	abs 430	Δabs	Δabs/2	(Δabs/2)*-1	$10^{-(\Delta abs/2)}$	I_{exp}	$I_{0,corr}$	$I_{0,corr}/I_{exp}$	$(I_0/I)-1$
0	2.87×10^{-3}	0	0	0	1.00	3.30×10^{4}	3.30×10^{4}	1.00	0.00
1.05×10^{-5}	4.58×10^{-2}	4.29×10^{-2}	2.15×10^{-2}	-2.15×10^{-2}	0.95	3.01×10^{4}	3.14×10^{4}	1.04	0.04
2.10×10^{-5}	8.65×10^{-2}	8.36×10^{-2}	4.18×10^{-2}	-4.18×10^{-2}	0.91	2.77×10^{4}	2.99×10^{4}	1.08	0.08
3.20×10^{-5}	1.38×10^{-1}	1.35×10^{-1}	6.75×10^{-2}	-6.75×10^{-2}	0.86	2.54×10^{4}	2.82×10^{4}	1.11	0.11
4.20×10^{-5}	1.84×10^{-1}	1.81×10^{-1}	9.05×10^{-2}	-9.05×10^{-2}	0.81	2.28×10^{4}	2.68×10^{4}	1.17	0.17
5.25×10^{-5}	2.27×10^{-1}	2.24×10^{-1}	1.12×10^{-1}	-1.12×10^{-1}	0.77	2.16×10^{4}	2.55×10^{4}	1.18	0.18
6.30×10^{-5}	2.67×10^{-1}	2.64×10^{-1}	1.32×10^{-1}	-1.32×10^{-1}	0.74	1.99×10^{4}	2.43×10^{4}	1.22	0.22
7.35×10^{-5}	2.69×10^{-1}	2.66×10^{-1}	1.33×10^{-1}	-1.33×10^{-1}	0.74	1.92×10^{4}	2.42×10^{4}	1.27	0.27
8.40×10^{-5}	3.55×10^{-1}	3.52×10^{-1}	1.76×10^{-1}	-1.76×10^{-1}	0.67	1.70×10^{4}	2.20×10^{4}	1.29	0.29
9.45×10^{-5}	4.01×10^{-1}	3.98×10^{-1}	1.99×10^{-1}	-1.99×10^{-1}	0.63	1.62×10^{4}	2.08×10^{4}	1.28	0.28
1.05×10^{-4}	4.47×10^{-1}	4.44×10^{-1}	2.22×10^{-1}	-2.22×10^{-1}	0.60	1.42×10^{4}	1.98×10^{4}	1.39	0.39
1.26×10^{-4}	5.44×10^{-1}	5.41×10^{-1}	2.71×10^{-1}	-2.71×10^{-1}	0.54	1.30×10^{4}	1.77×10^{4}	1.36	0.36
1.47×10^{-4}	6.30×10^{-1}	6.27×10^{-1}	3.13×10^{-1}	-3.13×10^{-1}	0.48	1.13×10^{4}	1.60×10^{4}	1.42	0.42
1.68×10^{-4}	7.22×10^{-1}	7.19×10^{-1}	3.60×10^{-1}	-3.60×10^{-1}	0.44	9.63×10^{3}	1.44×10^{4}	1.50	0.50
1.89×10^{-4}	8.04×10^{-1}	8.01×10^{-1}	4.01×10^{-1}	-4.01×10^{-1}	0.40	8.78×10^{3}	1.31×10^{4}	1.49	0.49
2.10×10^{-4}	8.94×10^{-1}	8.91×10^{-1}	4.45×10^{-1}	-4.45×10^{-1}	0.36	7.76×10^{3}	1.18×10^{4}	1.52	0.52

Table 15.3 Inner filter effect correction of Borissevitch for Stern-Volmer plot data.

$[Fe(acac)_3]$,M	A_{ex}	$1\text{-}10^{-Aex0}$	$1\text{-}10^{-Aex}$	IFE_{corr}	I_{exp}	I_0/I_{exp}	$(I_0/I_{exp})_{corr}$	$(I_0/I_{exp})_{corr}$-1
0	2.87×10^{-3}	6.59×10^{-3}	6.59×10^{-3}	1.00	3.30×10^{4}	1.00	1.00	0.00
1.05×10^{-5}	4.58×10^{-2}	6.59×10^{-3}	1.00×10^{-1}	0.95	3.01×10^{4}	1.09	1.04	0.04
2.10×10^{-5}	8.65×10^{-2}	6.59×10^{-3}	1.80×10^{-1}	0.91	2.77×10^{4}	1.19	1.08	0.08
3.20×10^{-5}	1.38×10^{-1}	6.59×10^{-3}	2.72×10^{-1}	0.86	2.54×10^{4}	1.30	1.12	0.12
4.20×10^{-5}	1.84×10^{-1}	6.59×10^{-3}	3.45×10^{-1}	0.82	2.28×10^{4}	1.45	1.18	0.18
5.25×10^{-5}	2.27×10^{-1}	6.59×10^{-3}	4.07×10^{-1}	0.78	2.16×10^{4}	1.53	1.20	0.20
6.30×10^{-5}	2.67×10^{-1}	6.59×10^{-3}	4.60×10^{-1}	0.75	1.99×10^{4}	1.66	1.24	0.24
7.35×10^{-5}	2.69×10^{-1}	6.59×10^{-3}	4.62×10^{-1}	0.75	1.92×10^{4}	1.72	1.29	0.29
8.40×10^{-5}	3.55×10^{-1}	6.59×10^{-3}	5.56×10^{-1}	0.68	1.70×10^{4}	1.93	1.33	0.33
9.45×10^{-5}	4.01×10^{-1}	6.59×10^{-3}	6.03×10^{-1}	0.66	1.62×10^{4}	2.03	1.33	0.33
1.05×10^{-4}	4.47×10^{-1}	6.59×10^{-3}	6.43×10^{-1}	0.63	1.42×10^{4}	2.32	1.45	0.45
1.26×10^{-4}	5.44×10^{-1}	6.59×10^{-3}	7.14×10^{-1}	0.57	1.30×10^{4}	2.54	1.45	0.45
1.47×10^{-4}	6.30×10^{-1}	6.59×10^{-3}	7.65×10^{-1}	0.53	1.13×10^{4}	2.93	1.55	0.55
1.68×10^{-4}	7.22×10^{-1}	6.59×10^{-3}	8.10×10^{-1}	0.49	9.63×10^{3}	3.42	1.67	0.67
1.89×10^{-4}	8.04×10^{-1}	6.59×10^{-3}	8.43×10^{-1}	0.46	8.78×10^{3}	3.76	1.72	0.72
2.10×10^{-4}	8.94×10^{-1}	6.59×10^{-3}	8.72×10^{-1}	0.42	7.76×10^{3}	4.25	1.81	0.81

Table 15.4 The apparent association constant (K_{app}) data.

[Fe(acac)$_3$]	**(I_0-I)**	**1/(I_0-I)**	**1/[Fe(acac)$_3$]**
0	0	-	-
1.00×10^{-5}	2.82×10^{3}	3.55×10^{-4}	9.52×10^{4}
2.10×10^{-5}	5.22×10^{3}	1.92×10^{-4}	4.76×10^{4}
3.20×10^{-5}	7.60×10^{3}	1.32×10^{-4}	3.12×10^{4}
4.20×10^{-5}	1.02×10^{4}	9.85×10^{-5}	2.38×10^{4}
5.20×10^{-5}	1.14×10^{4}	8.77×10^{-5}	1.90×10^{4}
6.30×10^{-5}	1.31×10^{4}	7.64×10^{-5}	1.59×10^{4}
7.40×10^{-5}	1.38×10^{4}	7.24×10^{-5}	1.36×10^{4}
8.40×10^{-5}	1.59×10^{4}	6.28×10^{-5}	1.19×10^{4}
9.40×10^{-5}	1.67×10^{4}	5.99×10^{-5}	1.06×10^{4}
1.05×10^{-4}	1.87×10^{4}	5.34×10^{-5}	9.52×10^{3}
1.26×10^{-4}	2.00×10^{4}	5.01×10^{-5}	7.94×10^{3}
1.47×10^{-4}	2.17×10^{4}	4.61×10^{-5}	6.80×10^{3}
1.68×10^{-4}	2.33×10^{4}	4.29×10^{-5}	5.95×10^{3}
1.89×10^{-4}	2.42×10^{4}	4.14×10^{-5}	5.29×10^{3}
2.10×10^{-4}	2.52×10^{4}	3.97×10^{-5}	4.76×10^{3}

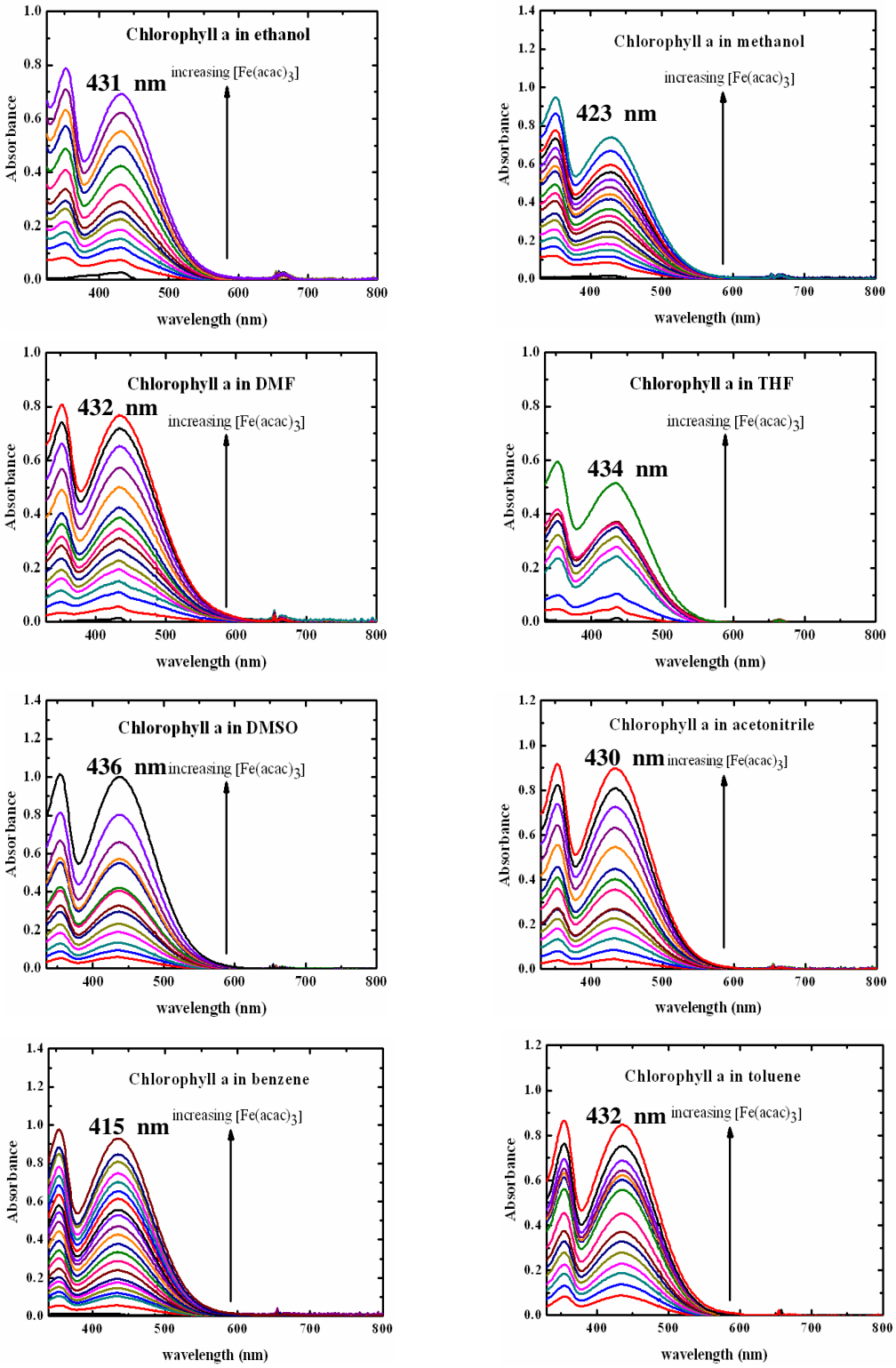

Figure 4 Absorption spectra of chlorophyll a when have $[Fe(acac)_3]$ in various solvents.

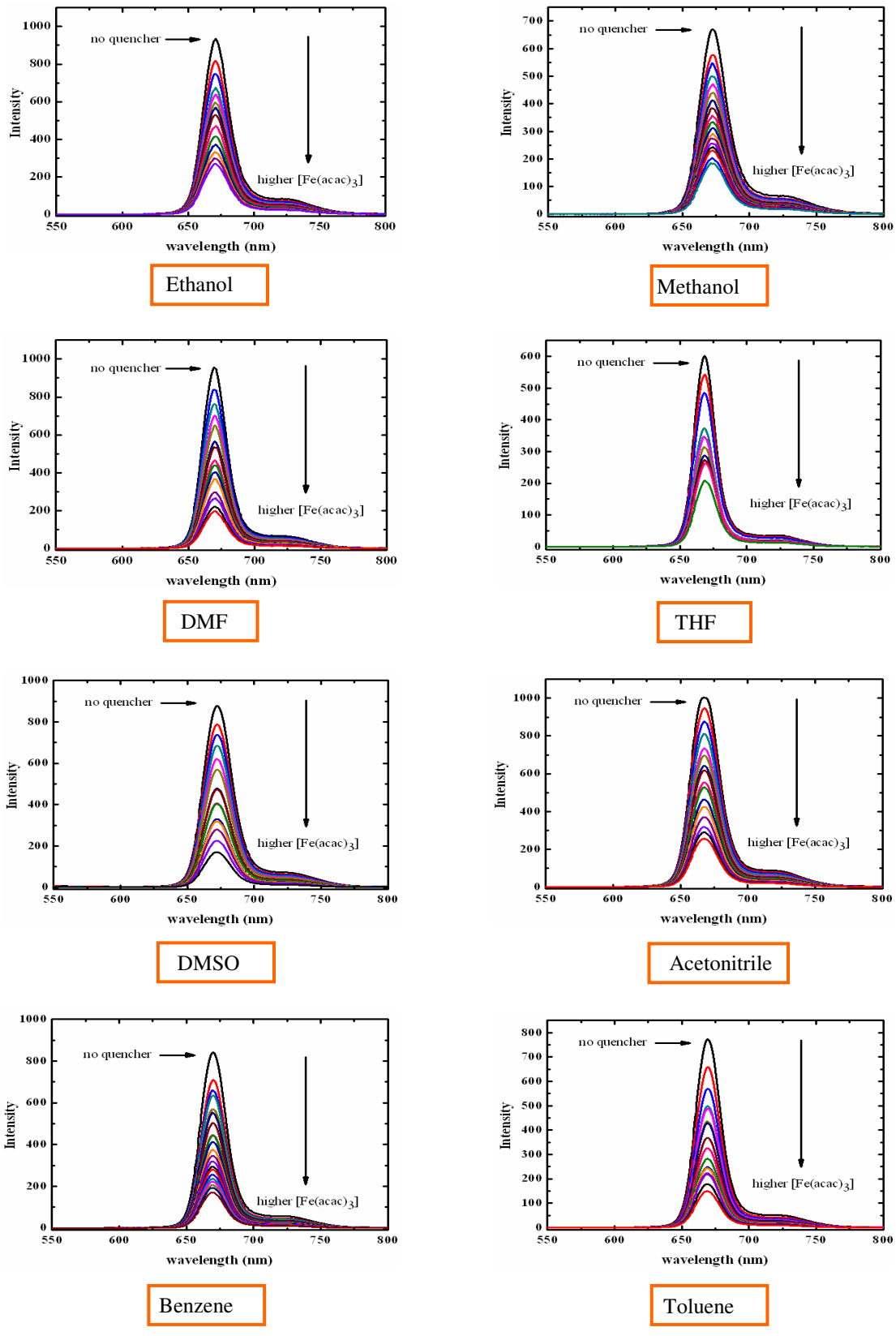

Figure 5 Emission spectra of chlorophyll a when have $[Fe(acac)_3]$ in various solvents.

VITAE

Name Miss Daweena Masen

Student ID 5010220050

Educational Attainment

Degree	Name of Institution	Year of Graduation
B. Ed. (Science-Chemistry)	Thaksin University	2006

Scholarship Awards during Enrolment

Center of Excellence for Innovation in Chemistry Commission on Higher Education, (PERCH-CIC)

List of Publication and Proceedings

Masen, D., Leesakul, N. 2009. Photo-Physical Properties and Quenching of the Excited State of Chlorophyll A. Proceeding of the 12th National Graduate Research Conference co - organized by CGAU and Khon Kaen University, Khon Kaen, Thailand, 12-13 February 2009. pp. 292-297.